

REACTIVE GASES IN GLOW DISCHARGE ION SOURCES:  
SPUTTERING AND IONIZATION CONSIDERATIONS

By

ELIZABETH PIERZ HASTINGS

A DISSERTATION PRESENTED TO THE GRADUATE SCHOOL  
OF THE UNIVERSITY OF FLORIDA IN PARTIAL FULFILLMENT  
OF THE REQUIREMENTS FOR THE DEGREE OF  
DOCTOR OF PHILOSOPHY

UNIVERSITY OF FLORIDA

2004

Copyright 2004

by

Elizabeth Pierz Hastings

**This document is dedicated to my parents, Ann and Jay, my brothers Brian and Chris, my cousin Erin, and my patient husband Jim.**

## ACKNOWLEDGMENTS

My career as a professional student has come to a close and now I must endure the uncertain future that beckons me. The success of my last few years in graduate school leaves me indebted to many people for their mentoring, continuing support, and comradeship. First, I wish to thank my advisor, Dr. W. W. Harrison, for granting me the opportunity to join the Harrison Group family, his guidance, and the endless words of wisdom.

I am forever grateful for the additional guidance and support from Dr. Jim Winefordner. His words of advice during a time of need steered me in a good direction. Also from the Winefordner group, special recognition goes to Dr. Ben Smith who has been an integral part of my success. The work here was made possible by the Harrison/Winefordner group laboratory cohesiveness and the support and help from my lab mates. Dr. Eric Oxley introduced me to the infamous technique of glow discharge and its small, yet close-knit community of scientists. I thank Eric for his advice and support during my writing period. Special attention goes to my sole lab mate (and friend) Kevin Turney. Our endless conversations not only about science, but on life helped me to grow as a person. Most of all, I appreciated his honesty. I also thank Tiffany Correll who brought laughter and lightheartedness into our group and for her friendship. I value Li Qian's support and friendship over the past couple of years. In addition, I must also thank the rest of the Winefordner group, new and old. Starbuck's anyone?

Finally, I thank my family and friends for their tremendous support throughout the past five years. My parents listened to my disappointments and achievements, and they provided daily encouragement with phone calls and occasional visits from New York. I appreciate my brothers' attentiveness during our conversations, and most of all their ability to relieve my stress with a bout of laughter! They have taught me to not take life too seriously all the time. Most of all, I will forever be indebted to my husband Jim. He has endlessly supported my endeavors and has supported me through the lows and highs. Also, many thanks go to him for the ice cream runs!

This work has been supported by the U.S. Department of Energy, Basic Energy Sciences, and LECO Corporation.

## TABLE OF CONTENTS

	<u>page</u>
ACKNOWLEDGMENTS .....	iv
LIST OF TABLES .....	ix
LIST OF FIGURES .....	x
ABSTRACT .....	xv
 CHAPTER	
1 GLOW DISCHARGE MASS SPECTROMETRY .....	1
Historical Background .....	1
Glow Discharge Fundamental Processes .....	3
The Glow Discharge .....	3
Discharge Operational Modes .....	8
Cathodic Sputtering .....	10
Ionization Processes .....	14
Instrumentation .....	17
Grimm-type Glow Discharge Ion Source .....	18
Time-of-Flight Mass Spectrometry .....	19
Pulsed Glow Discharge and Time-of-Flight Mass Spectrometer Timing .....	22
Gas Delivery System .....	25
2 GASES IN GLOW DISCHARGE ATOMIC EMISSION AND MASS SPECTROMETRY .....	27
Introduction .....	27
Inert Gases .....	28
Characteristics .....	29
Atmospheric Gases .....	31
Nitrogen .....	32
Oxygen .....	38
Organic Gases .....	40
Chemical Ionization .....	41
Penning Ionization .....	43
Considerations .....	43

3	CHARACTERIZATION OF THE MICROSECOND PULSED GLOW DISCHARGE PROCESSES IN NITROGEN.....	45
	Introduction.....	45
	Experimental.....	46
	Glow Discharge and Time-of-Flight Mass Spectrometer .....	46
	Gas Delivery System .....	49
	Plasma Gas .....	51
	Sample Material.....	52
	Results and Discussion .....	53
	Background.....	53
	Direct Current Glow Discharge: Comparison of Ar and N <sub>2</sub> .....	53
	Microsecond Pulsed Glow Discharge: Comparison of Ar and N <sub>2</sub> .....	63
	Conclusions.....	76
4	CHARACTERIZATION OF THE MICROSECOND PULSED GLOW DISCHARGE PROCESSES IN OXYGEN – REACTIVE SPUTTERING .....	77
	Introduction.....	77
	Experimental.....	78
	Glow Discharge Source and Time-of-Flight Mass Spectrometer .....	78
	Gas Delivery System .....	79
	Plasma Gas .....	79
	Sample Material.....	79
	Results and Discussion .....	80
	Background.....	80
	Direct Current Glow Discharge: Comparison of Ar and O <sub>2</sub> .....	81
	Microsecond Pulsed Glow Discharge: Comparison of Ar and O <sub>2</sub> .....	88
	Conclusions.....	101
5	EXAMINATION OF THE ROLE OF CHEMICAL IONIZATION IN A MICROSECOND PULSED GLOW DISCHARGE .....	103
	Introduction.....	103
	Experimental.....	104
	Glow Discharge Time-of-Flight Mass Spectrometer .....	104
	Gas Delivery System .....	104
	Plasma Gas .....	105
	Sample Material.....	106
	Results and Discussion .....	106
	Direct Current Glow Discharge: Comparison of Ar and 5%CH <sub>4</sub> .....	106
	Microsecond Pulsed Glow Discharge: Comparison of Ar and 5% CH <sub>4</sub> .....	114
	Conclusions.....	133
6	CONCLUDING REMARKS.....	135
7	FUTURE CONSIDERATIONS.....	139

LIST OF REFERENCES .....	142
BIOGRAPHICAL SKETCH .....	149

## LIST OF TABLES

<u>Table</u>	<u>page</u>
1-1 Ionization processes in a glow discharge plasma. Ionization is characterized by primary and secondary ionization processes. ....	15
2-1 Characteristics of noble gases used in glow discharge spectrometry. ....	29
2-2 Physical and chemical properties of nitrogen and oxygen gases. ....	31
2-3 Common nitrogen ions detected in glow discharge mass spectrometry. ....	35
2-4 List of methane ions detected in a radio frequency discharge in methane. ....	42
3-1 Typical operating conditions of the glow discharge source. ....	47
3-2 Typical operating conditions for a time-of-flight mass spectrometer with a dc and pulsed glow discharge. ....	48
3-3 A list of mass flow controllers, flow rate ranges, and their corresponding calibration gases. ....	49
3-4 Molecular structure correction factors to calculate the gas correction factor. ....	51
3-5 Secondary electron emission yields ( $\gamma_i$ ) of various metals for argon and nitrogen gases. ....	67
5-1 Comparison of methane ions in a conventional CI mass spectrum and a 5% CH <sub>4</sub> in argon direct current glow discharge mass spectrum. ....	110
5-2 Comparison of the methane derived ions in a dc glow discharge compared to a microsecond pulsed glow discharge. ....	124

## LIST OF FIGURES

<u>Figure</u>	<u>page</u>
1-1 Voltage versus current characteristics of various discharges – the operating regimes. (adapted from Howatson <sup>43</sup> ) .....	4
1-2 Architecture of an abnormal glow discharge. The three main regions are the cathode dark space (CDS), negative glow (NG), and Faraday dark space. ....	6
1-3 Simple glow discharge configuration highlighting the three main regions.....	7
1-4 Schematic of two different discharge modes .....	9
1-5 Representation of cathodic sputtering in a glow discharge.....	10
1-6 The number of electrons in the atomic “d” shell as a function of the atomic number.....	13
1-7 Sputter yield for various elements in the periodic table. The elements are bombarded with 400 eV argon ions. ....	14
1-8 Electron impact ionization (EI) process. ....	16
1-9 Penning ionization mechanism.....	17
1-10 Schematic of a Grimm-type source coupled to a time-of-flight mass spectrometer. ....	18
1-11 Schematic of the Renaissance time-of-flight mass spectrometer.....	22
1-12 Diagram of the microsecond pulsed glow discharge – time-of-flight mass spectrometry setup.....	23
1-13 Temporal profile concepts for a microsecond pulsed glow discharge and time-of-flight mass spectrometer.....	24
1-14 Schematic of the gas delivery system. The gas delivery system controls gas flow rate and gas mixing conditions.....	26
2-1 Plots of the emission intensities of copper and argon atom lines. A) Variation of peak intensities of Cu I 327.4 nm as a function of the nitrogen partial pressure. B) Variation of emission intensities of Ar I lines.....	33

2-2	Emission intensity as a function of nitrogen concentration. ....	34
2-3	The three regions of a pulsed glow discharge: prepeak, plateau, and afterpeak. ....	37
2-4	Effect of oxygen content (0-100%) .....	39
2-5	Effect of methane concentration on atomic absorption of copper atom and ion signals and the argon metastable. ....	43
3-1	Schematic of the vacuum system and pressure regimes of the time-of-flight mass spectrometer. ....	47
3-2	Direct current argon glow discharge mass spectra with a A) gold sample and B) NIST 1113 sample. ....	55
3-3	Direct current nitrogen glow discharge mass spectra for A) gold sample and B) NIST 1113 sample. ....	57
3-4	The effect of 0-100% nitrogen addition to an argon dc glow discharge on ion signals. The ion signals monitored were $N_2^+$ , $N_2H^+$ , $Ar^+$ , $ArH^+$ , and $Au^+$ (or $^{63}Cu^+$ and $^{65}Cu^+$ ). A) gold sample B) NIST 1113 sample. ....	60
3-5	Direct current glow discharge mass spectra of NIST 1113 sample in A) 10% $N_2$ and B) 60% $N_2$ . ....	61
3-6	Pure nitrogen direct current glow discharge mass spectra of a gold cathode at A) 10% $N_2$ and B) 80% $N_2$ . ....	62
3-7	Delay time plot of an argon microsecond pulsed glow discharge. Sample material: high purity gold. ....	64
3-8	Delay time plot of a nitrogen microsecond pulsed glow discharge. Sample material: high purity gold. ....	65
3-9	Microsecond pulsed glow discharge at early delay times illustrating electron impact ionization-like mass spectra. A) Argon discharge at 50 $\mu s$ delay time. B) Nitrogen discharge at 10 $\mu s$ delay time. ....	66
3-10	Secondary electron emission yields of tungsten and molybdenum for the noble gases. ....	66
3-11	Comparison of one MFC at 150 mL·min <sup>-1</sup> versus two MFCs totaling 150 mL·min <sup>-1</sup> . ....	68
3-12	Total number of ions of those investigated versus concentration of added gas when $N_2$ is added to the Ar matrix plasma. ....	70
3-13	Total number of ions of those investigated versus concentration of added gas when $N_2$ is added to the Ar matrix plasma. ....	72

3-14	Ionization efficiency as a function of electron energy. ....	73
3-15	Pulsed net sputter rate of gold, silver, and copper relative to nitrogen content. ....	75
4-1	Direct current glow discharge mass spectra in 100% argon using a gold cathode. ....	82
4-2	Direct current glow discharge mass spectra in 100% oxygen using a gold cathode. ....	84
4-3	A plot of the relationship between ion signal intensities and the oxygen content in a mixed argon-oxygen direct current glow discharge. ....	86
4-4	Direct current glow discharge mass spectra of A) 20% O <sub>2</sub> , B) 20% O <sub>2</sub> , 35x magnified m/z region 10-50, C) 80% O <sub>2</sub> , and D) 80% O <sub>2</sub> , 35x magnified m/z region 10-50. ....	87
4-5	Waterfall plot of an argon microsecond pulsed glow discharge. This plot corresponds to Figure 3-7 in Chapter 3. Sample material: gold. ....	89
4-6	Delay time plot of 100% oxygen microsecond pulsed glow discharge. Sample material: high purity gold. ....	89
4-7	Mass spectra of a 100% oxygen microsecond pulsed glow discharge at various delay times. A) 10 μs B) 30 μs C) 50 μs D) 90 μs. Sample material: high purity gold. ....	90
4-8	Total number of ions as a function of the oxygen content in an argon microsecond pulsed glow discharge. Sample material: high purity gold. ....	91
4-9	Total number of ions versus oxygen content in a μs pulsed argon glow discharge. The ions monitored are O <sub>2</sub> <sup>+</sup> , O <sub>2</sub> H <sup>+</sup> , Ar <sup>+</sup> , ArH <sup>+</sup> , and the isotopes of copper and silver. A) Sample material: NIST 1113 B) Sample material: high purity silver. ....	94
4-10	Log of MO <sup>+</sup> /M <sup>+</sup> as a function of the energy of formation of MO. ....	95
4-11	Ion currents versus oxygen pressure in A) oxygen-neon discharge and B) oxygen-argon discharge. ....	96
4-12	Mass spectra of a 20% oxygen glow discharge. Sample material: NIST 1113. ....	97
4-13	Pure oxygen microsecond pulsed glow discharge mass spectra. ....	98
4-14	Type 1 and type 2 configurations to determine the presence of an oxide layer. Sputter rate as a function of partial pressure of O <sub>2</sub> . ....	99
4-15	Net pulsed sputter rate (ng/pulse) of gold, silver, and copper as a function of oxygen content. ....	100

5-1	Mass spectra of an argon direct current glow discharge with time-of-flight mass spectrometry detection. Sample material: high purity gold. ....	107
5-2	Mass spectra of a 5% methane in argon direct current glow discharge with time-of-flight mass spectrometry detection. Sample material: high purity gold.....	109
5-3	The effect of methane addition to an argon dc glow discharge. Methane concentration ranges from 0-5% CH <sub>4</sub> . ....	112
5-4	Direct current glow discharge mass spectra of A) 0.5% methane, B) 1% methane, C) 2% methane, and D) 3% methane. <i>m/z</i> region 10-60. ....	113
5-5	Direct current glow discharge mass spectrum of 1% CH <sub>4</sub> in an argon matrix depicting the <i>m/z</i> region 190-240. Magnified 60x. This figure correlates to Figure 5-3. Sample material: high purity gold. ....	113
5-6	Direct current glow discharge mass spectrum of 3% CH <sub>4</sub> in argon.....	115
5-7	Microsecond pulsed glow discharge delay time plot of 5% CH <sub>4</sub> in argon. Sample material: high purity gold.....	116
5-8	Microsecond pulsed glow discharge mass spectrum of 5% CH <sub>4</sub> in argon at a 30 $\mu$ s delay time. Sample material: high purity gold. ....	117
5-9	Microsecond pulsed glow discharge mass spectra in 5% CH <sub>4</sub> at a 120 $\mu$ s delay time. Sample material: high purity gold.....	118
5-10	Microsecond pulsed glow discharge plot of ion population versus methane content in argon. Sample material: high purity gold.....	119
5-11	1% CH <sub>4</sub> $\mu$ sPGD. A series of mass spectra collected at delay times between 10-220 $\mu$ s compiled to generate a waterfall plot. Cathode material: high purity gold.....	120
5-12	Microsecond pulsed glow discharge mass spectrum of 1% CH <sub>4</sub> in argon collected at a 120 $\mu$ s delay time. Sample material: high purity gold. ....	121
5-13	Microsecond pulsed glow discharge mass spectrum of 1% CH <sub>4</sub> in argon collected at a 120 $\mu$ s delay time. Sample material: high purity gold. ....	123
5-14	Microsecond pulsed glow discharge of ion population with respect to methane concentration (0-5%). A) NIST 1113 and B) High purity silver. ....	125
5-15	1% CH <sub>4</sub> in argon $\mu$ s pulsed glow discharge mass spectrum at a 50 $\mu$ s delay time. Sample material: NIST 1113.....	126
5-16	Mass spectra of 1% CH <sub>4</sub> in argon for a $\mu$ sPGD collected at a 120 $\mu$ s delay time. A) <i>m/z</i> region 10-260 and B) <i>m/z</i> region 75-215. Sample material: NIST 1113...127	

5-17	Mass spectra generated from Isopro indicating the isotope distribution of copper dimers and trimers. ....	128
5-18	Microsecond pulsed glow discharge mass spectrum of 1% CH <sub>4</sub> in argon, A) experimental data. B) Distribution of silver dimers using Isopro calculation. ....	129
5-19	Net pulsed sputter rate of gold, copper, and silver as a function of methane concentration. ....	131
5-20	Mass spectrum of a microsecond pulsed glow discharge with a 1% methane in argon plasma gas. Toluene vapor was added to the plasma. Sample material: high purity gold. ....	132

Abstract of Dissertation Presented to the Graduate School  
of the University of Florida in Partial Fulfillment of the  
Requirements for the Degree of Doctor of Philosophy

REACTIVE GASES IN GLOW DISCHARGE ION SOURCES: SPUTTERING AND  
IONIZATION CONSIDERATIONS

By

Elizabeth Pierz Hastings

August 2004

Chair: Willard W. Harrison

Major Department: Chemistry

Glow discharge (GD) spectrometry is an established technique for the analysis of solid samples. The glow discharge source is simple yet versatile, providing information for both emission and mass spectrometry methods. A GD source shows stable operation in both direct current (dc) mode and pulsed mode, providing either a continuous supply of photons, atoms, and ions or a time-variant beam. Advantages accrue to both types of operation.

A glow discharge source commonly uses argon as the discharge gas due to its inert nature, discharge stability, and relatively simple spectra. Other noble gases have also been studied: helium, neon, krypton, and xenon; all sustain a workable GD plasma. The plasma gas employed in a glow discharge will have a significant effect on the type of ions produced. In analytical GD spectrometry, only high purity non-reactive gases are normally used in the discharge. However, oxygen, nitrogen, and water vapor are common impurities from trace leaks in the source or vacuum system. Mixed gas

plasmas, primarily the addition of small percentage increments of a reactive gas to a noble gas base discharge, have been explored for glow discharge – optical emission spectrometry (GD-OES). Limited information is available on reactive gases using glow discharge mass spectrometry.

In this work we are interested in the performance of a glow discharge as traditional, inert gases are systematically replaced by alternative reactive gases. Our main focus is to monitor the effect that type and composition of discharge gas have on the positive ion population. By varying the gas composition, there is also the possibility of controlling the reagent ion population for chemical ionization. A Grimm-type microsecond pulsed glow discharge time-of-flight mass analyzer was used.

To monitor how oxygen, nitrogen, or methane affect a normal argon discharge, the following studies were conducted: 1) comparison of argon versus mixed-gas discharge environments, 2) comparison of pulsed versus direct current discharges, 3) determination of ions of the gas species present in the discharge, and 4) comparison of the sputtering rates. Additionally, reactive versus potentially non-reactive cathodes were employed to further study the ionization and sputtering effects of unconventional gases. To decouple the reactive plasma from potentially reactive surface processes, gold was employed as a relatively non-reactive cathode material. For comparison, NIST SRM 1113, a copper-based standard, was used as a reactive cathode surface.

## CHAPTER 1 GLOW DISCHARGE MASS SPECTROMETRY

### **Historical Background**

The glow discharge device can be traced back to its birth over a century ago. Despite the long lineage of the technique, its prominence is still found extensively in academics and the metallurgical field. Popularity of the glow discharge is due to its simple operation and intense ion currents generated, which are essential for significant ion production.

In the late 1800s, investigation of the glow discharge (or work on gaseous conduction) commenced due to advancements in vacuum technology.<sup>1</sup> Revelation by Goldstein (1886) of “positive rays” of electricity, otherwise known as Kanalstrahlen, in a discharge tube providing a source of ions led to a series of discoveries.<sup>2</sup> The work of J. J. Thomson in the early 1900s brought the glow discharge to fruition as an ionization source. His interest in “positive rays” led to the discovery of the electron and the ratio of charge-to-mass recorded on a mass spectrograph.<sup>1,3</sup> Further advancements by Thomson and Aston contributed to the development of a glow discharge ion source coupled to a mass spectrometer for solids analysis. At this time Aston also discovered isotopes for a large number of elements.<sup>4,5</sup> K. T. Bainbridge improved the mass spectrometer to focus ion beams, which are non-uniform in both velocity and direction.<sup>6</sup> J. J. Thomson, Aston, and Bainbridge were the pioneers of coupling electrical discharges as ion sources to mass spectrometers.

Due to the poor reproducibility of glow discharge analyses and the implementation of the vacuum spark source, attractiveness of the glow discharge ion source declined. In the early 1970s the glow discharge experienced a rebirth with the implementation of direct current (dc) and radiofrequency (rf) powering discharge modes for glow discharge mass spectrometry (GDMS). Coburn and Kay introduced the dual powering modes for analysis of conducting and non-conducting solids.<sup>7-9</sup> Additionally, the development of both the Grimm<sup>10</sup> Glow Discharge in 1968 and later a commercial GD instrument (VG 9000, VG Isotopes) contributed to a resurgence of the electrical discharge. Renewed interest in the technique inspired research on a hollow cathode source,<sup>11-13</sup> solution residue analysis,<sup>14-18</sup> sputtering processes, and ionization phenomena.

At the present time, three discharge modes are in use: direct current (dc), radiofrequency (rf), and pulsed operation. Applications range from non-conducting samples using an rf discharge<sup>19,20</sup> to depth profiling using all discharge modes.<sup>21-27</sup> Li and coworkers utilized rf-GDMS for the analysis of bromine in flame-retardant plastics.<sup>28</sup> Davis and coworkers extended the use of particle beam-GDMS for the determination of nucleotides.<sup>29</sup> In addition to glow discharge applications, a comprehensive modeling network for a pulsed glow discharge<sup>30,31</sup> and for fundamental understandings provides further insight into GD properties.<sup>32</sup>

Applications and theoretical considerations have been enhanced by the implementation of alternative detection methods. An increasing number of glow discharge studies involve mass spectrometry for elemental<sup>33-35</sup> and molecular<sup>36-38</sup> detection, more specifically, time-of-flight mass spectrometry (TOFMS). An advantage of a TOFMS is the ability to synchronize timings of a pulsed plasma with the mass

spectrometer, enhancing analyte signal. My research takes advantage of the synchronization by using a microsecond pulsed glow discharge – time-of-flight mass spectrometer. The following sections describe the fundamental glow discharge processes and instrumentation used in the research.

### **Glow Discharge Fundamental Processes**

In general, a discharge is characterized by a particular voltage and current relationship. Based on operating regimes, the glow discharge is divided into two categories: the normal and abnormal, with the latter providing the important atomic spectroscopic information. The abnormal glow discharge can be further partitioned into eight regions, which comprise the plasma. Each region is integral for sustaining a steady-state discharge. The following section describes discharge formation, operating regimes, and architecture.

### **The Glow Discharge**

What events transpire during glow discharge (GD) formation? When two electrodes, a cathode (-) and anode (+), are immersed in an inert gas (e.g., argon) and a potential is applied, an electric breakdown of the gas occurs. Formation of electrons and ions results from gas breakdown, allowing current to flow. Current flowing through a gaseous medium is called a discharge or plasma. The gas breakdown potential depends on gas pressure, gas type, cathode material, and inter-electrode distance. The discharge is maintained by the electrons, positive ions, and negative ions, which were formed during breakdown. Positively and negatively charged species accelerate to the cathode and anode respectively, due to the electric field created between electrodes. The positive ions

bombard the sample surface initiating a sputtering event. Sputtering releases analyte atoms from the bulk sample for analysis. Charged species are continually produced due to collisional properties within the plasma (negative glow region) and the discharge becomes “self-sustaining.”<sup>39-42</sup>

**Glow Discharge Characterization.** Discharges are differentiated by their voltage and current characteristics, which define the operating regimes. The operating regimes of discharges, with features close to a glow discharge, are shown in Figure 1-1. Depicted in red is the abnormal GD region, which is most commonly employed in atomic spectroscopy; however, other discharge regions are prevalent before an abnormal discharge is maintained.

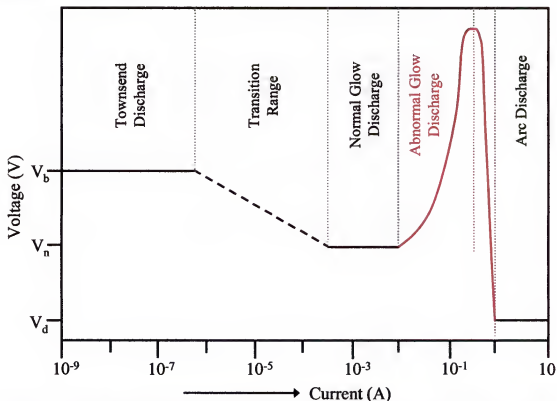


Figure 1-1 Voltage versus current characteristics of various discharges – the operating regimes. (Adapted from Howatson<sup>43</sup>)

In Figure 1-1,  $V_b$  represents the breakdown voltage (of the gas),  $V_n$  is the normal operating voltage, and  $V_d$  corresponds to the operating voltage of the arc discharge. Upon initial voltage ramping, a Townsend discharge forms at breakdown voltage conditions. Onset of a Townsend discharge induces gas breakdown forming few ions and electrons. An increase in the electrical current with a decrease in the required voltage corresponds to a transition region. The transition region is followed by the onset of a luminous glow – the normal glow discharge. At “normal” GD conditions, the constant current density is maintained as discharge current increases. However, the abnormal glow discharge region is most commonly used in atomic spectroscopy. The abnormal glow discharge is marked by an increase in current density as the discharge current increases. The second transition region is plagued by thermal vaporization of the cathode and the potential fields are perturbed. An arc forms at a lower discharge voltage when current levels reach the low ampere range.<sup>40,44</sup>

To obtain the greatest amount of analytical information, the discharge is maintained in the abnormal mode for both optical emission and mass spectrometry detection methods. Throughout this document, an abnormal glow discharge will be referred to as the “glow discharge.” An abnormal glow discharge can be defined further by its physical and electrical characteristics; hence, the architecture of the glow discharge.

**Glow Discharge Architecture.** Due to the potential difference between the anode and cathode, a distinct architecture defines the glow discharge. Eight regions exist in the discharge (Figure 1-2), although the shorter anode/cathode distance in analytical sources leads to the three major regions: the cathode dark space (CDS), negative glow (NG), and anode dark space. The CDS is where the majority of potential between the two

electrodes dropped. In this region, electrons are repelled, which creates a positive space charge near the cathode. Most analytically useful information is gained in the NG, which is a collision rich region of high luminosity. Adjacent to the anode is the Faraday dark space. The three regions that comprise a simple glow discharge are exemplified in Figure 1-3.<sup>40</sup> If argon is the discharge gas, a purple glow is typically visible due to gas-phase excitation and ionization collisions. This collision-rich region of the negative glow generates the analytically useful information.

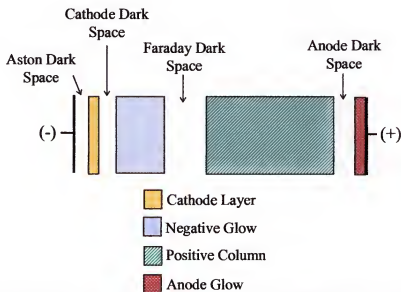


Figure 1-2 Architecture of an abnormal glow discharge. The three main regions are the cathode dark space (CDS), negative glow (NG), and Faraday dark space.

Figure 1-2 is a schematic illustrating the glow discharge regions<sup>44,45</sup> with the cathode (-) and anode (+), located on the left and right sides respectively, represented by black plates. Adjacent to the cathode surface is the *Aston dark space*, which forms during the sputtering process due to emitted secondary electrons, forming a net negative space charge above the cathode. A region of low luminosity arises from slow electrons and positive ions undergoing inelastic collisions to form neutrals – the *cathode layer*. The faint glow forms by radiative relaxation of the neutrals. Electrons that traverse the

cathode layer without colliding can acquire energy and form a net positive space charge. The majority of the discharge potential between the two electrodes is dropped across this region, the *cathode dark space* (CDS).

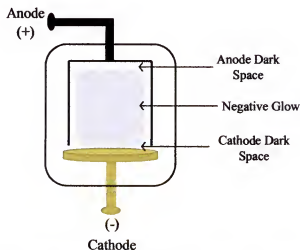


Figure 1-3 Simple glow discharge configuration highlighting the three main regions.

Beyond the CDS is the *negative glow* (NG) represented by a bright, collision-rich area due to the radiative relaxation of excited atoms. Most analytical information is obtained in the NG because of the extensive excitation and ionization collisions. The area where excitation of atoms is no longer prevalent, and thus electrons start to feel the anode potential, is the *Faraday dark space*. Electrons are accelerated in this region due to the potential gradient.

Because the electrons are accelerated, thus acquiring energy, they are again capable of excitation and ionization. This is a region of low luminosity called the *positive column*. Next to the positive column is the *anode dark space* where electrons are strongly attracted to the anode. In this region, increases in the field strength, negative space charge, and negative current density are apparent. Adjacent to the anode is the *anode glow*, where the negative current density is greatest. It is a luminous region

dictated by the high probability of electron impact excitation. The eight regions define the glow discharge's composition.<sup>40,44</sup>

### **Discharge Operational Modes**

Three discharge modes exist for powering the glow discharge: direct current (dc), pulsed, and radio frequency (rf). Each discharge mode spawns its own advantage(s) contributing to source versatility.

**Direct Current.** Early glow discharge studies used direct current (dc) to power the discharge. Direct current glow discharges normally operate by applying a constant negative potential to the cathode. Figure 1-4 is a schematic of a dc discharge showing the area of sputtered species in comparison to the glow region. Typical operating conditions are 1-3 kV and less than 30 mA current. This powering mode is the most conventional due to the simplicity, reproducibility, cost-effectiveness, and steady-state supply of ions produced. Disadvantages of a dc discharge are the low operating power (<10 W), and the inability to analyze non-conducting samples.

**Pulsed Discharge.** Instead of a steady-state supply of ions, a transient ion signal can be generated by pulsing the discharge voltage. Figure 1-4 shows a comparison of ion generation in a dc and pulsed discharge. A repetitive high voltage pulse is applied to the cathode in pulsed mode and at pulse initiation, electrical breakdown of argon atoms creates sputtering ions. The ions participate in analyte ejection from the cathode surface. Each atom packet is generated from an individual pulse and subjected to ionization. These ion packets expand and diffuse away from the cathode with each pulse. An induction period of ~0.5–1 ms occurs between gas and analyte ion measurements.<sup>46</sup> The elemental response in the induction period varies resulting in temporal profiles, which

provide discrimination between gas and analyte ions. A pulsed discharge offers high power operation (short term), enhanced sputter yield, greater excitation and ionization, less sample consumption, and temporal resolution. A limitation of pulsed mode is the requirement of a gated detector for temporal separation.

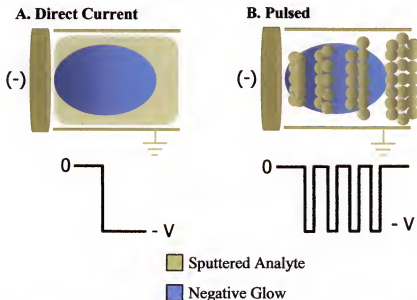


Figure 1-4 Schematic of two different discharge modes. (A) Direct current (dc) discharge mode generates a continuous supply of ions and (B) Pulsed mode generates packets of ions. (Adapted from Harrison et. al.<sup>46</sup>)

**Radio frequency.** The radio frequency powering mode allows the analysis of non-conducting samples, such as glass and ceramics. If a negative dc potential is applied to a non-conducting material, charge neutralization reactions result from the rapid decay of negative charge to a more positive potential. A discharge is not sustained because there is no net current flow. An alternating current applied at high pulse frequencies (1 MHz) induces a self (dc) biasing potential.<sup>40,44</sup> Each discharge mode has the capability to produce a population of sputtered analyte atoms. In the research that follows, only dc and pulsed discharges are studied.

## Cathodic Sputtering

Cathodic sputtering is the ejection of atoms from a bulk cathode into the gas phase. Ejection of atoms results from high energy positive ions (formed during gas breakdown) bombarding the cathode surface. The energetic positive ions are accelerated across the cathode fall region toward the cathode surface and experience penetration into the solid or backscattering. If penetration into the solid occurs, then the ion implants itself into the lattice, transferring kinetic energy and momentum to the surrounding atoms. A collisional cascade results from the transfer of kinetic energy, as shown in Figure 1-5. The arrows depict a random transfer of energy. Atoms can be released (or ejected) from the lattice if an atom absorbs energy greater than its binding energy. These atoms are ejected into the gas phase. For a given impact, the collisional cascade can last about 10-12 nanoseconds. Atoms, secondary ions, electrons, and clusters of atoms are released from the surface during the sputtering event; however, neutral atoms are the majority of sputtered material.<sup>40,47-49</sup>

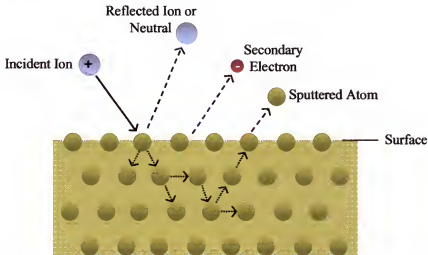


Figure 1-5 Representation of cathodic sputtering in a glow discharge.

The sputtered species are each affected by the electric field to differing extents. Electrons are accelerated toward the negative glow region acquiring energy for excitation

and ionization. Due to the strong electric field of the cathode, secondary ions return to the cathode surface. Individual sputtered atoms and clusters of atoms can experience two effects: 1) collisional redeposition onto sample surface (clusters dissociating due to collisions) and 2) diffusion into the negative glow for ionization. Sputtering is the atomization step in a glow discharge ionization source. Atomization is followed by ionization processes in the negative glow region. To describe the target collision phenomena of cathodic sputtering, two concepts are introduced: sputter rate and sputter yield.

**Sputter Rate.** Sputter rate describes the sputtering event and is expressed by the amount of material removed per unit time. It determines the rate of sample introduction into the mass analyzer. Net sputter rate ( $q$ ) for a direct current discharge is expressed as

$$q = \frac{\Delta W}{t} \quad (1-1)$$

where  $\Delta W$  is the change in weight and  $t$  is total sputtering time. Units are typically  $\mu\text{g}\cdot\text{s}^{-1}$ . When calculating the sputter rate for a pulsed discharge, the frequency must be factored into the equation. The net sputter rate for a pulsed discharge ( $\mu\text{g}/\text{pulse}$ ) is expressed as

$$q = \frac{\Delta W}{t \cdot f} \quad (1-2)$$

where  $f$  is the frequency (Hz) of the pulse and  $t$  is the total sputtering time. What affects the sputter rate? Target material, mass of incident ion, angle of incoming ion, mass of sputtering atom, incident ion energy, and surface binding energy all influence the sputter rate of a discharge. Discharge current and pressure are additional parameters that significantly alter the sputter rate.

**Sputter Yield.** Sputter yield is defined as the number of target atoms ejected from a surface per incident ion, which is a measure of the sputter efficiency. Energy of the incident ion is transferred to the target atom in the lattice (sputtered atom). The following is the expression for sputter yield ( $S$ )

$$S = \frac{3}{4} \pi^2 \alpha \left( \frac{4m_1 m_2}{(m_1 + m_2)^2} \right) \frac{E}{U_0} \quad (1-3)$$

where  $\alpha$  is the function of  $m_2/m_1$  and the angle of incidence of incident ion.<sup>50,51</sup> Energy of the incident ion and the surface binding energy are denoted by  $E$  and  $U_0$  respectively. The sputter yield depends on the relationship between the ion mass ( $m_1$ ) and the target atom mass ( $m_2$ ). The two masses determine the energy transfer function (mass transfer term), portraying the energy transfer in binary collisions

$$\frac{4m_1 m_2}{(m_1 + m_2)^2} \quad (1-4)$$

As  $m_1/m_2$  approaches unity, the mass transfer term maximizes, and thus sputter yield increases. Sputter yield is also closely related to an atom's electron concentration in the d-shell orbitals. In Figure 1-6, elements are plotted according to the d-shell filling as a function of atomic number.<sup>52,53</sup> Atomic radii decrease as the d-shells are filled, resulting in an increase in atomic density in the cathode. The penetration depth of primary ions is partly controlled by the electronic structure of the target atoms. In theory, the greater the d-shell filling, the greater the sputter yield. An incident ion can penetrate further into a cathode that has a more open electronic structure resulting in less efficient transmission of energy back to the cathode surface and a reduction in the sputtering process.

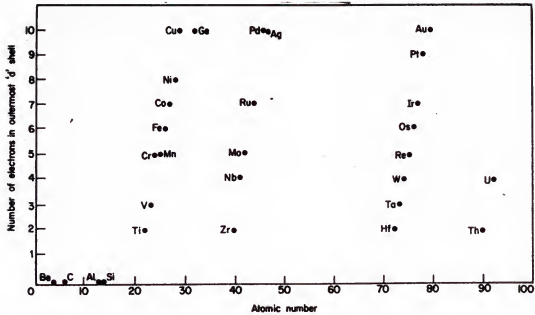


Figure 1-6 The number of electrons in the atomic "d" shell as a function of the atomic number. (Adapted from Laegreid et. al.<sup>54</sup>)

According to Figure 1-6, copper, silver, and gold should have similar sputter yields (and rates). The actual sputter yields of copper, silver, and gold with bombardment of the noble gas argon are depicted in Figure 1-7.<sup>54</sup> Figure 1-7 is a collection of sputter yields for various elements at conditions similar to a glow discharge, 400 eV argon ions. Sputter yield is reported in terms of  $S/(1 + \gamma)$  where  $S$  is the sputtering coefficient in atoms/ion and  $\gamma$  is the secondary electron coefficient. This shows a sputtering trend of  $\text{Ag} > \text{Au} > \text{Cu}$ . Laegreid and Wehner<sup>54</sup> report a sputtering trend of target materials that varies according to electron concentrations in the d-shells. Refer to Figure 1-6 for a plot of the number of electrons in the outermost d-shell as a function of the atomic number. Note that the results in Figures 1-6 and 1-7 are for ion beam, vacuum sputtering and not GD. What affects the sputter yield? Similar to sputter rate, the masses of incident ion and sputtered atom, incident ion energy, angle of incidence, and the surface binding

energy all affect the sputter yield. A higher sputter yield offers more neutral atoms for ionization. The following section describes how sputtered neutrals are ionized.

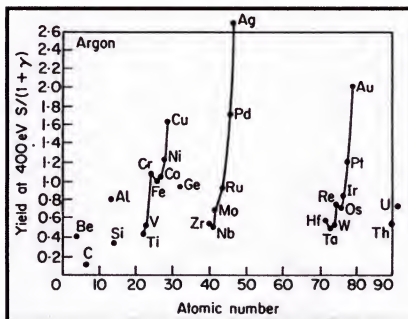


Figure 1-7 Sputter yield for various elements in the periodic table. The elements are bombarded with 400 eV argon ions. (Ref. 54)

### Ionization Processes

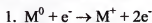
The glow discharge can be considered a two-step process separating the atomization and ionization steps. The sputtering event atomizes the sample material and, with sufficient energy transfer, sputtered atoms are ionized for elemental analysis. More specifically, as noble gas atoms strike the cathode surface, secondary electrons are released and rapidly accelerate. The electrons either strike the anode or undergo collisions in the negative glow, exciting and ionizing the sputtered atoms and noble gas atoms. Electron densities in the negative glow are around  $10^{14} \text{ cm}^{-3}$ .<sup>55</sup> Sputtered analyte atoms are ionized primarily by two ionization processes: electron impact ionization and Penning ionization. Depending on discharge conditions, charge exchange may also be prevalent. Table 1-1 lists other secondary ionization contributors. Factors that affect

ionization are gas pressure, discharge gas type, cathode geometry, and electron energy and number density.

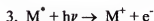
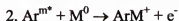
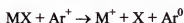
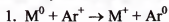
Many types of collisional processes in the negative glow contribute to analyte ionization. Collisions of the first kind transfer kinetic energy resulting in ionization, whereas collisions of the second kind transfer potential energy to promote ionization.<sup>56</sup> Electron ionization is considered a collision of the first kind and Penning ionization is a collision of the second kind.

Table 1-1 Ionization processes in a glow discharge plasma. Ionization is characterized by primary and secondary ionization processes.

### **I. Primary Ionization Processes**



### **II. Secondary Ionization Processes**



**Electron Impact Ionization.** Electron impact ionization is essential for sustaining a discharge, and is one of the best known processes. Electron impact involves the collision of an electron with a neutral atom; the electron energy must be higher than the ionization energy of the neutral atom. This collision removes an electron from the atom and produces a positive ion and two electrons, which are then accelerated by the electric

field and participate in further electron impact collisions (Figure 1-8). The multiplication process contributes to discharge stability.

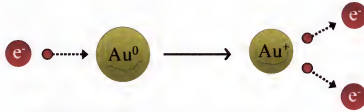


Figure 1-8 Electron impact ionization (EI) process.

Two principal types of electrons participate in the ionizing collisions: primary electrons and secondary electrons. Primary electrons, the same as secondary electrons emitted from the target surface, are accelerated by the electric field and have high energy upon entering the negative glow. They have the ability to ionize any element; however, due to their short interaction time and forward scattering they have a low probability of being involved in an ionizing collision. Secondary electrons are the by-product of ionizing collisions in the negative glow and have substantially lower energy. Secondary electrons are responsible for most ionization in the negative glow region.<sup>57,58</sup>

**Penning Ionization.** Penning ionization is another dominant ionization mechanism in the glow discharge. A collision between a metastable gas atom and a neutral atom may induce ionization (Figure 1-9). The ionization energy of the neutral atom must be below the excitation energy of the metastable species. Metastables are gas atoms that have been electronically excited to a level where radiative decay is forbidden. These species typically have a lifetime of several milliseconds. Argon, a common discharge gas, has metastable atoms with energies of 11.55 and 11.72 eV. These energies are sufficient enough to ionize most elements on the periodic table (e.g., IP: Au 9.2 eV). Penning ionization depends on the concentration of metastables in the negative glow

region and the population of metastables determines the ionization efficiency. Penning ionization has been considered the dominant ionization mechanism in low pressure discharges.<sup>59</sup> Furthermore, Penning ionization is thought to occur after pulse termination in a pulsed GD.<sup>60</sup>

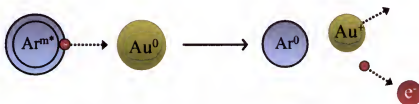


Figure 1-9 Penning ionization mechanism.

**Charge Transfer.** Charge transfer, more specifically asymmetric charge transfer, is an additional ionization mechanism in the glow discharge. Since transfer of charges will only occur between specific energy levels, asymmetric charge transfer is considered a very selective mechanism. For charge transfer to occur, a small energy difference between the gas ion ground state and the energy of the product ion is required.<sup>61</sup> Secondary ionization processes also contribute to the ionization of neutral species, but to a lesser degree. These include charge transfer, associative ionization, photoionization, and cumulative ionization.

### Instrumentation

Glow discharge mass spectrometry (GDMS) gained significant popularity in the mid-1970s when Harrison and Magee coupled glow discharge to a quadrupole mass spectrometer.<sup>13</sup> More recent developments prove that a Grimm-type glow discharge – time-of-flight mass spectrometer (GD-TOFMS) is a valuable instrument for solid sample analysis.<sup>34,35,38,62,63</sup> The glow discharge serves as an ion source for solid sample analysis, and ions are then directed into a time-of-flight mass spectrometer for separation and

detection. A pulsed ion source benefits from the inherent pulsed voltages in a time-of-flight mass spectrometer. The following sections describe in detail the glow discharge ion source, the mass spectrometer, and the gas delivery system.

### Grimm-type Glow Discharge Ion Source

A variety of glow discharge source configurations have been considered as ion sources such as the hollow cathode, Grimm-type, jet-enhanced, and coaxial cathode. However, the most widely used sources are the Grimm-type and the coaxial cathode.

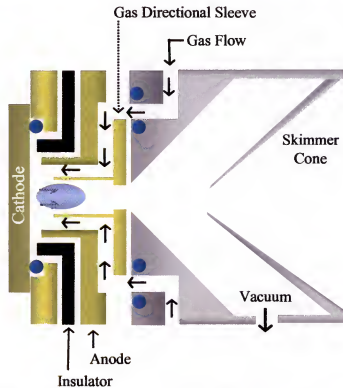


Figure 1-10 Schematic of a Grimm-type source coupled to a time-of-flight mass spectrometer.

The Grimm-type configuration was first introduced by Grimm in the 1960s for atomic emission spectrometry.<sup>10</sup> The Grimm-type configuration confines the plasma to the cathode surface and within the cylindrical anode. A distance between the cathode

surface and anode edge is kept at less than the electrons' mean free path to sustain discharge stability.<sup>64</sup> The sample must be flat and form a tight vacuum seal. Advantages of a Grimm-type source are flat sample analysis, ease of sample interchange (external mounting), depth profiling, and reproducibility. Limitations of the Grimm-type source, such as sample configurations, and ion transport, have been improved by implementing a new sample holder<sup>63</sup> and a transport gas mode.<sup>34</sup>

Figure 1-10 is a schematic of the Grimm-type glow discharge configuration utilized in experiments throughout this document. A vertical cross-section provides a view of all source components. The cathode plate and anode are machined of brass and isolated from each other by a Macor® plate. The cylindrical 4 mm (i.d.) anode sits approximately 0.25 mm from the sample surface. A stainless steel gas directing sleeve is mounted between the anode and instrument base. The gas directing sleeve, with an inner diameter slightly smaller than the 4 mm anode, is retained approximately 0.2 mm from the end of the anode. A gas flow is introduced through a ~1 mm orifice in the source mount and flows between the anode and sleeve. Figure 1-10 illustrates the projected path of gas flow. Directing the gas flow with this configuration has improved ion transport into the skimmer cone (i.d. 0.7 mm).<sup>34</sup> The total sampling distance between the source and skimmer cone orifice is approximately 13 mm. A flat sample is mounted onto the cathode plate and vacuum sealed with an o-ring. All source components are at ground potential except for the cathode plate and sample.

### **Time-of-Flight Mass Spectrometry**

Whether coupled to an inductively coupled plasma or glow discharge, time-of-flight mass spectrometry (TOFMS) has become a valuable tool for inorganic analysis.

The greatest benefit of TOFMS is the ability to simultaneously collect all mass-to-charge ( $m/z$ ) values within a desired range. This section will briefly describe the theory of TOFMS, basic operation, and instrument modifications.

**Fundamentals.** Time-of-flight mass spectrometry (TOFMS) is based on dispersion-in-time principle (ions in a field-free drift region).<sup>65</sup> Gas phase ions are accelerated in an electric field ( $10^3 - 10^4$  V) to an energy represented by

$$KE = \frac{1}{2}mv^2 \quad (1-1)$$

Since ions are accelerated to the same kinetic energy ( $KE$ ), they are separated based on velocity ( $v$ ). Ions of differing masses ( $m$ ), therefore have differing velocities. Based on ion flight times, a mass spectrum is compiled ranging from low mass to high mass ions. TOFMS is based on flight time in a field-free region, thus the time  $t$  (s) required for an ion to traverse length  $L$  (m) can be described by

$$t = \left( \frac{m}{zeV} \right)^{\frac{1}{2}} \bullet L \quad (1-2)$$

where  $z$  is the number of charges on an ion,  $e$  is the charge of an electron (eV), and  $V$  (V) is the accelerating voltage.<sup>66</sup> Flight time can be converted into a mass-to-charge ratio ( $m/z$ ). Lighter ions have higher velocities and reach the detector first. An added component of most TOFMSs is a reflectron, which improves mass resolution by correcting for KE distributions.<sup>67</sup>

The transient nature by which the TOF mass spectrometer accepts ions is an important aspect, and a distinct advantage for a pulsed glow discharge source. With each discharge pulse, a packet of ions is generated and sampled into the TOFMS providing

optimal ion sampling efficiency. GD-TOFMS timing and ion temporal resolution will be described in a subsequent section.

**Renaissance TOFMS.** The mass spectrometer employed in these studies is an axial time-of-flight mass spectrometer (LECO Corporation, St. Joseph, MI). The original instrument was developed for ICP analysis and was subsequently replaced by an in-house designed Grimm-type GD source. A schematic of the main components of the Renaissance TOFMS is shown in Figure 1-11.

Gas phase ions are formed in the source and transported to the skimmer cone *via* a gas flow. As described previously, gas flow is important because it aids in ion transport. Extracted ions are transferred by a series of lenses (ion extraction lens and ion transfer lens) before entering the modulation region. A ~1.5 cm long ion packet is selected in the modulation region; this packet of ions is introduced into the mass spectrometer by applying a negative voltage to the modulation component. Switching the modulation electrode to a positive potential prevents additional ions from entering the drift region. A positive repeller voltage pulses the ion packet into the acceleration region of the mass spectrometer. Ions attain their final kinetic energy in the acceleration region. After being accelerated, a series of Einzel and X,Y-steering lenses focus and steer the ions into the flight tube. Ions enter the “field-free” drift region and then traverse through a reflectron to correct for any kinetic energy distributions. Finally, ions are detected with a discrete dynode electron multiplier tube.

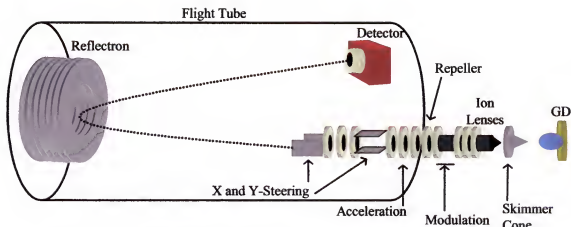


Figure 1-11 Schematic of the Renaissance time-of-flight mass spectrometer.

Ions are generated in the GD and traverse through the ion optics as shown. Since the Renaissance TOFMS was originally tailored for an ICP source, modifications were made to accept a pulsed glow discharge source. This includes software modifications to control the discharge frequency (100-1000 Hz), an added repeller delay function, and a trigger for the pulsed power supply (shown in Figure 1-12).

The rapid duty cycle, generating thousands of complete mass spectra per second, and integrating the spectra (improving S/N) are added benefits of a TOFMS. Theoretically, TOFMS has an unlimited mass range, yet the number of events that can be recorded in time is limited by electronics. Since elemental analysis generally requires the lower atomic mass range, this instrument only collects up to approximately  $m/z$  300.

### Pulsed Glow Discharge and Time-of-Flight Mass Spectrometer Timing

An advantage of a pulsed glow discharge source coupled to a time-of-flight mass spectrometer is the ability to temporally resolve background gas and sputtered species. The inherent timing properties of the TOF's ion optics are advantageous for a pulsed glow discharge since the TOFMS requires a pulsed ion source. A diagram of the entire

$\mu$ sPGD-TOFMS is shown in Figure 1-12. As shown in Figure 1-12, the Renaissance TOFMS triggers the pulsed power supply, which then supplies a transient voltage to the Grimm-type source. With the glow discharge pulsed voltage triggered by the mass spectrometer, both components can be synchronized for maximum ion sampling efficiency. A digital oscilloscope is beneficial to synchronizing and monitoring these processes. Upon applying a pulsed voltage, ions are created in the source and then traverse into the mass spectrometer for detection. An electrical signal output from the detector is converted to a mass spectrum with the readout displayed on a computer.

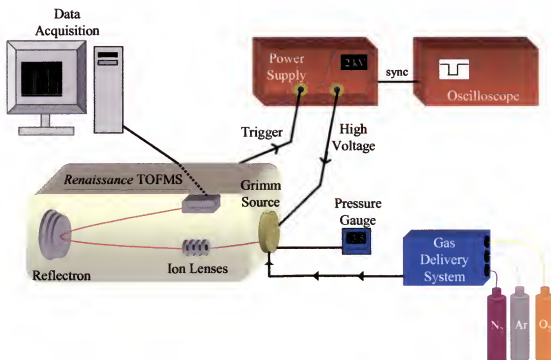


Figure 1-12 Diagram of the microsecond pulsed glow discharge – time-of-flight mass spectrometry setup.

As mentioned previously, one of the greatest assets of a pulsed glow discharge is temporal response. With a temporal response, discharge gas ions are detected earlier in time than sputtered ions. For example, calcium was detected in the presence of argon using a millisecond pulsed glow discharge – quadrupole mass spectrometer.<sup>68</sup> Despite

this advantage, the greatest benefit of a pulsed source can be gained by coupling a microsecond pulsed glow discharge to a time-of-flight mass spectrometer. Individual mass spectra are collected for each pulsed packet of ions at a particular duty cycle. A  $\mu$ sPGD produces ion packets that are compatible with the duty cycle of a time-of-flight. These time-dependent events offer additional opportunities.<sup>55,69</sup>

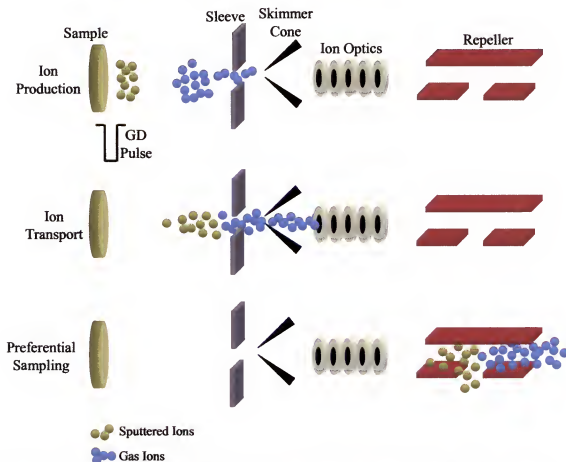


Figure 1-13 Temporal profile concepts for a microsecond pulsed glow discharge and time-of-flight mass spectrometer.

The pulsed voltage is triggered by the mass spectrometer. The time-resolving principle for a microsecond pulsed glow discharge – time-of-flight mass spectrometer is shown in Figure 1-13. In Figure 1-13 the gold spheres represent sputtered analyte ions and the purple spheres the discharge gas ions. At gas breakdown voltage, discharge gas

ions form, followed by the production of sputtered analyte. After ion production, the ions traverse through a series of lenses and then enter the repeller region. In this region, ions are directed into the flight tube by applying a high positive voltage (1 kV) to the repeller. Any ions in the repeller region during the “voltage on” period have the potential to be sampled and detected. With the Renaissance TOFMS, the repeller pulse timing can be controlled allowing discrimination of ions based on their temporal properties. The repeller delay can be set between 10-300  $\mu$ s. Delay times between 10-100  $\mu$ s are typical for detecting argon ions; sputtered analyte ions are detected at longer delay times (80 - 250  $\mu$ s). Operating conditions and source configuration contribute to the magnitude of the delay time for gas and analyte ions.

### **Gas Delivery System**

A flexible and convenient gas delivery system was prepared as shown in Figure 14. The gas delivery system replaces a single mass flow meter used in the original setup. The gas flow controller module, four-channel readout (Model: 247D, MKS Instruments, Andover, MA), allows up to four mass controllers to be used simultaneously. The flows are controlled by a 0-5 V signal, which corresponds to a specific flow rate. Three calibrated mass flow controllers (MFC) were connected to the control module and used for introduction of argon, nitrogen, oxygen, and methane. Even though each MFC is calibrated for a specific gas, recalibration *via* the flow controller module permits the use of other gases.

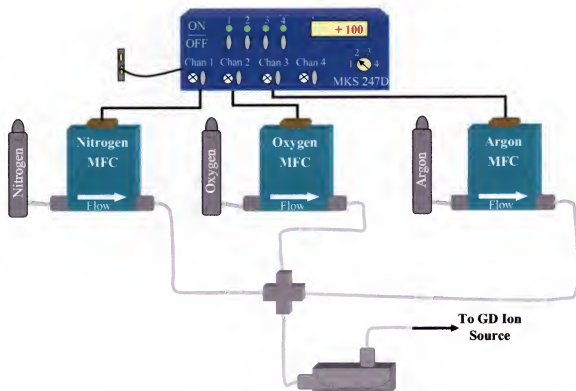


Figure 1-14 Schematic of the gas delivery system. The gas delivery system controls gas flow rate and gas mixing conditions.

## CHAPTER 2

### GASES IN GLOW DISCHARGE ATOMIC EMISSION AND MASS SPECTROMETRY

#### Introduction

The plasma gas is an essential component of the glow discharge source, participating in both the physical and chemical phenomena of sputtering and ionization. Gases are the medium of choice for the glow discharge since atoms, the most abundant sputtered species, are more easily ionized in the gaseous state.<sup>48</sup> Since the plasma support gas serves multiple roles, it may be helpful to review the role of the discharge gas. Under an electric field, plasma gas atoms (or molecules) break down forming ions and electrons. The plasma gas ions accelerate toward the cathode surface and are the main participant in the sputtering process; therefore, the plasma gas is also expressed as the “sputtering gas.”<sup>40</sup> As a result of sputtering, atoms are liberated from the sample surface, ionized by collisions with gas ions in the negative glow, and are subsequently analyzed. A glow discharge is sustained by the continuous sputtering and ionization. Even though inert gases are the most common plasma gases, the GD can be easily maintained when using alternative plasma gases.

The extent of sputtering and ionization is determined largely by the type of discharge gas, yet other parameters, such as pressure, voltage, and cathode-anode distance, also influence sputtering. By using inert gases, chemical reactivity is minimized leaving physical phenomena to dominate. Argon is the most commonly used GD gas. However, implementing alternative gases, ranging from inert to highly reactive,

alters chemical characteristics of the discharge. Both the sputtering and ionization are chemically altered. The characteristics of argon are much different than molecular gases (e.g.,  $N_2$ ,  $O_2$ , and  $CH_4$ ) including atomic (molecular) mass, atom (molecule) size, ionization energy, and metastable energy. By using molecular plasma gases, changes in discharge phenomena are observed, which may offer additional analytical opportunities. The following section describes various types of plasma gases used in both dc and pulsed glow discharge sources monitored with emission and mass spectrometry.

### **Inert Gases**

While many gases can be ionized under the influence of an electric field and support a self-sustaining discharge, inert gases are most widely used. A benefit of noble gases is their lack of chemical reactivity with the cathode surface rendering only physical sputtering; therefore, since a glow discharge produces a significant flux of gas ions, noble gases are preferred for efficient sputtering.<sup>51</sup> Bombardment of a target with reactive gas ions causes surface layer reactions. If a stable surface layer forms on the sample, then sputtering rates (and yields) can decrease. Sputter yields decrease due to the impurity predominantly being removed. Additionally, sputtering of primarily the impurities interferes with efficient sputtering of the metal surface atoms. A decrease in the sputter yield negatively affects atomic emission and ion signal intensities. However, the surface layer can also act as a protective coating for the sample.<sup>48,53</sup> To prevent unwanted surface buildup, noble gases are used for routine glow discharge analyses.

## Characteristics

Helium (He), neon (Ne), argon (Ar), krypton, (Kr), and xenon (Xe) are the inert gases historically studied with a glow discharge source.<sup>54,70,71</sup> Radon (Ra) is excluded from discharge studies due to its radioactive nature. About one-percent by volume of the atmosphere consists of the noble gases (primarily argon). These gases are used because of their chemical inertness, ease of handling, ready availability, and high energy metastable states. Table 2.1 lists the characteristics of noble gases.<sup>42</sup>

As shown in Table 2-1, the elemental characteristics of each gas are much different. As the atomic weight and radius increase, the ionization potential of each element decreases. Compared to most elements in the periodic table, these gases exhibit high ionization potentials making them desirable gases for ionization. Besides their high ionization potentials, the presence of metastable energy levels makes noble gases suitable for ionization.

Table 2-1 Characteristics of noble gases used in glow discharge spectrometry.

	He	Ne	Ar	Kr	Xe
<b>Atomic Radius (pm)</b>	31	71	98	112	131
<b>Atomic Weight (g/mol)</b>	4.003	20.18	39.95	83.80	131.3
<b>Ionization Potential (eV)</b>	24.6	21.5	15.8	14	12.1
<b>Metastable States (eV)</b>	19.8 20.6	16.6 16.7	11.5 11.7	9.9 10.5	8.3 9.4

**Metastables.** Metastable species are long-lived excited atoms – radiative relaxation to the ground state is spin-forbidden thus providing an effective source of potential

energy. Inert gas atoms benefit from these metastable states since their excitation and ionization potentials (energies) are higher than most other elements. The ionization potentials of common transition metals range from 7-10 eV (e.g., Ag: IP 7.5 eV). Within the plasma, the number density of metastables is  $10^{11} - 10^{12} \text{ cm}^{-3}$ .<sup>40</sup> The high number density, high potential energy, and long lifetime make metastables ideal in plasma ionization. Penning ionization (Chapter 1) in the negative glow results from the collision between a metastable gas atom ( $X^m$ ) and a sputtered atom ( $M^0$ ). As reported in the literature,<sup>60,72</sup> residual gases, such as those from a vacuum leak, can greatly perturb ionization by depopulating the metastables.

**Sputter Yield.** The physical phenomenon of sputtering in a glow discharge is significantly influenced by gas selection. A review of sputter yield from Chapter 1 shows that the energy transfer function is crucial in predicting sputter yield. According to the energy transfer function, as  $m_1/m_2$  approaches unity ( $m_1$ : mass of incident ion,  $m_2$ : mass of target atom), sputter yield increases. Therefore, sputtering of the first row transition elements by argon ions is the best choice, and krypton for the second row, etc.; however, argon has higher energy metastable states and the sputtering of mixed row elements is not a concern.<sup>40,48</sup> Figure 1-7 in Chapter 1 shows the sputter yield for various elements of the periodic table when bombarded with argon. Since argon's characteristics fall in the middle of the noble gases, it is often used.

**Argon.** Argon has been used almost exclusively for glow discharge, and is a well-characterized gas in the glow discharge ion source. Both krypton and xenon produce similar results to argon, but argon has only one major isotope ( $^{40}\text{Ar}$  at 99.6%). In addition, argon is more readily available, cost effective, and is an efficient sputter gas for

many materials. Despite these attractive features, there is interest in studying alternative gases.

### Atmospheric Gases

Nitrogen (78%) and oxygen (20%) are the main constituents in the earth's atmosphere. These gases are commonly employed for atmospheric pressure ion sources,<sup>73-75</sup> but not for glow discharge analysis. As mentioned above, only high purity inert gases are normally used in the discharge. However, nitrogen, oxygen, and water vapor are common impurities from trace leaks in the source or vacuum system. The appearance of these peaks at  $m/z$  18, 28, and 32 in glow discharge mass spectra may also be due to an impure argon source. Interferences at these  $m/z$  values, (e.g., <sup>28</sup>Si and <sup>32</sup>S) limit the ability to measure analyte peaks if they co-exist. Unfortunately, gas species associated with these gases is unavoidable.

Table 2-2 Physical and chemical properties of nitrogen and oxygen gases.

	N <sub>2</sub>	O <sub>2</sub>
<b>Molecular Weight (g/mol)</b>	28	32
<b>Ionization Potential (eV)</b>	15.6	12.3
<b>Metastable States (eV)</b>	6.2, 8.4	0.98, 1.63, 4.2-4.5 <sup>†</sup>
<b>Binding Energy (eV)</b>	9.8	5.2
<b>Atomic Radius (pm)</b>	65	60

<sup>†</sup> Three metastable states exist between 4.2 and 4.5 eV.

To better understand the effect of contaminants, studies have been conducted that monitor plasma changes after introducing small amounts of an alternative gas into the

glow discharge ion source.<sup>60,76-83</sup> Little research has focused on nitrogen and oxygen as the main constituent of the plasma gas.<sup>83,84</sup> Some of the physical and chemical properties of diatomic nitrogen and oxygen are listed in Table 2-2.<sup>85,86</sup> The effect of gas impurities on emission yields, atom and ion emission intensities, discharge current, sputter rate, and target material has been analyzed.

## Nitrogen

If molecular nitrogen is subjected to an electrical potential, then the gas becomes chemically reactive and is referred to as “active nitrogen.” Pure molecular nitrogen electrical discharges are stable and often appear yellow in the “nitrogen afterglow” region. The existence of ground state nitrogen atoms in the afterglow may contribute to nitrogen’s reactivity.<sup>86</sup> The emission (or glow) of the nitrogen discharge is due to a positive band system:  $N_2(B^3\Pi_g) \rightarrow N_2(A^3\Sigma_u^+)$ .

Reports indicate that nitrogen mixed-gas discharges are stable when powered by all three major operational modes of the discharge: direct current,<sup>77,78,81,82,87</sup> radio frequency,<sup>76,84,88</sup> or pulsed voltages.<sup>60</sup> Each study reports similar results of emission ion (and atom) signals and sputter rates. Glow discharge – optical emission spectrometry (GD-OES) is the technique of choice for studying nitrogen mixed-gas plasmas; however, a few studies have incorporated glow discharge mass spectrometry (GDMS).

**Glow Discharge – Optical Emission Spectrometry.** Mixed-gas plasmas, primarily the addition of small percentage increments of nitrogen to a noble gas discharge, have been explored for GD-OES. Wagatsuma<sup>78</sup> reports that nitrogen acts as a quenching agent after comparing nitrogen-argon and nitrogen-neon discharges. With the addition of ~20%  $N_2$ , drastic decreases in argon and copper atom and ion emission

intensities are evident, yet the nitrogen emission bands ( $C^3\Pi_u \rightarrow B^3\Pi_g$ ) are very intense. Figure 2-1 shows the trend of both copper (A) and argon (B) atom emission intensities as a function of nitrogen partial pressure. A few argon atom emission lines are monitored. Both copper and argon show similar trends with increasing concentration of nitrogen. Two factors account for the decrease in copper emission intensities. First, as nitrogen concentration is increased, the sputter rate decreases indicating a possible reduction in projectiles impinging on the target surface. A lower sputter yield is generally related fewer copper atoms available for ionization. Second, emission intensities of argon metastable species decrease with the addition of nitrogen, inherently lowering the contribution of Penning ionization in the plasma.

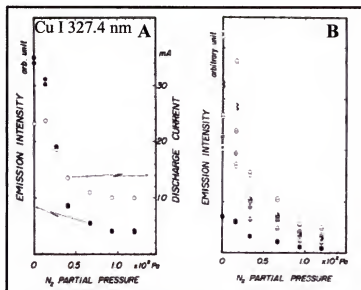


Figure 2-1 Plots of the emission intensities of copper and argon atom lines. A) Variation of peak intensities of Cu I 327.4 nm as a function of the nitrogen partial pressure. B) Variation of emission intensities of Ar I lines. (Ref. 78)

Other studies of nitrogen addition (0-3%  $N_2$ ) to an argon glow discharge have been reported by Fischer et. al.<sup>81,82</sup> In agreement with Wagatsuma, Fischer reports a decrease in sputter rate with increasing nitrogen concentration using GD-OES. Furthermore, two groups of metals were investigated: elements that form stable nitrides (Al and Ti) and

elements that do not react with nitrogen (Fe, Ni, Cu, and Ag). As expected, the elements that form stable nitrides showed an abrupt decrease in the sputter rate and atomic emission signals indicating possible  $N_2$  surface layer formation. An unusual phenomenon occurred when copper, a non-nitride forming element, was exposed to  $N_2$ . A gradual decrease in copper sputter rate occurred when conditions ranged from pure argon to 3%  $N_2$ ; however, the copper atom emission signal (327.4 nm) increased slightly (1.5%  $N_2$ ) and then decreased to the original level of pure argon. The other elements, which do not react with nitrogen, show a more gradual decrease in emission intensities. Figure 2-2 shows an argon atomic emission line (426.6 nm) decreasing in intensity (A), yet a nitrogen atomic emission line (174.2 nm) increasing in intensity (B). Each line represents a different metal used in the analysis.<sup>81,82</sup> These studies show that nitrogen contamination (up to 3%) in a discharge alters the primary ionization, sample surface, and sputtering.

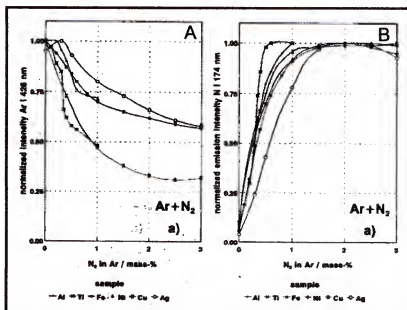


Figure 2-2 Emission intensity as a function of nitrogen concentration. A) Ar I 426.6 nm and B) N I 174.2 nm. (Ref. 81 and 82)

Additional studies agree that small amounts of nitrogen (up to 2%) have a significant effect on the glow discharge plasma. A high resolution Fourier transform spectrometer was used to study the reactivity of nitrogen with titanium and iron.<sup>77</sup> As expected, both atomic and ionic emission lines of Ti abruptly decrease with 0.2% N<sub>2</sub>, yet the emission lines of Fe decrease more gradually. In agreement with Fischer, the N I 174 nm emission line increases with greater amounts of nitrogen gas.

Even though nitrogen has been historically studied as an impurity, discharges may benefit from molecular gas addition. Radio frequency glow discharge optical emission spectrometry was employed to investigate the effect of nitrogen on depth-profiling.<sup>76,88</sup> A N<sub>2</sub>-Ar gas mixture improved the analytical performance of the source for depth-profiling of both conducting and non-conducting samples. Since the addition of nitrogen lowers the sputtering rate, depth resolution improves allowing nanometer layer analysis (<100 nm).

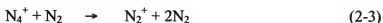
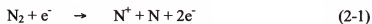
Table 2-3 Common nitrogen ions detected in glow discharge mass spectrometry.

<i>m/z</i>	Ion
28	N <sub>2</sub> <sup>+</sup>
29	N <sub>2</sub> H <sup>+</sup>
30	NO <sup>+</sup>
42	N <sub>3</sub> <sup>+</sup>
56	N <sub>4</sub> <sup>+</sup>
70	N <sub>5</sub> <sup>+</sup>

**Glow Discharge Mass Spectrometry.** Mass spectrometry offers additional insight into the effect of gas mixtures on direct current glow discharge plasmas. In mass spectrometric analysis, peaks at *m/z* 28 and 29 (N<sub>2</sub><sup>+</sup> and N<sub>2</sub>H<sup>+</sup>) are observed when a measurable amount of nitrogen exists in the plasma. Nitrogen based polyatomic ions fall

in the mass range of 28-30 and at  $m/z$  42, 56, 70.<sup>84</sup> The trend of nitrogen-based ions is seen as combinations of  $m/z$  14 +  $x$ . Table 2-3 lists common ions formed in a nitrogen glow discharge source.

How do these nitrogen ions form? Proposed mechanisms for nitrogen ion formation can be found in the literature.<sup>84,89-94</sup> Formation of  $N^+$  and  $N_2^+$  occurs by high energy processes typical of negative glow conditions. Dissociative ionization of a nitrogen molecule by electron bombardment will result in the formation of  $N^+$  if the electron energy is at least 24 eV<sup>91</sup> (Equation 2-1). Atomic nitrogen ions are found at the base of the negative glow closest to the cathode. Formation of  $N_2^+$  also occurs by electron impact ionization (required energy for this reaction is 15.6 eV) or charge transfer as shown in Equations 2-2 and 2-3.

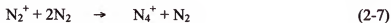


Molecular nitrogen ions are most abundant in the negative glow region. Evidence of the  $N_3^+$  molecular ion has been reported and forms by Equation 2-4.  $N_2^{+*}$  is an excited molecular ion.<sup>94</sup> Knewstubb and Tickner<sup>90</sup> report that a decay in  $N^+$  corresponds to an increase in concentration of  $N_3^+$ , thus Equation 2-5 represents the proposed mechanism.



For the formation of the nitrogen tetramer ( $N_4^+$ ), three mechanisms are proposed based on vibrational excitation, a three-body reaction, and an excited neutral nitrogen

molecule ( $N_2^+$ ). Purity of the nitrogen gas determines the extent of nitrogen tetramer formation.



These proposed mechanisms are based on a pure nitrogen environment.<sup>90-94</sup> If contaminants are present in the nitrogen gas, then additional reactions involving water and oxygen would be evident.

**Pulsed Source Mass Spectrometry.** All studies described previously involve a continuous voltage supply to generate ions; however, pulsing a discharge generates packets of ions as described in Chapter 1.

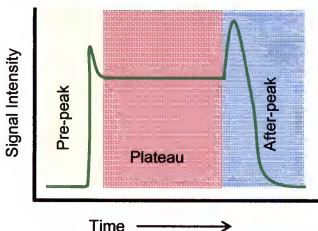


Figure 2-3 The three regions of a pulsed glow discharge: prepeak, plateau, and afterpeak.

Recent work by Jackson and King<sup>60</sup> focuses on the addition of 1%  $N_2$  to an argon millisecond pulsed glow discharge (msPGD) for diagnostic measurements. Similar to a dc glow discharge, signals arising from argon and sputtered analyte are greatly influenced by the addition of 1% nitrogen. In the afterpeak region of an argon msPGD, an influx of argon metastables ( $Ar^m$ ) is evident. For example, if monitoring an  $Ar^m$  emission line

( $\lambda=811.5$  nm), a spike in signal intensity would occur in the afterpeak region. Figure 2-3 illustrates the three regions of a msPGD: prepeak, plateau, and afterpeak. With the addition of 1% N<sub>2</sub>, the afterpeak spike is not observed and the argon ion signal is reduced by a factor of ten. As mentioned previously, Wagatsuma<sup>78</sup> observed a similar effect. The loss of metastables is due to either the nitrogen preventing them from forming or quenching after they form.

## Oxygen

Oxygen is another common glow discharge impurity. In spite of oxygen being a contaminant in glow discharges, it benefits as a gas for negative ionization sources.<sup>95</sup> Controlled additions of oxygen, both in low and high concentrations, have been reported in the literature for a dcGD.<sup>8,76,81-83,88,96-101</sup> A general trend reveals that small amounts of molecular oxygen greatly perturb the argon glow discharge.

**Glow Discharge – Optical Emission Spectrometry.** Wagatsuma<sup>83</sup> reports that oxygen (O<sub>2</sub>) acts as a strong quenching agent in a dc glow discharge. Figure 2-4 shows the effect of 0-100% O<sub>2</sub> addition on the emission intensity of Cu I 327.4 nm (A) and the sputter rate (B) of copper. Addition of 4% O<sub>2</sub> results in an 800 fold decrease in the copper emission intensity (A), which parallels the decrease in copper sputter rate (B). A decrease in the copper emission signal corresponds to a reduction in argon atom and ion emission lines. An abrupt decrease in both the copper and argon emission intensities is possibly due to oxide surface layers forming, which hinders effective sputtering of the surface. The oxide layer prevents impinging ions from penetrating into the cathode surface, thus reducing the sputtered analyte population.<sup>80</sup>

Various studies report an abrupt decrease in sputtering rate when oxygen is added to an argon plasma. Heller<sup>98</sup> states that a chemical surface reaction occurring on the cathode is related to the sharp decrease in sputtering rate. Another study reports that as the copper ion signal decreases, the  $O^+$  and  $O_2^+$  ion signals increase.<sup>101</sup>

One purpose for changing the plasma gas is to improve the analytical utility of the glow discharge. Similar to nitrogen, oxygen can be used to improve the depth profiling in thin layer analysis because of a lower penetration rate. The rfGD penetration rate of stainless steel in a pure argon and 0.5%  $O_2$  discharge is  $4.5 \mu\text{m}\cdot\text{min}^{-1}$  and  $0.25 \mu\text{m}\cdot\text{min}^{-1}$  respectively.<sup>76</sup>

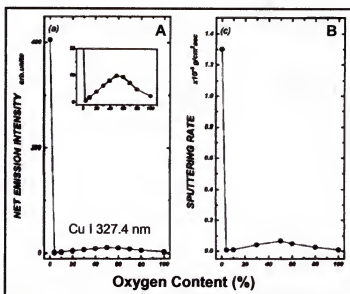


Figure 2-4 Effect of oxygen content (0-100%) on A) Cu I 327.4 nm emission intensity and B) the sputter rate of copper. (Ref. 83)

**Oxygen Discharge Reactions.** The following section describes what is occurring in a mixed-gas plasma of a diatomic molecule and rare gas atomic ions. Equations 2-9 and 2-10 are two proposed mechanisms for the formation of oxygen ions. Significant destruction of the atomic oxygen ion can occur by the reaction in Equation 2-11. A

termolecular oxygen ion can form through association (Equation 2-12). These are all possible mechanisms for oxygen ion formation in the presence of rare gases.<sup>99,102</sup>



Since positive ions are sampled in the negative glow, in a 99.7% purity  $\text{O}_2$  discharge the molecular oxygen ion ( $\text{O}_2^+$ ) should be the major constituent. The molecular oxygen ion can also be formed *via* electron bombardment. At the region of the negative glow closest to the cathode, high energy electrons bombard oxygen molecules forming  $\text{O}^+$  ions. The  $\text{O}^+$  concentration is rapidly reduced as a result of charge transfer to oxygen molecules (Equation 2-11). Under glow discharge conditions, ozone ( $\text{O}_3^+$ ) has been found to form; however, the lifetime of ozone under these conditions is short because of charge transfer to diatomic oxygen.<sup>99</sup> Closer to the anode in the positive column, and at higher pressures (and current densities) formation of  $\text{O}_4^+$  is observed.

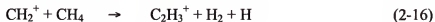
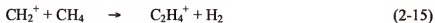
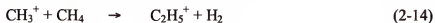
### Organic Gases

The type of gas employed in a plasma is important in determining its analytical utility. Plasma gas affects sputter rate, ion formation, and discharge stability. Common impurities, such as nitrogen or oxygen, have been shown to produce negative effects on the plasma; however, advantages such as improving depth profiling emerge from the addition of alternative gases. The majority of ionization occurring in the plasma is due to

electron impact. What happens if a different type of ionization dominates in the discharge?

### Chemical Ionization

One alternative to electron impact ionization is chemical ionization (CI). For chemical ionization to occur, a reagent gas is introduced into the reaction vessel (e.g., GD confines). The reagent gas is ionized, producing reagent ions (those that do not react further with the reagent gas), which then react chemically with the analyte molecule. In mass spectrometry, a spectrum of ions characteristic of the analyte material is generated.<sup>74,103-105</sup> The most common organic gas used for chemical ionization is methane (CH<sub>4</sub>). The dominant ion-molecule reactions in methane are as follows<sup>106</sup>



Each of the methane products formed in these ion-molecule reactions serves as a reagent ion for chemical ionization with an analyte molecule. The few studies done on a methane glow discharge include the study of ionic species in an rf discharge,<sup>107</sup> the role of Penning ionization in low pressure discharges,<sup>72,108</sup> and analysis of rapid desorption chemical ionization spectra.<sup>109</sup> The major ions formed in a radiofrequency discharge can be categorized into C<sub>1</sub>, C<sub>2</sub>, and C<sub>3</sub>-based species. Table 2-4 lists the main methane ions detected in rf discharge mass spectrometry.

The dominant C<sub>1</sub>, C<sub>2</sub>, and C<sub>3</sub>-based hydrocarbons are CH<sub>5</sub><sup>+</sup>, C<sub>2</sub>H<sub>5</sub><sup>+</sup>, and C<sub>3</sub>H<sub>5</sub><sup>+</sup> respectively. Species of low concentration, C<sup>+</sup>, CH<sup>+</sup>, or CH<sub>2</sub><sup>+</sup>, may tend to have a higher reactivity. In addition to studying methane-based ions, organic compounds were deposited onto a cathode surface, rapidly desorbed from the surface, and probed by chemical ionization. Methane was added to promote proton transfer and moderate the extensive low molecular weight peaks formed in an argon discharge. A significant difference between a 3% CH<sub>4</sub> glow discharge and a conventional chemical ionization spectrum is the extensive interferences in the lower *m/z* region (i.e., hydrocarbon series) in the 3% CH<sub>4</sub> glow discharge. This shows that methane is an unsuitable reagent gas in a direct current glow discharge for chemical ionization of organic molecules due to interferences.<sup>107,109</sup> The advantage of using a pulsed glow discharge has yet to be determined.

Table 2-4 List of methane ions detected in a radio frequency discharge in methane.

<u>Ion</u>	<u><i>m/z</i></u>
CH <sub>5</sub> <sup>+</sup>	17
C <sub>2</sub> H <sub>3</sub> <sup>+</sup>	27
C <sub>2</sub> H <sub>4</sub> <sup>+</sup>	28
C <sub>2</sub> H <sub>5</sub> <sup>+</sup>	29
C <sub>3</sub> H <sub>3</sub> <sup>+</sup>	39
C <sub>3</sub> H <sub>4</sub> <sup>+</sup>	40
C <sub>3</sub> H <sub>5</sub> <sup>+</sup>	41
C <sub>3</sub> H <sub>9</sub> <sup>+</sup>	45
C <sub>4</sub> H <sub>11</sub> <sup>+</sup>	59
C <sub>5</sub> H <sub>13</sub> <sup>+</sup>	73

## Penning Ionization

Even though methane is not analytically useful for chemical ionization in a dc glow discharge, it proves useful for studying the role of Penning ionization in a low pressure dc glow discharge. Methane is employed as a quenching agent due to its ability to effectively quench the argon metastable ( $\text{Ar}^m$ ) population. The  $^3\text{P}_2$  metastable population ( $\lambda = 811.5 \text{ nm}$ ), was monitored by atomic absorption to observe the impact of quenching.<sup>72,108</sup> With 2%  $\text{CH}_4$ , the  $\text{Ar}^m$  population is quickly quenched as shown in Figure 2-5. Following the decrease in  $\text{Ar}^m$  population, a decrease in the copper ion signal is observed.

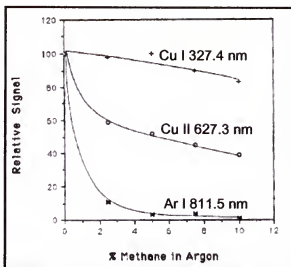


Figure 2-5 Effect of methane concentration on atomic absorption of copper atom and ion signals and the argon metastable. (Ref. 108)

## Considerations

Gases ranging from inert to highly reactive have been considered for glow discharge analysis. Noble gases are most commonly used for GD research due to their lack of reactivity. Reports in the literature show that reactive gases could potentially be beneficial by improving the analytical utility of the glow discharge source. The research in this document involves mixing alternative gases ( $\text{N}_2$ ,  $\text{O}_2$ , and  $\text{CH}_4$ ) to an argon glow

discharge, generating ions, and analyzing them with mass spectrometry. The focus is on a  $\mu$ sPGD, though a traditional dcGD is also employed. Since the inherent nature of a pulsed glow discharge involves a duty cycle, it is of interest to learn how it can affect ion formation.

## CHAPTER 3

### CHARACTERIZATION OF THE MICROSECOND PULSED GLOW DISCHARGE PROCESSES IN NITROGEN

#### Introduction

The glow discharge (GD) is a versatile source routinely used for the elemental analysis of solids. With the production of atoms, ions, and photons in the source, multiple techniques are available for plasma analysis: atomic absorption, fluorescence, emission, and mass spectrometry.<sup>110</sup> In GD an ion population, representative of the sample composition, is generated directly from the sputtered sample atoms. With mass spectrometry (MS), a mass spectrum is produced based on the representative ion population. An advantage of GDMS is the simple mass spectra, compared to atomic emission, typically displaying 1-3 peaks per element (based on the number of isotopes). The glow discharge has been interfaced to all types of mass spectrometers; however, our focus is time-of-flight mass spectrometry (TOFMS). An inherent advantage of TOFMS is the pulsed nature of the analyzer which provides a unique opportunity to utilize a pulsed source. In our laboratory, a microsecond pulsed Grimm-type glow discharge source has been interfaced to a commercial axial TOFMS.

Since GD-TOFMS produces simplistic spectra, it is easier to identify foreign peaks in a mass spectrum. For example, ion signals associated with atmospheric contaminants, such as oxygen and nitrogen, would be prevalent if a vacuum leak existed in the system. Reports indicate that small amounts of N<sub>2</sub> or O<sub>2</sub> added to an argon glow discharge can cause significant changes in plasma characteristics.<sup>60,80,81,88</sup> Very little evidence is found

in the literature dealing with sputtering and ionization of a mixed nitrogen-argon  $\mu$ sPGD with mass spectrometric analysis. The role the discharge gas plays in sputtering and ionization was examined. More specifically, this chapter will describe the effect of nitrogen addition on dc and microsecond pulsed glow discharge plasmas with time-of-flight mass spectrometry analysis. Since the extent of sputtering and ionization also depends on cathode material, gold, silver, and copper cathodes are used for comparison.

## **Experimental**

### **Glow Discharge and Time-of-Flight Mass Spectrometer**

An in-house designed Grimm-type glow discharge configuration was used in this research. The source was operated in both direct current and microsecond pulsed modes, as described previously in Chapter 1. For direct current data, a high voltage dc power supply (Model: 105, Bertan, Vahalla, NY) produces a steady-state supply of ions. Additionally, the TOFMS has been modified to accept a high voltage pulsed power supply (Model: M3k-20, Instrument Research Company, MD) to produce a transient ion signal.

The Grimm-type glow discharge source (Figure 1-9) is interfaced to a commercial axial time-of-flight mass spectrometer (Renaissance, LECO Corporation, St. Joseph, MI). Refer to Figure 1-10 for the TOFMS configuration and Figure 1-11 for GD-TOFMS setup. To maintain optimal pressures in the various stages of the mass spectrometer, an extensive vacuum system is required.

Three main pressure regimes exist in the mass spectrometer, as shown in Figure 3-1, controlled and monitored by instrument software. The pressure in the glow discharge source is controlled by manually adjusting a diaphragm valve (Model: Sp35K, BOC

Edwards, Wilmington, MA) located in the vacuum line of the first stage. The source pressure is measured with a dual sensor vacuum gauge (Model: 2002, Teledyne Hastings Instruments, Hampton, VA) and provides a digital readout on a corresponding unit. Pressure in the glow discharge source is also affected by a gas flow, which is described in the following section. Typical operating conditions of the glow discharge are listed in Table 3-1. Table 3-2 lists the typical operating conditions of the time-of-flight mass spectrometer for pulsed and dc glow discharges. The operational frequency of the mass spectrometer for a dc GD is 20 kHz.

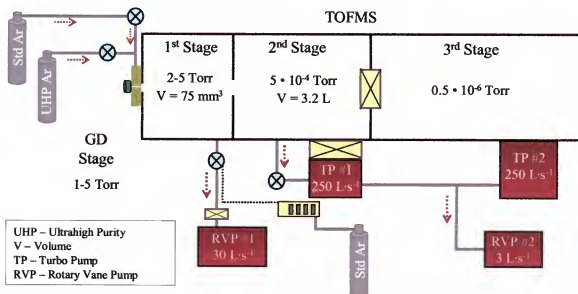


Figure 3-1 Schematic of the vacuum system and pressure regimes of the time-of-flight mass spectrometer.

Table 3-1 Typical operating conditions of the glow discharge source.

**Direct Current Glow Discharge Source**

Discharge Voltage	1.1 – 1.3 kV
Source Pressure	2.5 – 4.5 Torr
Current	5 – 8 mA (Au) 16 – 19 mA (Cu)
Flow Rate	150 mL·min <sup>-1</sup>

Table 3-1. Continued.

**Microsecond Pulsed Glow Discharge Source**

Pulse Magnitude	1.75 kV
Pulse Width	20 $\mu$ s
Pulse Frequency	600 Hz
Source Pressure	2.5 – 4.5 Torr
Average Current	2-2.4 mA
Flow Rate	150 mL $\cdot$ min <sup>-1</sup>

Table 3-2 Typical operating conditions for a time-of-flight mass spectrometer with a dc and pulsed glow discharge.

<b>Time-of-Flight Mass Spectrometer</b>	<b>Pulsed GD</b>	<b>dc GD</b>
Ion Lens 1	-710 V	-390 V
Ion Lens 2	-700 V	-781 V
Flight Tube	-1490 V	-1500 V
Reflectron Low	215 V	205 V
Reflectron High	1550 V	1550 V
Noise Reduction	500 V	500 V
X-Steering	- 1480 V	-1500 V
Y-Steering	- 1640 V	-1620 V
Einzel Lens 1	- 1370 V	-2000 V
Einzel Lens 2	- 800 V	-700 V
Modulation Positive	100 V	100 V
Modulation Negative	- 133 V	-170 V
Modulation Delay	45 $\mu$ s	45 $\mu$ s
Modulation Pulse Width	5 $\mu$ s	5 $\mu$ s
Repeller Bias	- 4 V	-6 V
Repeller Pulse	1000 V	1000 V
Repeller Pulse Width	1.2 $\mu$ s	5 $\mu$ s
Third Stage Pressure	0.4 – 0.9 $\mu$ Torr	0.4 – 0.9 $\mu$ Torr
Integration Time	5 $\cdot$ 10 <sup>-3</sup> s	5 $\cdot$ 10 <sup>-3</sup> s

## Gas Delivery System

To control gas flow rate and mixed-gas plasma composition, a flexible and convenient gas delivery system was implemented. Operation of the gas delivery system was described briefly in Chapter 1 (Figure 1-13); however, a more detailed description is provided below.

**Gas Mixing.** In the research throughout the remainder of this dissertation, gases are mixed to alter the discharge gas composition. One method to effectively mix different gases is to control their gas flow rate *via* a mass flow controller (MFC). The MFCs (Model: M100B, MKS Instruments, Andover, MA) employed accurately measure and control the mass flow rates of gases. The control range of the MFC is 2-100% of full scale with an accuracy of  $\pm 1\%$ . Table 3-3 lists the three MFCs used in the experiments and their operating flow rates.

Mixing the three gases in various combinations is simplified by a four channel readout, which operates as both a mass flow controller power supply and readout module. In addition, the four channel module is a set point source for four analog mass flow controllers and also displays the flow rate of a single MFC on a digital panel meter. The greatest advantage of this module is the ability to provide set points for multiple gas control; thus, all four readout channels can be utilized simultaneously.

Table 3-3 A list of the three mass flow controllers used in experiments, flow rate ranges, and their corresponding calibration gases.

Flow Rate Range (mL·min <sup>-1</sup> )	Calibrated Gas	Gauge Factor
0-20	O <sub>2</sub>	200
0-200	N <sub>2</sub>	200
0-200	Ar	200

For the digital panel meter to display flow rate and set point correctly, a potentiometer on the control module must be adjusted to correspond to the individual mass flow controllers. The +5 V output voltage from the MFC must correspond to the 1000 counts full-scale readout on the potentiometer. The amount by which the MFC output voltage is offset is the *Scaling Control Factor* (SCF).<sup>111</sup>

$$\text{Scaling Control Factor} = \text{Gauge Factor} \times \text{Gas Correction Factor} \quad (3-1)$$

The gauge factor is based on the MFC flow range, and Table 3-3 lists gauge factors for the MFCs used. To calculate the Gas Correction Factor (GCF) for pure gases ( $x$ ), the following equation is used

$$GCF_x = \frac{(0.3106)(s)}{(d_x)(cp_x)} \quad (3-2)$$

This equation assumes the MFC is calibrated for nitrogen because a mass flow controller will be calibrated for nitrogen unless requested otherwise. The standard density of  $N_2$  multiplied by the specific heat of  $N_2$  is equivalent to 0.3106. If the MFC is calibrated for a different gas, then this value must be recalculated. In the GCF equation,  $d_x$  is the standard density of gas  $X$  ( $\text{g}\cdot\text{L}^{-1}$ ) and the specific heat of gas  $X$  is  $cp_x$  ( $\text{cal}\cdot\text{g}^{-1}\cdot^\circ\text{C}^{-1}$ ). The molecular structure correction factor is denoted by  $s$  and Table 3-4 lists correction factors for various molecular structures.

With values for the gas correction factor and gauge factor, a scaling control factor can be calculated. Since each MFC is calibrated for its own gas, the potentiometer setting will be the same. However, if an alternative gas flows through the MFC, the potentiometer setting will vary. A mass flow controller can be “recalibrated” *via* the

control module permitting the use of other gases. This concept is covered in the following segment.

Table 3-4 Molecular structure correction factors to calculate the gas correction factor.

Molecular Structure	Correction Factor (s)
Monoatomic Gases	1.030
Diatomic Gases	1.000
Triatomic Gases	0.941
Polyatomic Gases	0.880

**Pre-mixed Gas.** The mass flow controllers are calibrated for a pure gas. For gas mixtures, such as a 5% CH<sub>4</sub>/ 90% Ar gas mixture, a gas correction factor for a mixture (GCF<sub>M</sub>) is necessary; however, the GCF<sub>M</sub> is not simply a weighted average of each component. Relative to nitrogen, the GCF<sub>M</sub> is expressed as

$$GCF_M = \frac{(0.3106)(a_1s_1 + a_2s_2 + \dots a_ns_n)}{a_1d_1cp_1 + a_2d_2cp_2 + \dots a_nd_ncp_n} \quad (3-3)$$

In this equation,  $a_1$  and  $a_2$  are the fractional flow of gases 1 and 2 ( $a_1 + a_2 = 1$ ) and  $s_1$  and  $s_2$  are the molecular structure correction factors for gases 1 and 2 (Table 3-4). Accordingly,  $d_1$  and  $d_2$  are the standard densities for gases 1 and 2, and  $cp_1$  and  $cp_2$  are the specific heats of gases 1 and 2. These mass flow controller concepts are applied to experiments in the remainder of this document to exploit the available MFCs.

### Plasma Gas

The plasma gas is an integral component of the glow discharge source. Plasma gas composition affects discharge stability, sputtering, and the ionization processes that sustain a discharge. The gases employed in this research include ultra high purity argon

(5 Grade, Strate Welding, Gainesville, FL) and ultra high purity nitrogen (5 Grade, Praxair, Gainesville, FL). In this research, argon was systematically replaced with nitrogen until a pure nitrogen plasma was sustained. Nitrogen concentrations ranged from 0-100% N<sub>2</sub>. The total gas flow rate was maintained at 150 mL·min<sup>-1</sup> *via* the gas delivery system. Additional argon (research grade, Strate Welding) was required for the pneumatic valves to work properly.

### **Sample Material**

Three types of cathode material were used in these studies: gold, silver, and copper. The gold (Gold Target, 99.99% Pure, Kurt J. Lesker, Clairton, PA) and silver (Silver Target, 99.99% Pure, Kurt J. Lesker, Clairton, PA) are high purity ingots of metal. The copper cathode is a certified standard reference material, NIST 1113 (National Institute of Standards and Technology, Gaithersburg, MD). NIST 1113 is 95.03% Cu and 4.80% Zinc.

Samples for obtaining sputter rates were high purity elemental foils (gold, silver, copper) approximately 1 mm thick (Puratronic, 99.9%, Alfa Aesar, Ward Hill, MA). The foils were cut into small discs 15 mm in diameter and weighed with an analytical microbalance (Model: M2P, Sartorius, Corp., Edgewood, NY). To calculate the weight difference, the foils were weighed prior to and after sputter analysis. Each sample was sputtered for 30 minutes (3x), using a new sample for each analysis.

## Results and Discussion

### Background

The glow discharge is an established ionization source used for the elemental analysis of solids that produces ions through sputtering and collisional processes as described in Chapter 1. To promote the physical and chemical phenomena of a glow discharge, a gas is required. This discharge gas is often overlooked as a critical parameter in GDMS. Selection of the appropriate discharge gas offers the opportunity to influence sputter ablation of the solid sample and subsequently the ionization reactions of analytical importance. The following sections detail the comparisons of argon and nitrogen gases in the glow discharge. Interest focuses on the role of nitrogen in a mixed or pure gas discharge, beginning with its activity in a low pressure glow discharge. How does nitrogen influence the sputtered species and the net complement of discharge ions? In these studies, argon was systematically replaced with nitrogen at increasing levels, eventually reaching 100% nitrogen. Three sample materials of varying reactivity (e.g., Au, Ag, and Cu) were compared to provide additional information on sputtering and ionization in a mixed nitrogen-argon plasma.

### Direct Current Glow Discharge: Comparison of Ar and N<sub>2</sub>

Despite the analytical advantages of a microsecond pulsed glow discharge, a direct current (dc) GD provides information otherwise not obtainable. A conventional dcGD generates a continuous supply of ions, thereby preventing extensive buildup of contamination. Before analyzing mixed-gas plasmas with a pulsed discharge, it is beneficial to establish information on ion production with a steady-state source.

**Pure Argon.** Argon is the most widely used plasma gas for glow discharge elemental analysis. Similar to other noble gases, argon presents little interference due to a small number of isotopes and minimal reactivity with other species. Besides a signal at  $m/z$  40, the other greatest interference appears at  $m/z$  41, indicative of argon hydride ( $^{40}\text{ArH}^+$ ). To decouple the plasma (reactive or non-reactive) from potentially reactive surface processes, gold was employed as a relatively non-reactive cathode material. For comparison, a copper-based standard (NIST 1113) was used to represent a more reactive sample material. Figure 3-2 displays conventional responses of gold (A) and NIST 1113 (B) in an argon dc glow discharge. The sputtered analyte ion signal of gold is at  $m/z$  197 compared to copper, which has two isotopes at  $m/z$  63 and 65.

Each plot in Figure 3-2 has an inset illustrating the peaks  $\text{H}_2\text{O}^+$ ,  $\text{H}_3\text{O}^+$ , and  $\text{Ar}^{2+}$  with magnifications of 12x (A) and 60x (B). Peaks in the lower  $m/z$  region are inevitable due to gas tank impurities and vacuum system leaks. Since the ionization potentials of the various background gases (water, nitrogen, and oxygen) are above the argon metastable energies, they are a result of electron impact ionization.

Argon sputters both gold and copper well, as indicated by the large signals for  $^{197}\text{Au}^+$ ,  $^{63}\text{Cu}^+$ , and  $^{65}\text{Cu}^+$  with respect to other species in the discharge. Even though the argon ion signals are lower than the analyte signal, the neutral atom density of argon is much greater than that of gold or copper; hence, Penning ionization of gold or copper is favored.<sup>112</sup>

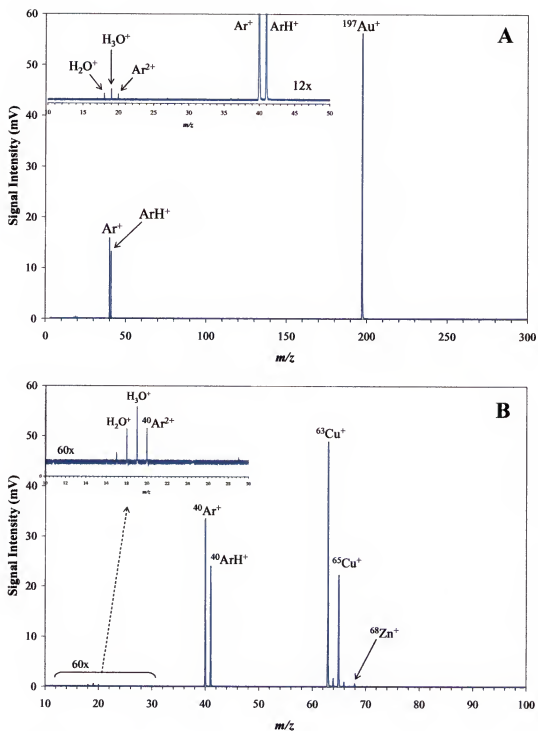


Figure 3-2 Direct current argon glow discharge mass spectra with a A) gold sample and B) NIST 1113 sample. Insets in each plot are magnified views of the  $m/z$  region 10-50 (12x) and 10-30 (60x).

**Pure Nitrogen.** When comparing an argon and nitrogen discharge, it is apparent that the ionization patterns in the glow discharge are altered by modifications in gas composition. For comparison, Figure 3-3 shows mass spectra of a pure nitrogen plasma for both gold and NIST 1113 samples. By replacing argon with nitrogen, the gold ion signal ( $A$ ) decreases in intensity by a factor of 1.5 and the argon ion signals are replaced by nitrogen containing species. The peak intensities of nitrogen species vary accordingly:  $N_2^+ > N_4^+ > N_3^+ > N_2H^+$ . While the majority of nitrogen-containing species appear in the lower molecular weight region, two nitrogen adducts are detected at  $m/z$  values higher than gold. The nitrogen dimer and tetramer form adducts with gold ( $m/z$  225 and 253) as illustrated in the inset of Figure 3-3A. Changing the cathode material to copper results in over a 100 fold reduction in copper ion signal and a single peak for the nitrogen dimer.

Given that argon and nitrogen have distinct properties, it is expected that ion signal responses will vary. Even though the ionization potentials of Ar and  $N_2$  are close in value, 15.8 eV and 15.6 eV respectively, the gold ion signal is 1.5 fold lower in a nitrogen discharge and the copper ion signal is over 100 fold lower. There are two possible reasons for a drop in the gold (and copper) signal intensity with nitrogen addition: 1) molecular weight differences and 2) metastable atom production. According to the mass transfer function, as  $m_1/m_2$  reaches unity, where  $m_1$  is the incident ion and  $m_2$  is the mass of the sample atom, the sputter yield and also the analyte ion signal should reach a maximum. With a  $N_2$  discharge, the simplified mass transfer function gets further from unity for both Au and Cu and these ion signals decrease. Also, nitrogen is a diatomic molecule thus spreading its energy over two atoms as opposed to conserving all

of its energy for one atom. Besides diatomic nitrogen impinging on the sample surface, monoatomic nitrogen is likely participating in this event.

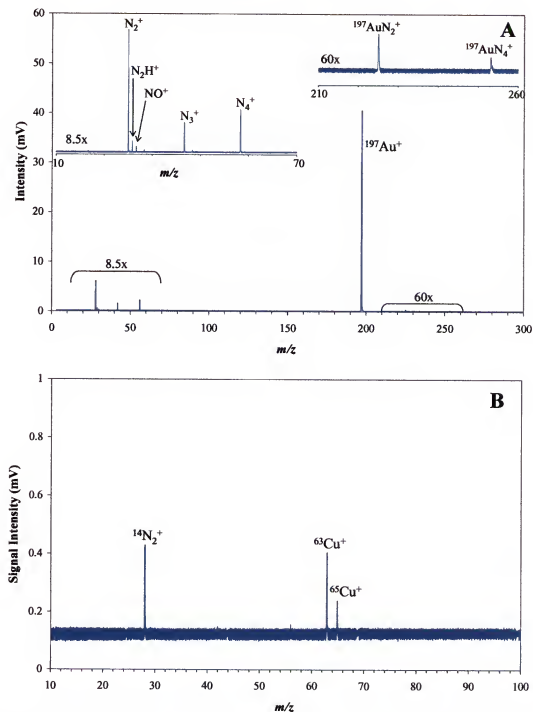


Figure 3-3 Direct current nitrogen glow discharge mass spectra for A) gold sample and B) NIST 1113 sample. Insets in plot A are magnified views of  $m/z$  10-70 and  $m/z$  210-260.

The transfer of energy from a nitrogen atom to the sample surface may not be as great as  $N_2$ , thus affecting the sputter yield. If a smaller number of atoms are ejected from the sample surface, then fewer atoms are available for ionization. An important difference between the two gases is the participation of metastable species. As described in Chapter 2, Penning ionization plays a significant role in the glow discharge. For example, argon has metastable states of 11.5 eV and 11.7 eV, sufficient to ionize most elements. In contrast, nitrogen's metastable states are 6.2 eV and 8.4 eV,<sup>113</sup> which are close to the ionization potential of many elements of interest. A reduction in the ion signal of gold (IP 9.2 eV) could be attributed to the loss of Penning ionization.

The greatest difference can be seen between the nitrogen discharges. For the gold cathode, a number of nitrogen species are detected; however, NIST 1113 produces only the nitrogen molecule. Discharge conditions for the NIST 1113 cathode analysis vary considerably from the gold cathode. This may contribute to the variations, yet, at the higher powers used for NIST 1113, the copper ion signal intensity should be higher. A dcGD introduces harsh conditions for the source and the skimmer cone, which could contribute to a lower signal for copper. With a dcGD, noticeable deposition of sputtered analyte on the skimmer cone interferes with ion focusing. Since a drastic difference exists between the argon and nitrogen plasmas, it is of interest to probe the mixed-gas plasmas.

**Effect of Gas Concentration on Ionization.** From the data reported above, obvious changes take place when argon is replaced with nitrogen as the plasma gas. When altering the plasma gas, the ionization processes in the discharge will change due to different gas species available. To more closely examine ionization processes in the dc

discharge, such as electron impact and Penning ionization, ion signals were monitored relative to discharge gas concentration. In the following experiments, argon was systematically replaced with nitrogen. A constant voltage and current was maintained for all experiments.

Figure 3-4 illustrates the ions detected at various mixed gas levels, 0 – 100% N<sub>2</sub>, in a dcGD. The ions monitored in the discharge were Ar<sup>+</sup>, ArH<sup>+</sup>, N<sub>2</sub><sup>+</sup>, and N<sub>2</sub>H<sup>+</sup>, and based on sample material, <sup>197</sup>Au<sup>+</sup>, <sup>63</sup>Cu<sup>+</sup>, and <sup>65</sup>Cu<sup>+</sup>. The signal intensity of gold, after an initial drop (5% N<sub>2</sub>), remained relatively constant until another decrease appeared at 100% N<sub>2</sub>. Our results show certain differences compared to previous publications, which generally featured reactive cathode materials.

For the addition of ~5% N<sub>2</sub> gas added to argon, Wagatsuma and Hirokawa<sup>78</sup> report that both the copper atom (327.4 nm) and ion (224.7 nm) emission signal intensities showed a reduction of ~10 fold, while at ~15% N<sub>2</sub> addition, the copper ion emission intensity became virtually undetectable. However, based on our results, the gold ion signal is still strong even at higher nitrogen concentrations. In agreement with Wagatsuma's copper ion results, the copper ion signals drop drastically with 5% N<sub>2</sub> addition as illustrated in Figure 3-4B, and very little copper ion signal remains at 10% N<sub>2</sub>. At 10% N<sub>2</sub>, <sup>63</sup>Cu<sup>+</sup> has decreased in intensity approximately 20 fold (Figure 3-5A). Similar to the gold sample experiments, the nitrogen ion signals are very low in intensity.

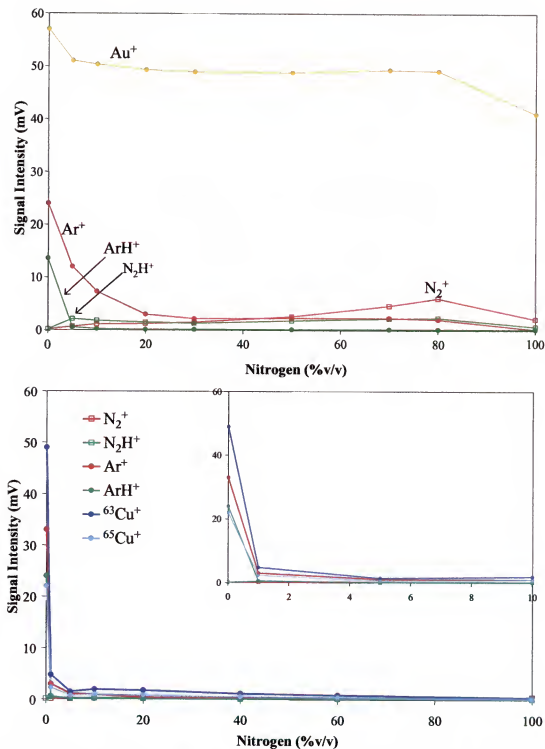


Figure 3-4 The effect of 0-100% nitrogen addition to an argon dc glow discharge on ion signals. The ion signals monitored were N<sub>2</sub><sup>+</sup>, N<sub>2</sub>H<sup>+</sup>, Ar<sup>+</sup>, ArH<sup>+</sup>, and Au<sup>+</sup> (or <sup>63</sup>Cu<sup>+</sup> and <sup>65</sup>Cu<sup>+</sup>). A) gold sample B) NIST 1113 sample.

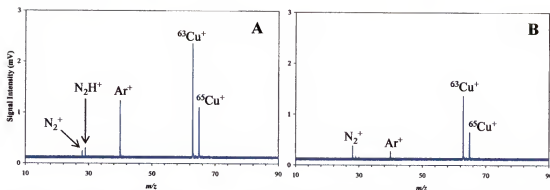


Figure 3-5 Direct current glow discharge mass spectra of NIST 1113 sample in A) 10% N<sub>2</sub> and B) 60% N<sub>2</sub>.

The difference in reactivity is an important factor here. Fischer et. al.<sup>81,82</sup> report a different finding with the addition of N<sub>2</sub> to an argon discharge. The copper atom emission signal (327.4 nm) increases with the addition of 1% N<sub>2</sub> gas, followed by a slight decrease in the emission intensity at 3% N<sub>2</sub>. They were not able to explain this phenomenon, but it does indicate a sustained analyte signal, more in keeping with our gold results in the dcGD. Direct current glow discharge mass spectra of 10% and 80% N<sub>2</sub> with a gold cathode are shown in Figure 3-6. At 80% N<sub>2</sub> (B), the nitrogen trimer, tetramer, and adducts with gold are prevalent. (Note that experiments were run at different conditions).

As shown in this section, a direct current glow discharge source provides a steady-state supply of ions. The continuous supply of ions is generated by a constant applied voltage; and the sample surface is continually being cleaned with an endless supply of bombarding gas ions. The data generated from a direct current glow discharge serves as reference spectra for the experiments that follow. With the addition of nitrogen, background ion signals are diminished. A reduction in background interferences can be beneficial for detection of isobaric interferences. It is known that by pulsing the voltage,

ion signals increase and ionization patterns change. What happens to the ions in the argon-nitrogen mixed plasma if the discharge voltage is pulsed?

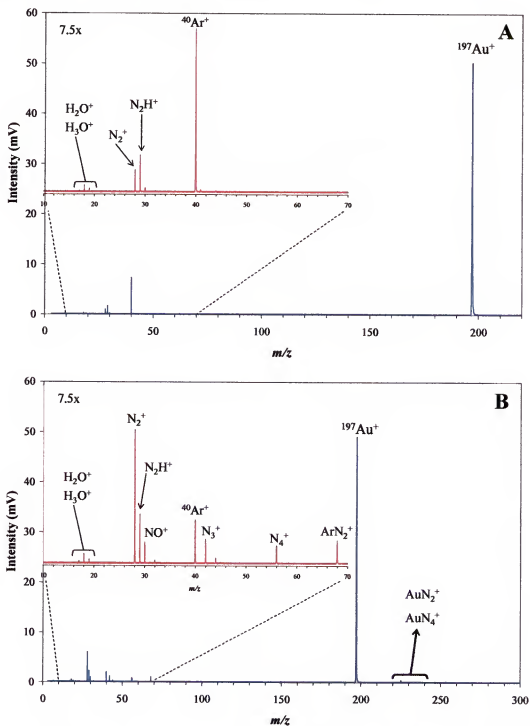


Figure 3-6 Pure nitrogen direct current glow discharge mass spectra of a gold cathode at A) 10%  $N_2$  and B) 80%  $N_2$ .

### **Microsecond Pulsed Glow Discharge: Comparison of Ar and N<sub>2</sub>**

Instead of gas ions continuously impinging on the sample surface and quickly eroding away analyte material, the discharge can be pulsed, generating packets of ions. For a microsecond pulsed discharge, sputtering occurs when the voltage is on – the pulse width is 20  $\mu$ s and is set at a 600 Hz frequency. Because of the short duty cycle (~1%), the total erosion rate is lower than the dcGD, yet due to a higher instantaneous current in a pulsed discharge, the sputtering is enhanced during the short pulse. A pulsed voltage offers enhanced sputtering, excitation, and ionization over a continuous voltage because of high peak voltages and currents. Since the voltage is greater for each pulse than the continuous voltage in dc mode, higher energy ions strike the surface and enhance sputter yield. The creation of a more energetic plasma increases the number of ionized sputtered atoms. Additionally, pulsed-mode operation offers the opportunity of temporal resolution.

**Pure Argon.** Similar to the dcGD experiments, argon was systematically replaced with nitrogen until a pure nitrogen discharge was maintained for a pulsed glow discharge. Instead of a steady state supply of ions, a pulsed discharge offers discrimination between gas and analyte species by means of the transient ion signal. For all experiments, the duty cycle of a 20  $\mu$ s pulse width and 600 Hz frequency discharge is ~1.2%. Pulsed operation requires that spectra be obtained at some specific temporal window. As illustrated in Figure 3-7, spectral composition changes continually with gated detection delay times. Early in the measurement cycle, Ar<sup>+</sup> and ArH<sup>+</sup> are prevalent, yet at longer delay times the gold ion dominates. Intermediate delay times are thought to represent conditions more similar to dc. The yellow shaded area under the delay time plot of Au<sup>+</sup> was integrated and represents the total number of ions detected.

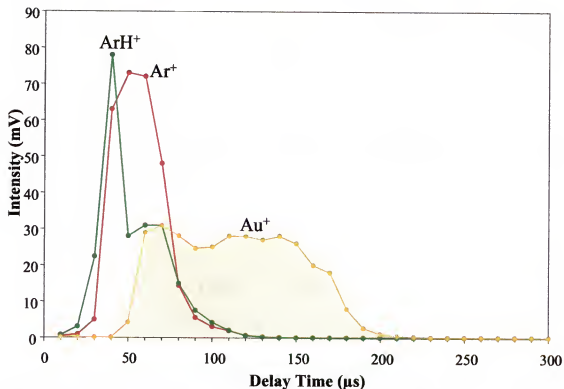


Figure 3-7 Delay time plot of an argon microsecond pulsed glow discharge. The yellow shaded area represents the total number of gold ions. Sample material: high purity gold.

**Pure Nitrogen.** A pure nitrogen discharge produces a delay time plot as shown in Figure 3-8, and the inset is a magnified view (12x) of the nitrogen gas species. Compared to the argon discharge, the  $\text{Au}^+$  signal drops in intensity by 1.5 fold, and the argon gas ions are replaced by nitrogen gas ions. Despite a pure nitrogen discharge, the signal intensity of the nitrogen ions is ~20 fold lower than the argon ions in a pure argon plasma. The pure argon and nitrogen pulsed plasmas serve as references to the mixed-gas plasmas.

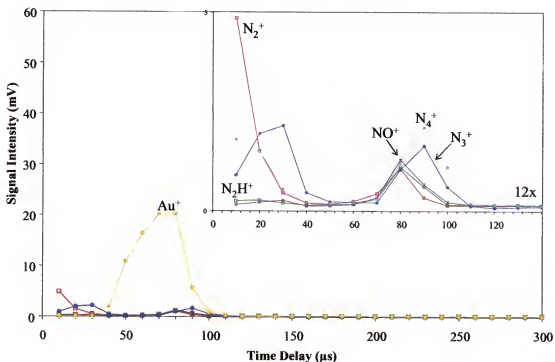


Figure 3-8 Delay time plot of a nitrogen microsecond pulsed glow discharge. Sample material: high purity gold. The inset is a 12x magnified view of 0-140  $\mu$ s delay time.

**Electron Impact Ionization.** During the pulsed cycle different modes of ionization exist. At early delay times, electron impact dominates producing discharge gas ions for sample bombardment. Breakdown of the gas occurs when a high negative voltage is applied to the cathode; positive gas ions are accelerated towards the cathode to participate in sputtering while electrons are accelerated away from the cathode. Time-of-flight mass spectra taken at early delay times are representative of discharge gas composition. Figure 3-9A and 3-9B (magnified  $\sim 10\times$ ) show mass spectra for an argon and nitrogen discharge at delay times of 50 and 10  $\mu$ s, respectively. The delay times in Figure 3-9 illustrate optimal signal intensities of gas ions for each gas. The  $\text{Ar}^+$  signal intensities are approximately ten times greater in intensity than the nitrogen gas ions. Discharge gas ions, as well as electrons, are critical in sustaining the plasma.

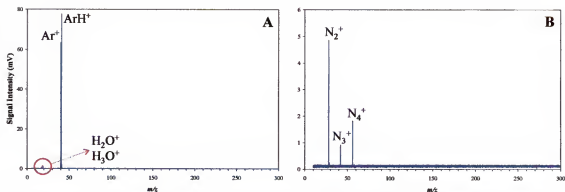


Figure 3-9 Microsecond pulsed glow discharge at early delay times illustrating electron impact ionization-like mass spectra. A) Argon discharge at 50  $\mu\text{s}$  delay time. B) Nitrogen discharge at 10  $\mu\text{s}$  delay time.

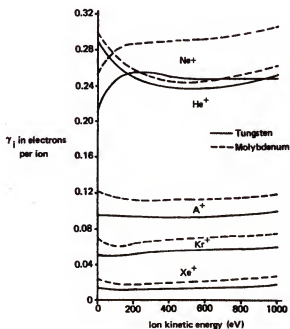


Figure 3-10 Secondary electron emission yields of tungsten and molybdenum for the noble gases. (Ref. 115)

As mentioned previously, discharge gas ions strike the cathode surface and induce ejection of analyte atoms. Besides analyte atoms being liberated from the surface, electrons (i.e., secondary electrons) are also emitted. In Figure 3-9B, the lower nitrogen gas ion signals could be due to a lower number of electrons emitted per incident ion. The secondary electron emission coefficient ( $\gamma_i$ ) for the noble gases is shown in Figure 3-10.

This plot does not show  $\gamma_i$  for nitrogen;<sup>114</sup> however,  $\gamma_i$  has been reported for various metals<sup>115</sup> as listed in Table 3-1. The secondary electron emission coefficient for N<sub>2</sub> compared to Ar for the metals listed is over two times less. A lower yield  $\gamma_i$  corresponds to fewer electrons participating in ionization during the 20  $\mu$ s pulse duration. This may be a factor for the lower signal intensities of nitrogen gas ions in the pure N<sub>2</sub> discharge. Lower ionization is also advantageous because of the reduction in background signals.

Table 3-5 Secondary electron emission yields ( $\gamma_i$ ) of various metals for argon and nitrogen gases.

Metal	Ar	N <sub>2</sub>
Al	0.12	0.10
Cu	0.058	0.025
Fe	0.058	0.020
Ni	0.058	0.036
Pt	0.058	0.017

**Effect of Gas Concentration on Ionization.** The influence of a controlled addition of nitrogen to argon on the net sputtering rate and ion signals in a microsecond pulsed glow discharge has been investigated. Initial studies implement a high purity gold sample to eliminate possible surface reactions. The nitrogen concentrations in the discharge gas were varied in the range 0-100% N<sub>2</sub>. The total flow rate was maintained at 150 mL·min<sup>-1</sup>. To verify that a single mass flow controller (MFC) set at 150 mL·min<sup>-1</sup> Ar is equivalent to two tandem MFCs totaling 150 mL·min<sup>-1</sup> Ar delay time plots were compared for each mode. Figure 3-11 illustrates a similar response, signal intensity and trend, for both flow modes. A slight shift to higher delay times for the dual mode is apparent; however, any differences are within discharge-to-discharge reproducibility variation.

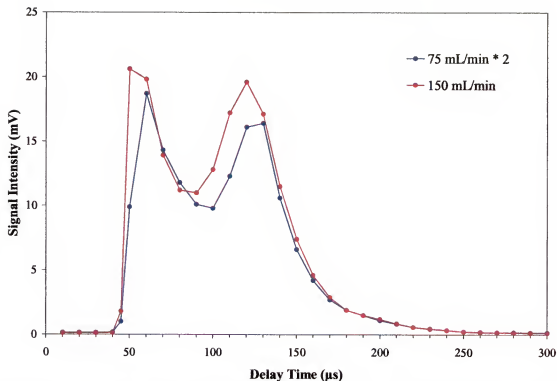


Figure 3-11 Comparison of one MFC at 150 mL·min<sup>-1</sup> versus two MFCs totaling 150 mL·min<sup>-1</sup>.

Pulsed discharge voltage and pressure were maintained at -1750 kV and ~3.5 Torr, respectively. With the controlled addition of nitrogen to an argon plasma, a trend is observed for gas and analyte ion production. Figure 3-12 is a plot of ion population versus percent nitrogen gas. The ions monitored in the discharge were  $N_2^+$ ,  $N_2H^+$ ,  $Ar^+$ ,  $ArH^+$ , and  $Au^+$ . The  $\mu$ sPGD gold response (Figure 3-12A) shows a continual decline as nitrogen was added, until at pure  $N_2$  the gold signal has decreased to less than half of that observed in a pure argon discharge. Signal response of the pulsed gas ions was not significantly different compared to the dcGD. The  $Ar^+$  signal drops sharply to a minimum and subsequently steady-state level by ~20%  $N_2$ . Comparing this to literature results for optical emission studies, several argon atom emission lines show a similar trend with the emission intensities reaching a minimum level at ~15%  $N_2$ .<sup>78</sup> In Figure 3-

12A, at 5%  $N_2$  the  $ArH^+$  signal essentially disappears in both a dc (Figure 3-4) and pulsed glow discharge. As the argon-hydride ions decrease appreciably the  $N_2H^+$  shows an initial increase perhaps, from a proton transfer reaction between the argon-hydride and nitrogen as shown in Figure 3-12B.

In partial agreement with these results, Jackson and King<sup>60</sup> report mass spectrometric data that show a vast reduction in  $ArH^+$  (factor of 10-100) with the addition of 1%  $N_2$  and a reduction in argon ions by a factor of 5-13. They also mention “large quantities” of  $N_2H^+$  with 1% nitrogen added. Our results do not show significant levels of nitrogen-hydride. More closely matching the data trends shown above are the emission results by Wagatsuma,<sup>78</sup> who demonstrated that the nitrogen emission band at 337.1 nm increases drastically; however, the  $N_2^+$  emission band at 391.4 nm shows only a slight increase in intensity with the addition of up to ~18% nitrogen. The  $\mu$ sPGD results show that at higher concentrations of nitrogen (> 40%),  $N_3^+$  and  $N_4^+$  are also present in the pulsed glow discharge (Figure 3-12B). Giglio and Caruso<sup>84</sup> also observed these polyatomic ions in their nitrogen discharge experiments. Before finalizing conclusions about possible ionization schemes in mixed gas plasmas, it is important to consider more reactive cathodes such as copper (NIST 1113) and silver. In addition, the sputter rates and trends for each element are also crucial for determining the type of sputtering.

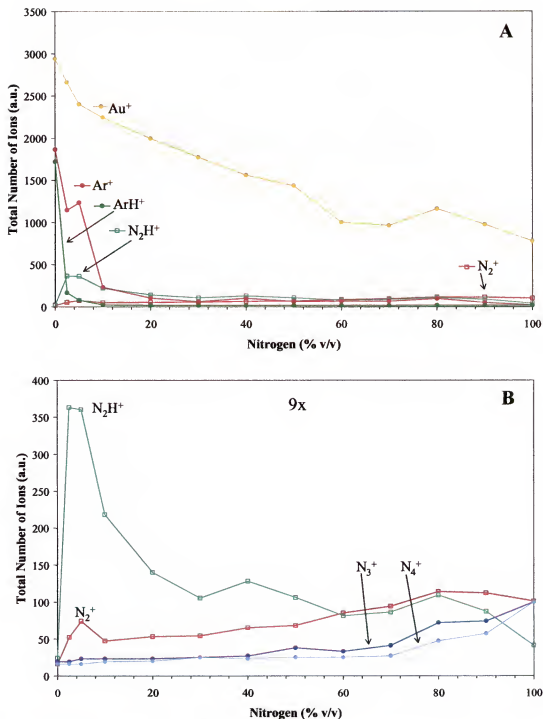


Figure 3-12 Total number of ions of those investigated versus concentration of added gas when  $\text{N}_2$  is added to the Ar matrix plasma. A) Normal signal intensity view of ions. B) 9x magnified view of plot A.

**Mixed Gas Plasma – Alternative Elements.** To observe the effect of nitrogen addition to an argon  $\mu$ sPGD under alternative conditions, silver and copper-based samples were analyzed. Each element in the periodic table will influence the discharge sputtering and ionization differently; yet, similarities will occur. Similar to Figure 3-12 where gold is the sample material, Figure 3-13 illustrates the effect of 0-100%  $N_2$  addition to an argon  $\mu$ sPGD using a copper-based sample (A) and a high purity silver sample (B). Conditions were maintained at a constant voltage, duty cycle, and relatively constant pressure.

The most noticeable difference between the gold, copper, and silver is the analyte ion trend as argon is systematically replaced by nitrogen. Despite the relatively similar ion signal intensities of  $^{197}\text{Au}^+$ ,  $^{63}\text{Cu}^+$ ,  $^{65}\text{Cu}^+$ ,  $^{107}\text{Ag}^+$ , and  $^{109}\text{Ag}^+$  at 100% Ar, the ion profiles are different. As mentioned previously, the gold ion signal gradually decreases and at 100%  $N_2$  is approximately one-third of the intensity in pure argon. In contrast, both copper and silver analyte ions show a drastic drop in signal with 20% or less nitrogen concentration followed by a gradual decrease in intensity.

A factor to consider is the ionization potential of both the sputtered atom and gas atom (or molecule). The ionization potentials of argon and nitrogen gases are close in value at 15.8 eV and 15.6 eV, respectively. Metals are typically ionized easily due to their much lower ionization potentials: Au at 9.22 eV, Ag at 7.57 eV, and Cu at 7.72 eV. Even though the ionization potentials of Ar and  $N_2$  are close in value, their ionization efficiencies might provide insight into the significant difference in analyte ion signals between a pure argon and pure nitrogen discharge.

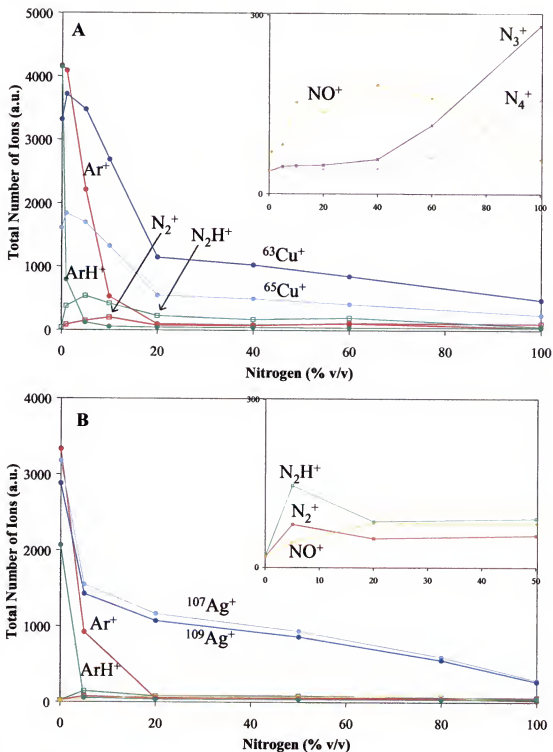


Figure 3-13 Total number of ions of those investigated versus concentration of added gas when N<sub>2</sub> is added to the Ar matrix plasma. A) Sample material: NIST 1113. B) Sample material: high purity silver.

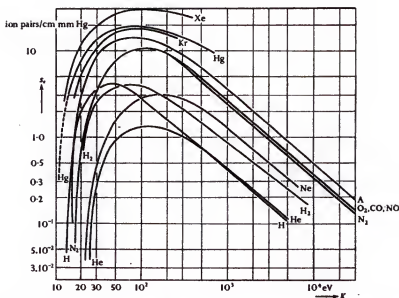


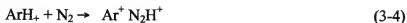
Figure 3-14 Ionization efficiency as a function of electron energy. (Ref. 117)

Figure 3-14 is a plot of ionization efficiency as a function of electron energy. At all electron energies, the ionization efficiency of argon is greater than nitrogen.<sup>116</sup> A greater ionization efficiency would theoretically result in a greater number of sputtered atoms being ionized, which can be monitored with mass spectrometry. The greater analyte ion signals in a pure argon discharge may be due to the higher ionization efficiency of argon. While ionization efficiency may play a role in signal reduction, a loss of metastables could also contribute to lower analyte ion signals.

**Penning Ionization.** In Chapter 1, three main types of ionization occurring in a glow discharge were described. At longer delay times in a microsecond pulsed glow discharge ( $>80 \mu\text{s}$ ), Penning ionization dominates as was shown in Figures 3-7 and 3-8. For Penning ionization to take place, metastable states of the gas are required. The metastable states of argon (i.e., 11.55 eV and 11.72 eV) can easily ionize gold, silver, or copper atoms. If the population of argon metastables is quenched or is prevented from forming, a reduction in ionization of sputtered atoms is observed. Reports for both dc<sup>78</sup>

and pulsed<sup>60</sup> glow discharges, using optical emission spectrometry, state that small amounts of nitrogen (<5%) added to an argon plasma quench the argon metastables. In the millisecond pulsed discharge, 1% N<sub>2</sub> eliminated the characteristic “afterpeak” of analyte emission. As reported in Chapter 2, the nitrogen metastable state is 6.2 eV, which is insufficient energy to ionize gold, copper, or silver. Other evidence that nitrogen contributes to quenching is the drastic drop in argon ion signals.

**Argon and Nitrogen Gas Ions.** As the signal intensity of Ar<sup>+</sup> decreases, an increase in N<sub>2</sub><sup>+</sup> is evident; however, a more pronounced change is apparent for ArH<sup>+</sup> and N<sub>2</sub>H<sup>+</sup>. Since the proton affinity of N<sub>2</sub> (118 kcal·mol<sup>-1</sup>) is greater than that of Ar (88 kcal·mol<sup>-1</sup>), proton transfer between the two ions likely occurs.



In addition to the formation of N<sub>2</sub>H<sup>+</sup>, levels of the nitrogen trimer and tetramer become more pronounced at higher concentrations of nitrogen. As mentioned in Chapter 2, the purity of the nitrogen gas determines the extent of nitrogen tetramer formation; hence, the highest levels of N<sub>4</sub><sup>+</sup> are found at 100% N<sub>2</sub>.

**Sputter Rate.** Ionization efficiency, metastable levels, and type of gas ions all influence the level of analyte ion signals. Not only does the gas composition affect ionization, the sputter rate is affected as well. The trend in sputter rate indicates the extent of surface reactions occurring, and the qualitative number of sputtered atoms available for ionization. Figure 3-15 shows the effect of nitrogen addition to an argon μsPGD on the net sputter rate of gold, silver, and copper. In this experiment, a pure copper sample was used in place of NIST 1113. Figure 1-7 in Chapter 1 plots sputter yield for elements of the periodic table as a function of atomic number (surfaces were

bombarded with 400 eV of argon).<sup>49,53</sup> The net sputter rates of gold, silver, and copper for an argon  $\mu$ sPGD do not correspond to the data published by Wehner.<sup>49,54</sup> Differences between results is partly due to the method used to measure sputtering effects.

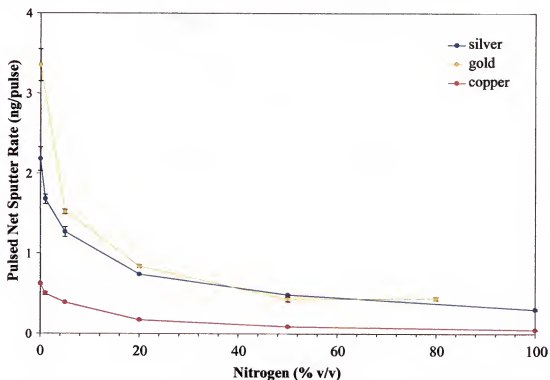


Figure 3-15 Pulsed net sputter rate of gold, silver, and copper relative to nitrogen content.

Despite discrepancies in the data, the net sputter rate trends are of importance. As nitrogen concentration in the discharge increases, the sputter rate of gold, silver, and copper decreases. A lower sputter rate is evidence of fewer atoms being liberated from the sample surface; therefore, fewer atoms are available for ionization. The decrease in net sputter rate is an additional explanation for a lower analyte signal in a pure nitrogen discharge.

### Conclusions

Argon is the most common plasma gas employed in glow discharge analysis; however, benefits arise from implementing and studying the use of alternative plasma gases. A common impurity in an argon glow discharge is nitrogen, and therefore it is important to study its effect on the plasma and possible analytical utility. Nitrogen has been successfully analyzed in a microsecond pulsed glow discharge using time-of-flight mass spectrometry. Synchronization of the pulsed discharge and time-of-flight offered the opportunity for temporal resolution of ions. This allowed discrimination between gas and analyte ions, and thus further studying of electron ionization and Penning ionization.

Addition of nitrogen to an argon glow discharge significantly reduces the argon ion signals, lowers the analyte ion population, and reduces the sputter rate. Despite these negative effects, nitrogen addition eliminates spectral interferences at  $m/z$  40 and 41 allowing analysis of  $^{40}\text{Ca}$  and with a lower sputter rate improves resolution for thin layer analysis.

## CHAPTER 4

### CHARACTERIZATION OF THE MICROSECOND PULSED GLOW DISCHARGE PROCESSES IN OXYGEN – REACTIVE SPUTTERING

#### **Introduction**

The sputtering mechanisms discussed to this point have included physical sputtering and semi-reactive sputtering. Physical sputtering encompasses the interactions between inert gases and sputtering atoms. If bombarding ions combine chemically with the sputtered atoms at the sample surface (or in the gas phase), then sputtering is considered reactive (chemical sputtering). Depending on the sample material, nitrogen can be categorized as either a reactive or non-reactive plasma gas, thus indicating a semi-reactive sputtering gas. Metals can be divided into two groups: 1) metals that form stable nitrides (e.g., Al and Ti) and 2) metals that do not react with nitrogen (e.g., Ni, Cu, Ag, and Au).<sup>77,81,82</sup> Small amounts of a reactive gas, such as oxygen, added to an inert sputtering medium can cause drastic effects on sputtering and therefore, type and magnitude of observed ion species are affected. Chemical sputtering is typically enhanced with oxygen gas. Oxygen has been shown to significantly affect sputter rate, atom and ion analyte emission signals, and gas species emission signals in a direct current glow discharge.<sup>76,80-83,88,95-100,102,117</sup>

Addition of alternative gases to an inert sputtering medium not only affects sputtering and emission signals, but also alters the ionization processes. Previous studies utilize oxygen (or mixed oxygen-argon gas) as a discharge gas for a negative ion reagent gas system. For a negative ion reagent gas system, argon acts as a buffer gas since it does

not form a stable anion. In essence, oxygen acts as the substrate molecule and captures an electron thus forming a stable anion.<sup>118</sup> The possibility of enhanced sensitivity is the attraction of electron capture chemical ionization. Due to limitations of the TOFMS described in Chapter 1, detection of only positive ions is possible for our instrument.

In the work described here, the types of ion species formed from sputtering elements of varying reactivity are examined in a mixed oxygen-argon plasma. To date, no attention has been given to the positive ions (related to the sputtered species) arising from an argon-oxygen microsecond pulsed glow discharge with time-of-flight mass spectrometry. The purpose of this study is to study the effect that adding oxygen to an argon plasma (0-100%) has on both analyte and gas ions. In addition, analyte samples of varying reactivity were analyzed to investigate the effect of physical and chemical sputtering.

## **Experimental**

### **Glow Discharge Source and Time-of-Flight Mass Spectrometer**

The Grimm-type glow discharge (GD) source configuration employed in this research was operated in the microsecond pulsed time regime. Details of the source were described in Chapter 1 and Chapter 3. A commercial time-of-flight mass spectrometer (Renaissance, LECO Corporation, St. Joseph, MI) is operated as described in Chapter 2. Refer to Figure 1-9 and 1-10 for the glow discharge source configuration and TOFMS setup, respectively. Operating conditions for the GD source and mass spectrometer were listed in Tables 3-1 and 3-2 of Chapter 3.

### **Gas Delivery System**

As described previously, gases are mixed using a four-channel readout module in combination with three mass flow controllers (MFCs). The gas delivery system allows control of gas flow rates and therefore gas composition. Three MFCs are available and individually calibrated for a specified gas. A  $200 \text{ mL}\cdot\text{min}^{-1}$  argon MFC is designated for argon-only use. The oxygen MFC is limited by a  $20 \text{ mL}\cdot\text{min}^{-1}$  flow rate, which corresponds to a maximum of 13%  $\text{O}_2$ . However, as described in Chapter 3, a mass flow controller can be “recalibrated,” permitting the use of other gases. For oxygen concentrations greater than 10%, the  $\text{N}_2$  MFC was recalibrated to accept oxygen gas. The scaling control factor, which is the product of the gauge factor and gas correction factor, was calculated and adjusted on the four-channel readout module.

### **Plasma Gas**

The gas is an essential medium for a glow discharge source to operate properly. Sputtering, ionization, and discharge stability are all influenced by the type and grade of plasma gas employed. The gases employed in this research include high purity argon (5 Grade, Strate Welding, Gainesville, FL, USA) and research grade oxygen (99.9%  $\text{O}_2$ , The BOC Group Inc., Murray Hill, NJ, USA). In this research, argon was systematically replaced with oxygen until a pure oxygen plasma was sustained. The total gas flow rate was maintained at  $150 \text{ mL}\cdot\text{min}^{-1}$  by utilizing the gas delivery system.

### **Sample Material**

Three types of cathode material were used in these studies: gold, silver, and copper. The gold (Gold Target, 99.99% Pure, Kurt J. Lesker, Clairton, PA) and silver (Silver

Target, 99.99% Pure, Kurt J. Lesker, Clairton, PA) cathodes are high purity ingots. The copper cathode is a certified standard reference material, NIST 1113, consisting of 95.03% Cu and 4.80% Zinc.

The same procedure was employed for sputter rate determination as described for the nitrogen studies in Chapter 3. Samples for obtaining sputter rates were high purity elemental foils (gold, silver, and copper) approximately 1 mm thick (Puratronic, 99.9%, Alfa Aesar, Ward Hill, MA). The foils were cut into small discs 15 mm in diameter and weighed with an analytical microbalance (Model: M2P, Sartorius, Corp., Edgewood, NY). To calculate the weight difference, the foils were weighed prior to and after sputter analysis. Each sample was sputtered three times for 30 minutes, using a new sample for each analysis.

## **Results and Discussion**

### **Background**

Argon is the most commonly used inert gas for glow discharge sources. As shown in the previous chapter, benefits can be gained by using an alternative gas, such as N<sub>2</sub>, since it can reduce potential isobaric interferences and can improve depth profiling. Despite oxygen's ability to quench an argon signal, there is the potential for analytical utility of an oxygen-argon discharge. More specifically, focusing on positive ion mass spectrometry for analysis. Similar to nitrogen, oxygen is often an indicator of a vacuum leak or gas tank impurity. Previous studies focused on low concentrations of oxygen in an argon plasma that mimic a possible system leak. Emission intensities of pertinent analyte and gas species were monitored along with sputter rate. The emission studies are complementary to mass spectrometry in that they provide information about excited

atoms and metastable species; however, mass spectrometry provides evidence for the utility of oxygen as a reagent gas.

In the following studies a pure argon discharge is compared to a pure oxygen discharge. The gold sample is used for direct current glow discharge (dcGD) mass spectrometry analysis, while gold, silver, and copper were employed for the microsecond pulsed glow discharge ( $\mu$ sPGD) experiments.

### **Direct Current Glow Discharge: Comparison of Ar and O<sub>2</sub>**

Oxygen is considered a reactive gas since, during sputtering, a chemical interaction occurs between the implanted oxygen and the atoms of the solid. Because of the chemical reactivity, the mixed oxygen-argon plasma was first analyzed using a dcGD to determine the extent of chemical influence when a continuous voltage is applied. In theory, the sample surface is continually cleaned by the continuous supply of ions generated by a direct current, preventing extensive oxide-layer formation. Since gold is perhaps the least reactive of all metals, it was used in the following experiments to minimize surface reactions and chemical sputtering.

**Pure Argon.** The primary ions formed in a pure argon direct current glow discharge are  $\text{Ar}^+$ ,  $\text{ArH}^+$ , and ionized sample material. Figure 4-1C is a dcGD mass spectrum of gold in a pure argon environment. Recall Figure 3-2A in Chapter 3 which is representative of a similar discharge, but collected under different conditions. By using the relatively non-reactive gold cathode, only one major ion is present,  $^{197}\text{Au}^+$ . Minor species detected in the lower molecular weight region of the discharge are  $\text{H}_2\text{O}^+$ ,  $\text{H}_3\text{O}^+$ , and  $\text{Ar}^{2+}$  (Figure 4-1A). Adducts with gold, such as  $^{197}\text{Au}^{40}\text{Ar}^+$ , are typically present, but at levels approximately 200 fold less than the analyte ion signal (Figure 4-1B). As

illustrated in Figure 4-1C, argon ion signals are similar in intensity to the gold ion signal, which possibly means that electron impact ionization is prevalent. Since argon provides a stable environment, then what happens if the plasma is sustained solely by oxygen?

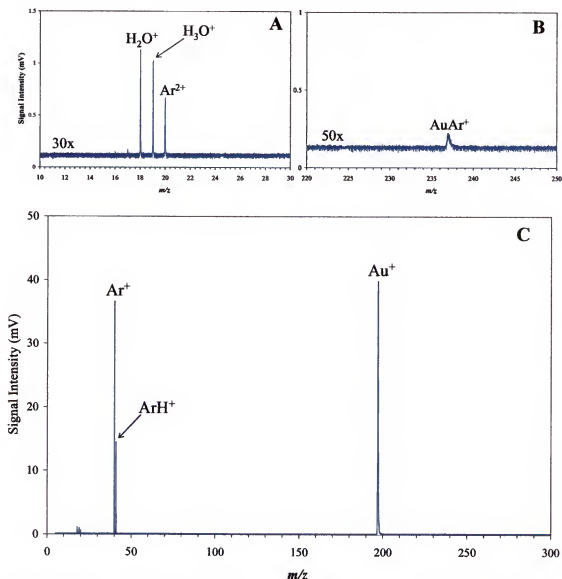


Figure 4-1 Direct current glow discharge mass spectra in 100% argon using a gold cathode. A) 30x magnified view of  $m/z$  range 10-30. B) 50x magnified view of  $m/z$  range 220-250. C) Full mass spectrum.

**Pure Oxygen.** Oxygen is commonly used as a reagent gas for negative ion chemical ionization, but in conjunction with a buffer gas, such as argon or methane. In these studies, oxygen is the sole provider that promotes ionization.

When comparing an argon and oxygen discharge, it is apparent that ionization patterns change and can be monitored by the gas ions formed and detected. Figure 4-2C is a dcGD mass spectrum of gold in a pure oxygen environment. When comparing the pure oxygen discharge to the pure argon discharge, the primary difference is the replacement of argon ions with oxygen ions (primarily  $O_2^+$ ). In addition, the interfering ions at  $m/z$  18-20 ( $H_2O^+$ ,  $H_3O^+$ , and  $Ar^{2+}$ ) in an argon plasma are not present in an oxygen discharge. Instead, the  $^{16}O^+$  monoatomic species forms, which is ~100 fold lower in signal than  $O_2^+$  as seen in Figure 4-2A. The inset is a magnified view (60x) of  $m/z$  region 10-20. A low concentration of oxygen atoms may be indicative of charge transfer to oxygen molecules as shown in equation 2-11 in Chapter 2. Charge transfer between an atomic oxygen ion and oxygen molecule is expressed as



This may contribute to the high concentration of molecular oxygen ions. The larger  $O_2^+$  signal compared to the  $Ar^+$  signal (in an argon plasma) may be attributed to a more easily ionizable species ( $IP_{Ar}$ : 15.8 eV and  $IP_{O_2}$ : 12.3 eV).

As seen in Chapter 3, the nitrogen monoatomic ion is not present in a pure nitrogen dcGD mass spectrum. The reason for this is partly due to the bond dissociation energy of  $N_2$  compared to  $O_2$ . Oxygen ( $O=O$ ), which contains a double bond, exhibits a bond dissociation energy of  $119 \text{ kcal}\cdot\text{mol}^{-1}$  compared to a much higher value for the triple

bonded nitrogen ( $\text{N}\equiv\text{N}$ ) at  $225 \text{ kcal}\cdot\text{mol}^{-1}$ . The triple bond in nitrogen is strong and therefore requires a greater amount of energy to break the bond.

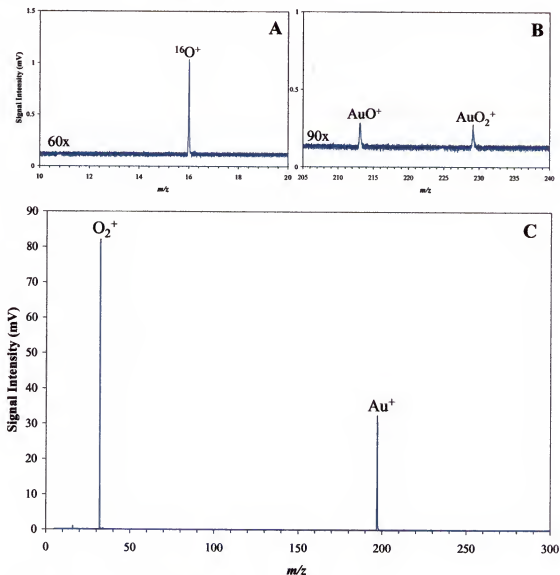


Figure 4-2 Direct current glow discharge mass spectra in 100% oxygen using a gold cathode. A) 60x magnified view of  $m/z$  range 10-20. B) 90x magnified view of  $m/z$  range 205-240. C) Full mass spectrum.

One approach to determine the extent of reactive sputtering is by examining the metal adducts that form in the discharge. For example, Figure 4-2B is a 90x magnified view of  $m/z$  region 205-240. This region displays the gold adducts  $\text{Au}^{16}\text{O}^+$  and  $\text{Au}^{16}\text{O}_2^+$  located at  $m/z$  213 and 229, respectively. The low signal intensity of the gold adducts

indicates a low extent of reactive sputtering. As stated by Roth,<sup>119</sup> if impinging ions and target atoms form molecules and are observed then chemical sputtered may be inferred.

Little information exists pertaining to the relationship between the molecular oxygen ion and sputtered analyte ion. A short communication reports<sup>99</sup> that the main ion in the negative glow is  $O_2^+$ , yet information on the sputtered analyte ion is not reported. The oxygen metastable energy levels are inefficient for ionizing gold atoms, and this may contribute to the two-fold decrease in  $Au^+$ .

Additional factors contributing to a reduced gold signals in an oxygen plasma include lower molecular weight differences and low energy metastable species. The metastable states of oxygen are 0.98 eV, 1.63 eV, and three states between 4.2 eV and 4.5 eV. These energy levels are over two times lower in energy than argon metastable states. Oxygen metastables are deficient in energy to ionize a gold atom, which requires at least 9.2 eV of energy. A loss of metastable contribution to plasma ionization (i.e., Penning ionization) would significantly affect analyte ion signals. The following section presents data for mixed-gas plasmas.

**Effect of Gas Concentration on Ionization.** From the data reported in the previous section, obvious changes occur when the inert plasma gas is replaced by a more reactive, diatomic gas. To examine the plasma dynamics changes taking place as argon is systematically replaced with oxygen, Figure 4-3 illustrates the changes in ion signals for a dcGD. Signal intensity of  $O_2^+$ ,  $O_2H^+$ ,  $Ar^+$ ,  $ArH^+$ , and  $Au^+$  are monitored as a function of percentage oxygen in argon. A constant current and pressure are maintained for the various mixed-gas plasmas.

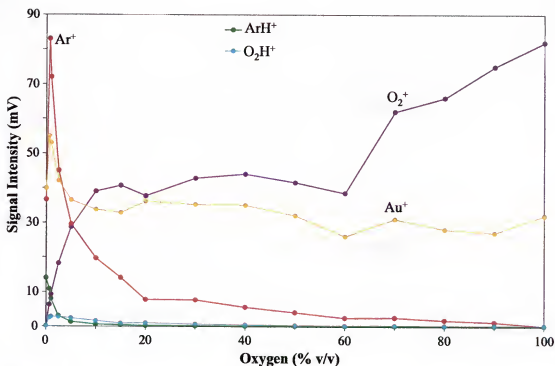


Figure 4-3 A plot of the relationship between ion signal intensities and the oxygen content in a mixed argon-oxygen direct current glow discharge. Oxygen content ranges from 0-100%.

In Figure 4-3, distinct changes take place for the gas ions as increasing amounts of oxygen are added to the inert gas medium, yet the gold ion signal experiences little change. Argon and gold ion signals surprisingly rise slightly with the first small increment of oxygen (< 1%), before dropping as more oxygen is added. The gold ion signal decreases to about the 10% oxygen level, but remains fairly constant at mixtures of increasing oxygen content. The gas species show a different trend. Significant changes occur in the 0-20% oxygen range (Figure 4-3). The  $\text{Ar}^+$  signal decreases by 8 fold with the addition of 20% oxygen, as it is replaced by  $\text{O}_2^+$  which continues to increase up to 100% oxygen. As the  $\text{ArH}^+$  signal decreases there is a slight increase in the  $\text{O}_2\text{H}^+$  ion signal, possibly due to a proton transfer reaction. In an rf discharge, Purdes et. al. report a continual increase (1000 fold) in the  $\text{O}_2^+$  signal from zero to 7.5% oxygen addition to

argon. The  $\text{Cu}^+$  ion signal increases slightly with  $\sim 1\%$   $\text{O}_2$  followed by a gradual decrease with increasing amounts of oxygen. Figure 4-4 illustrates the changes in ion signals between 20%  $\text{O}_2$  (A and B) and 80%  $\text{O}_2$  (C and D) plasmas. These mass spectra correlate with the data in Figure 4-3.

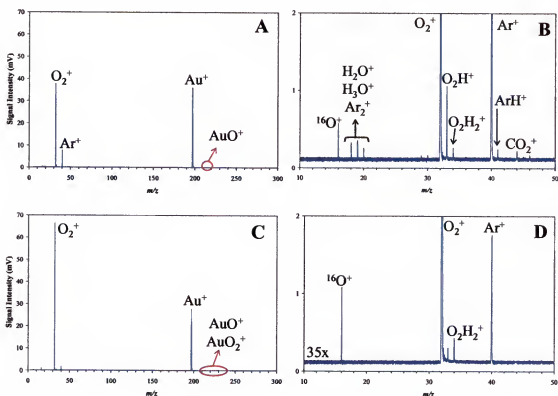


Figure 4-4 Direct current glow discharge mass spectra of A) 20%  $\text{O}_2$ , B) 20%  $\text{O}_2$ , 35x magnified  $m/z$  region 10-50, C) 80%  $\text{O}_2$ , and D) 80%  $\text{O}_2$ , 35x magnified  $m/z$  region 10-50.

The direct current glow discharge data for argon-oxygen plasmas serve as reference spectra for comparison to results in the microsecond pulsed mode of operation. Since the small change in the gold ion signal indicates little or no chemical sputtering, gold was studied initially in the pulsed studies.

### Microsecond Pulsed Glow Discharge: Comparison of Ar and O<sub>2</sub>

Previous studies report that oxygen acts as a quenching agent in a direct current glow discharge, which was determined by the drastic reduction of the argon atom (and ion) emission signals.<sup>83</sup> Due to the limitations of emission spectrometry, certain ions such as the molecular oxygen ion, were unable to be monitored. In addition, most known studies employed a copper sample, which easily forms an oxidation layer on the surface. Finally, oxygen has not been studied in the microsecond pulsed mode for positive ion mass spectrometry. With this information, an argon-oxygen mixed gas plasma was studied using the  $\mu$ sPGD-TOFMS system and a gold cathode to ensure little chemical sputtering.

**Pure Argon.** Similar to the dcGD experiments, argon was systematically replaced with oxygen until a pure oxygen discharge was maintained for a pulsed glow discharge. In pulsed mode, sputtering and ionization are enhanced as a result of high peak voltage and currents. For all the pulsed mode experiments in this dissertation, a 20  $\mu$ s pulse width and 600 Hz frequency is employed. The discharge frequency can be set between 100-1000 Hz; however, 600 Hz provided the most stable plasma.

A delay time plot is shown in Figure 3-7 for an argon  $\mu$ sPGD using a gold sample. This data can be viewed in an alternative mode to enhance the changes occurring over time. Figure 4-5 is a three-dimensional temporal plot corresponding to the data in Figure 3-7 of Chapter 3. This three-dimensional plot allows for a series of mass spectra to be viewed simultaneously and demonstrates the concept of temporal resolution. The green line correlates to the argon ion peaks and the yellow line to the gold ion signal. As described in Chapter 3, Ar<sup>+</sup>, ArH<sup>+</sup>, and Au<sup>+</sup> are the primary ions detected in an argon  $\mu$ sPGD providing a relatively simplistic spectrum with few interferences. The argon gas

ions are detected at early delay times, while sputtered analyte ions are detected at the longer delay times.

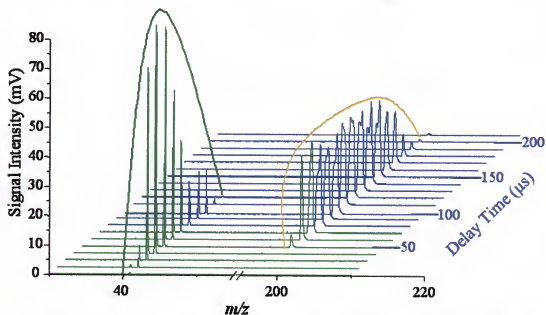


Figure 4-5 Waterfall plot of an argon microsecond pulsed glow discharge. The green line follows the trend of argon ions at early delay times, and the yellow line follows the trend of the gold ion at longer delay times. This plot corresponds to Figure 3-7 in Chapter 3. Sample material: gold.

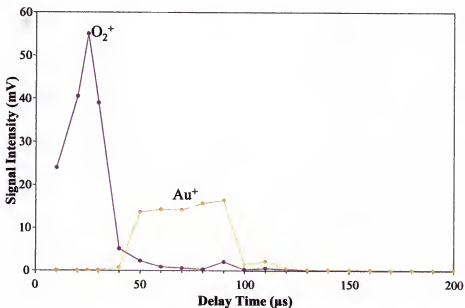


Figure 4-6 Delay time plot of 100% oxygen microsecond pulsed glow discharge. Sample material: high purity gold.

**Pure Oxygen.** A pure oxygen microsecond pulsed discharge produces a delay time plot as shown in Figure 4-6. The pure oxygen discharge was stable using the gold cathode. Similar to a pure argon discharge, the mass spectra which correspond to the delay time plot in Figure 4-6 are simplistic. Figure 4-7 displays a series of mass spectra at the delay times 10  $\mu$ s, 30  $\mu$ s, 50  $\mu$ s, and 90  $\mu$ s. At the 30  $\mu$ s delay time, a peak at  $m/z$  34 is evidence of either  $\text{O}_2\text{H}_2^+$  or  $^{16}\text{O}^{18}\text{O}^+$ ; however, the calculation of isotopic ratios by Isopro did not correspond to the ratio of  $^{16}\text{O}_2^+ / ^{16}\text{O}^{18}\text{O}^+$  as shown in Figure 4-7B. An FTICR mass spectrometer is required to determine which ion is dominant. In addition, the signal level of  $\text{O}_2^+$  is relatively close to  $\text{Ar}^+$  thus concluding that approximately the same number of gas ions is available to participate in ionization. The gold ion signal decreases by only approximately one-third compared to the argon discharge.

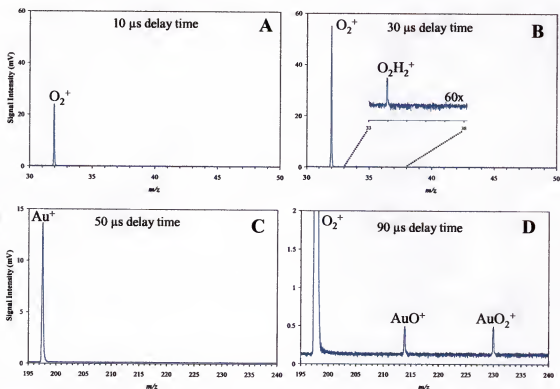


Figure 4-7. Mass spectra of a 100% oxygen microsecond pulsed glow discharge at various delay times. A) 10  $\mu$ s B) 30  $\mu$ s C) 50  $\mu$ s D) 90  $\mu$ s. Sample material: high purity gold.

**Effect of Gas Concentration on Ionization.** The influence of a controlled addition of oxygen to argon on the net sputtering rate and ion signals in a microsecond pulsed glow discharge has been investigated. The previous section compared an oxygen and argon discharge, which serve as reference spectra for the mixed gas plasmas. To prevent excessive chemical sputtering, a gold cathode was implemented for differentiation between plasma ionization processes and those associated with chemical sputtering. The oxygen content in the argon discharge ranged from 0-100%  $O_2$ . Total flow rate was maintained at  $150 \text{ mL}\cdot\text{min}^{-1}$ . The pulsed discharge voltage and pressure was maintained at  $-1750 \text{ kV}$  and  $\sim 3.5 \text{ Torr}$ , respectively.

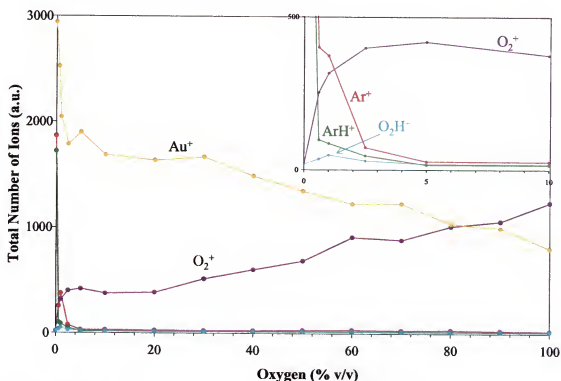


Figure 4-8 Total number of ions as a function of the oxygen content in an argon microsecond pulsed glow discharge. The inset is a zoomed-in view of 0-10%  $O_2$  magnified by a factor of 6. Sample material: high purity gold.

As argon is replaced with oxygen, noticeable changes in the ion signals are apparent. Figure 4-8 illustrates the trend of ion signals as a function of oxygen content.

The ions monitored in the discharge were  $O_2^+$ ,  $O_2H^+$ ,  $Ar^+$ ,  $ArH^+$ , and  $Au^+$ . The greatest drop in gold ion signal occurred within the first 5% of oxygen addition; however, the gold ion signal then remained relatively constant to 30%  $O_2$ , beyond which it continually decreased as the oxygen content in the gas plasma increased. Hecq included gold in a series of metals he studied to determine metal-oxide formation, but data comparing gold ions and gas ions was not shown.<sup>97,120</sup>

The gas species show a different trend. In the  $\mu$ sPGD, large ion signal changes occur between 0-5%  $O_2$ . With 1%  $O_2$  addition to an argon discharge, the argon ion signal is nearly depleted; however, the  $O_2^+$  ion signal increases significantly. Unlike the dcGD, the  $O_2^+$  signal increases to just below the  $Ar^+$  level (pure argon discharge) in the  $\mu$ sPGD. Both the  $Au^+$  and  $O_2^+$  ion signals have plateau regions between 10% and 20%  $O_2$ , which could be associated with initial surface layer formation and chemical sputtering.<sup>101</sup> The microsecond pulsed glow discharge provides a different type of plasma environment compared to a direct current discharge. In the  $\mu$ sPGD, the voltage-on time is 20  $\mu$ s with a short duty cycle, while the dcGD supplies a constant potential. Long off-times allows plasma equilibration and the gold cathode can become coated with surface layers of absorbed gases ( $O_2$ ).

According to Wagatsuma *et. al.*,<sup>80,83</sup> who used a copper cathode in dcGD, the copper atom emission signal is reduced by a factor of 800 with the addition of ~4% oxygen, which they attributed to oxide layer formation on the copper cathode. Silver, which is similar in reactivity to gold, showed that even 1%  $O_2$  addition decreases the silver atom emission intensity by half, but then reaches a steady state. So the response for gold that we observed is in keeping with literature trends, although the magnitude of

the changes is not comparable. What happens if copper and silver are subjected to a mixed oxygen-argon plasma with a microsecond pulsed glow discharged instead of the direct current mode? The following section examines the effect that alternative elements have in a  $\mu$ sPGD.

**Mixed Gas Plasma – Alternative Elements.** In the literature, oxygen has been shown to reduce the emission signals of both analyte and gas ions in a dcGD. Reactive sputtering of the copper (NIST 1113) and silver was studied by glow discharge mass spectrometry. Figure 4-9 illustrates the effect of 0-100%  $O_2$  addition to an argon  $\mu$ sPGD using a 95% copper-based sample (A) and a high purity silver sample (B). The surface on each sample was cleaned of possible oxide layer formation by polishing with emery paper and rinsing with ethanol. For each Ar- $O_2$  mixed-gas plasma analyzed, a clean section of the sample was sputtered.

Both silver ion signals ( $^{107}Ag^+$  and  $^{109}Ag^+$ ) show the greatest signal reduction with between 0-10%  $O_2$  in argon; however the silver ion signal remained relatively constant to 80%  $O_2$  followed by a slight decrease in intensity at 100%  $O_2$  (Figure 4-9B). The molecular oxygen ion signal experienced an initial sharp increase (5%  $O_2$ ), followed by a plateau region (5-20%  $O_2$ ), and then gradually increased as the oxygen content in the plasma gas increased. Both  $Ar^+$  and  $ArH^+$  are replaced with  $O_2^+$  with increasing amounts of oxygen. Silver reacts to an oxidizing atmosphere in a similar way to gold.

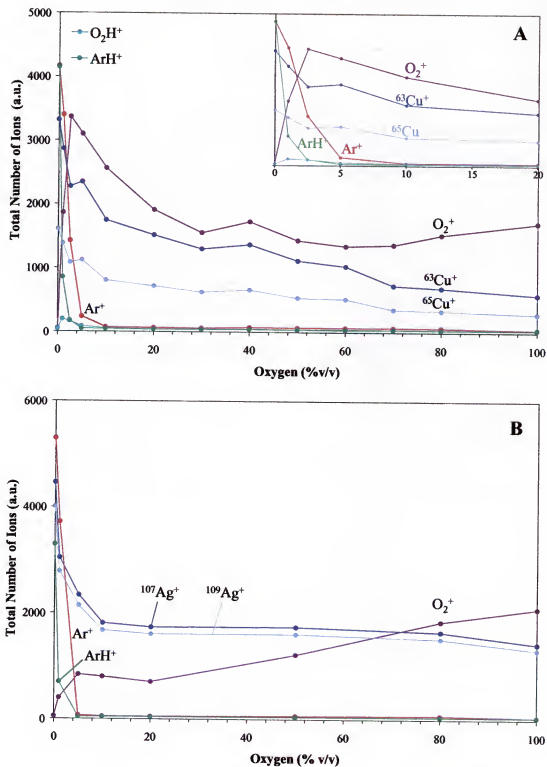


Figure 4-9 Total number of ions versus oxygen content in a  $\mu s$  pulsed argon glow discharge. The ions monitored are  $O_2^+$ ,  $O_2H^+$ ,  $Ar^+$ ,  $ArH^+$ , and the isotopes of copper and silver. A) Sample material: NIST 1113 B) Sample material: high purity silver.

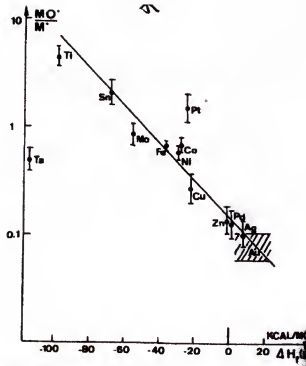


Figure 4-10 Log of  $MO^+/M^+$  as a function of the energy of formation of MO. (Ref. 97)

Silver and gold samples are considered relatively inactive elements when exposed to an oxidizing atmosphere; however, copper is known to readily form a visible oxide layer on the surface when left exposed to the atmosphere for an extended period of time. Evidence of chemical sputtering is the formation of metallic oxides ( $MO^+$  or  $MO_2^+$ ). Figure 4-10 illustrates the ratio of  $MO^+$  and  $M^+$  currents relative to the formation energy based on the reaction<sup>97</sup>



As shown in Figure 4-10, copper has a higher probability of forming an oxide compared to silver and gold, which have the lowest probability. Evidence of oxide formation on the sample surface is often a decrease in analyte ion signal accompanied by a decrease in the sputtering rate. Figure 4-9A reveals the effect of oxygen content in an argon plasma on the ion signals. With up to 5%  $O_2$  addition, the copper isotope ion

signals drastically decrease, yet the  $O_2^+$  signal reaches a maximum. The molecular oxygen ion follows  $^{63}\text{Cu}^+$  and  $^{65}\text{Cu}^+$  signal trend until 60%  $O_2$ ; the oxygen ion signal increases to the pure oxygen discharge.

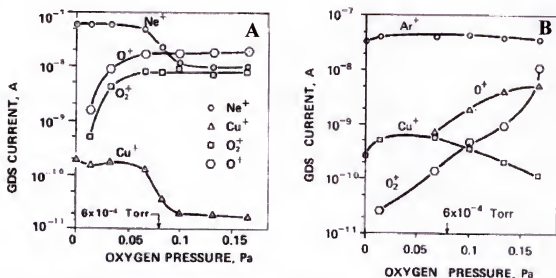


Figure 4-11 Ion currents versus oxygen pressure in A) oxygen-neon discharge and B) oxygen-argon discharge. Total pressure is 2 Pa. (Ref 101)

Figure 4-11 reveals the effect of oxygen content on an rf glow discharge with matrix gases neon (A) and argon (B).<sup>101</sup> The metastable states of neon are high enough to Penning ionize oxygen opposed to the inefficient transfer of energy from an argon metastable to oxygen. As the sputtered analyte ion decreases ( $\text{Cu}^+$ ) the  $\text{O}_2^+$  signal gradually increases. A reason for the decrease in analyte ion signals may involve the pulsed nature of the discharge, with its attendant short duty cycle, which causes relatively long off-times during which the plasma equilibrates, and the gold cathode becomes coated with surface layers of adsorbed gases/impurities that may influence sputtering.

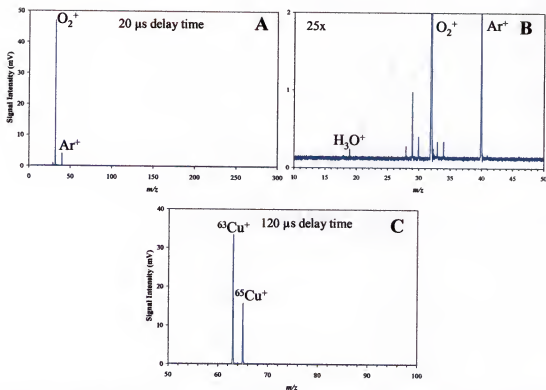


Figure 4-12 Mass spectra of a 20% oxygen glow discharge. A) 20  $\mu$ s delay time B)  $m/z$  region 10-50 at a 20  $\mu$ s delay time magnified 25x C) 120  $\mu$ s delay time. Sample material: NIST 1113.

Figures 4-12 and 4-13 are mass spectra of a 20% O<sub>2</sub> plasma and 100% O<sub>2</sub> plasma, respectively with a copper-based cathode. When comparing plot B of both figures, the low molecular weight ions associated with the gases, have changed considerably. A signal for Ar<sup>+</sup> remains at 20% O<sub>2</sub>; however, ozone and O<sub>4</sub><sup>+</sup> are formed in a pure oxygen discharge. The likelihood of O<sub>4</sub><sup>+</sup> formation in an oxygen discharge is high due to the large concentration of O<sub>2</sub><sup>+</sup> and neutral oxygen molecules. As described in Chapter 2, the oxygen tetramer forms through association. Oxygen also forms an adduct with copper as shown in Figure 4-12B in high oxygen concentrations. The ion trend as a function of oxygen content and the mass spectra revealing differences in ions only partly explain the effect of oxygen addition on the plasma.

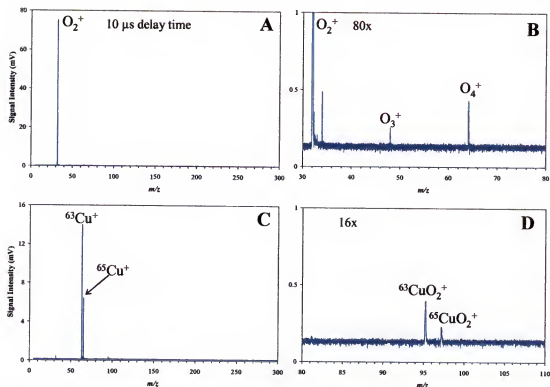


Figure 4-13 Pure oxygen microsecond pulsed glow discharge mass spectra. A) 10  $\mu$ s delay time, B) 10  $\mu$ s delay time and magnified 80x, C) 110  $\mu$ s delay time, and D) 110  $\mu$ s delay time magnified 16x.

**Sputter Rate.** In theory, each element should respond to oxygen to a different extent. Heller<sup>98</sup> reported on a sputtering model for a dc glow discharge that included oxide formation on a target surface. In the model, a sharp decrease in sputter rate can occur at definite oxygen concentrations; thereby indicating spontaneous oxide formation on the sample surface. An oxide layer is related to a chemical surface reaction on the sample. Oxidation rate on a metal is expressed as

$$Y(x) = \rho \frac{dx}{dt} = A(p)e^{\frac{-x}{B}} \quad (4-2)$$

In this equation  $Y(x)$  is the oxidation rate ( $\text{g}\cdot\text{cm}^{-2}\cdot\text{s}^{-1}$ ),  $\rho$  is the mass density of the oxide,  $A$  is a function of oxygen pressure ( $p$ ), and  $B$  is a constant based on target material. Sputtering rate is denoted by  $R$ . If the oxidation rate ( $Y$ ) is less than the sputter rate ( $R$ ),

then theoretically no oxide will form on the target surface; type 1 configuration. A type 2 configuration is defined as  $Y > R$  in which an oxidation layer forms. These two configurations are depicted in Figure 4-14 where sputter rate is plotted as a function of partial pressure  $O_2$ . Plot A is typical of no oxide layer formation (Type 1) and plot B is typical of oxide layer formation (Type 2).

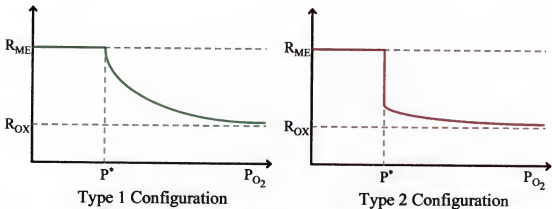


Figure 4-14. Type 1 and type 2 configurations to determine the presence of an oxide layer. Sputter rate as a function of partial pressure of  $O_2$ . (Adapted from Heller<sup>98</sup>)

If sputter rate is a determination of reactive (chemical) sputtering, then it is important to monitor what is occurring in the microsecond pulsed glow discharge source. Figure 4-15 is a figure of net sputter rate for pulsed mode as a function of oxygen content for gold, silver, and copper targets. Due to the instability of the discharge greater than 20%  $O_2$  with a copper cathode, the net sputter rate could not be determined. The net sputter rate of gold correlates with the  $Au^+$  ion signal trend as shown in Figure 4-8; however, the sputter rate trend more closely resembles a Type 2 configuration indicating an oxide layer. As mentioned previously, the voltage-on time for the  $\mu sPGD$  is 20  $\mu s$  with a short duty cycle, while the dcGD supplies a constant potential. These long off-times allow plasma equilibration and could result in oxidation of the gold surface with

layers of absorbed gases ( $O_2$ ). This is also true for silver and copper targets. In an rf glow discharge, Fernández et. al. report that 1%  $O_2$  reduces the nickel sputter rate by three-fold and remains constant up to 10%  $O_2$ . As shown in Figure 4-10, nickel has a slightly higher energy of oxide formation than copper.

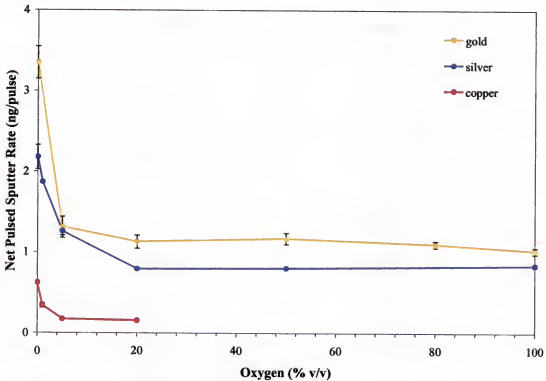


Figure 4-15 Net pulsed sputter rate (ng/pulse) of gold, silver, and copper as a function of oxygen content.

With increasing amounts of oxygen, the discharge current increases for all elements analyzed. A higher discharge current often corresponds to a more energetic plasma, but is not a direct indication of the sputter rate. Generation of negative ions on the target surface can contribute to an increase in discharge current. The negative ions would be accelerated away from the cathode and thus not participate in sputtering. Since the sputter rate decreases, fewer sputtered atoms are available for ionization. As shown with gold, silver, and copper, the signals decrease with increasing amounts of oxygen.

**Penning Ionization.** A decrease in the sputtered atom ion signals is partly due to negative oxygen ion formation, yet the argon ion concentration is also decreasing. Lounsbury<sup>100</sup> has reported that addition of 1% O<sub>2</sub> to argon decreases the metastable argon concentration in an rf glow discharge. A decrease in the metastable argon population results in the reduction of Penning ionization because this ionization mechanism is not possible in an oxygen plasma. The energies of the oxygen metastable states (0.98 eV, 1.63 eV and three states between 4.2 and 4.5 eV) are below the ionization potentials of most metals.<sup>97</sup> This leaves electron transfer ionization to dominate in the oxygen discharge.

**Electron Transfer Ionization.** Since the transfer of energy from an oxygen metastable to a sputtered atom is inefficient, electron impact ionization or electron transfer ionization must dominate. The ionization potential of molecular oxygen (12 eV) is greater than the ionization energy of most metals and their oxides. If atomic oxygen is present in the discharge (IP: 13.5 eV), it could contribute to electron ionization.

### Conclusions

Oxygen is a known reagent gas used successfully for negative ion mass spectrometry. In our laboratory negative ion direct current glow discharge mass spectrometry has been employed using oxygen to examine the potential of the GD to generate negative ions.<sup>95</sup> Current studies reveal that discharge current increases as a function of oxygen content, which is partly due to a large population of negative oxygen ions; however, the potential of oxygen for positive ion mass spectrometry in a  $\mu$ sPGD was investigated in the present research.

In a pure oxygen plasma, a large population of positive molecular oxygen ions is generated, which parallels the population level of argon ions in a pure argon plasma. Argon ions contribute heavily to the ionization of sputtered analyte ions through Penning ionization, yet the low metastable energy levels for molecular oxygen are inefficient to promote Penning ionization. Ion populations of the sputtered analyte atoms of gold, silver, and copper, decrease by approximately half in an oxygen discharge compared to argon. Decreases in ion populations result from a loss of Penning ionization. Electron impact ionization compensates for the loss of metastable ionization. The decrease in analyte ion signals is also due in part to oxide layer formation on the target surface. In the microsecond pulsed glow discharge, the voltage-on time is 20  $\mu\text{s}$  with a short duty cycle, while the dcGD supplies a constant potential. These long off-times allow plasma equilibration and the gold cathode can become coated with surface layers of absorbed gases ( $\text{O}_2$ ); therefore, there are lower net sputter rates and analyte ion populations.

With the large molecular oxygen ion population generated by a  $\mu\text{sPGD}$ , opportunities exist for supplementing argon with oxygen as the plasma gas. Further investigation is required to determine the extent of analytical utility.

## CHAPTER 5

### EXAMINATION OF THE ROLE OF CHEMICAL IONIZATION IN A MICROSECOND PULSED GLOW DISCHARGE

#### Introduction

Chemical ionization involves the process of gas phase ion/molecule reactions. For chemical ionization (CI), a reaction gas is required that produces a set of ions (either nonreactive or slightly reactive with the reagent gas), which are capable of reacting with other molecules. Stable ions of the reaction gas (reagent ions) will react with an analyte molecule producing a mass spectrum of ions characteristic of the molecule. The advantages of chemical ionization are molecular mass determination, structure elucidation, and identification.<sup>105,118</sup>

Various reaction gases are applicable for chemical ionization; however, this discussion and research is restricted to methane. Methane is a suitable reaction gas commonly employed for CI mass spectrometry. For dc glow discharge mass spectrometry (and emission spectrometry), methane has been used to study the role of Penning ionization as an ionization mechanism for sputtered atoms.<sup>72,112</sup> Since methane acts as a quenching agent in a low pressure argon glow discharge, it is employed to study the argon metastable population. Methane may act as a quenching agent, in effect reducing the analyte ion population, yet the utility of methane as a CI reaction gas in a low pressure microsecond pulsed glow discharge has not been investigated. Enhancements in analyte emission have been noted in an inductively coupled plasma by

methane and propane addition; the proposed mechanism involves the formation of CO thus reducing the metal-oxide species.<sup>121,122</sup>

With the possibility of chemical ionization reactions and signal enhancement, methane was examined as a component in the argon plasma gas of a low pressure microsecond pulsed glow discharge with time-of-flight mass spectrometry. In the following research, 0-5% CH<sub>4</sub> was introduced in an argon plasma gas. The type of ions produced and changes in ion signals relative to methane content were studied. For possible chemical ionization contributions, toluene vapor was continuously added to the discharge to observe the possible CI effects.

## **Experimental**

### **Glow Discharge Time-of-Flight Mass Spectrometer**

The Grimm-type glow discharge (GD) source configuration employed in this research was operated in the microsecond pulsed time regime. Details of the source were described previously in Chapter 1 and Chapter 3 of this document. A commercial time-of-flight mass spectrometer (Renaissance, LECO Corporation, St. Joseph, MI) is operated in the same mode as described in Chapter 2. Refer to Figure 1-9 and 1-10 for the glow discharge source configuration and TOFMS setup, respectively. Operating conditions for the GD source and mass spectrometer were listed in Tables 3-1 and 3-2 of Chapter 3.

### **Gas Delivery System**

As described previously, gases are mixed using a four-channel readout module in combination with three mass flow controllers (MFCs). The gas delivery system allows

control of the gas flow rates and therefore control of gas composition. Three MFCs are available and each calibrated for a specified gas. A  $200 \text{ mL}\cdot\text{min}^{-1}$  argon MFC is designated for argon-only use. Of the three MFCs available, none are calibrated for methane. However, as described in Chapter 3, a mass flow controller can be “recalibrated” permitting the use of other gases. The mass flow controllers are calibrated for a pure gas. For gas mixtures, such as a 5%  $\text{CH}_4$ /95% Ar gas mixture, a gas correction factor for a mixture ( $\text{GCF}_M$ ) is necessary. Equation 3-2 was used to calculate the  $\text{GCF}_M$  of 5%  $\text{CH}_4$ /99% Ar gas mixture. The scaling control factor, which is the product of the gauge factor and gas correction factor, was calculated and adjusted on the four-channel readout module. The nitrogen mass flow controller was used for the methane gas mixture due to the higher flow capabilities.

### Plasma Gas

In order for a glow discharge to operate properly, a gas medium is essential. Sputtering, ionization, and discharge stability are all influenced by the type and grade of plasma gas employed. The matrix gas employed in this research is a high purity argon (5 Grade, Strate Welding, Gainesville, FL). A pre-mixed gas of 5% methane and 95% argon was used (P-5 Mixture, Praxair, Gainesville, FL) to introduce low concentrations of methane into the discharge. The methane mixture was diluted with the high purity argon. In this research, argon was systematically replaced with the argon-methane mixture until a 5% methane plasma was sustained. Methane concentrations ranged from 0-5%  $\text{CH}_4$  and the total gas flow rate was maintained at  $150 \text{ mL}\cdot\text{min}^{-1}$  by utilizing the gas delivery system.

### **Sample Material**

As described in Chapter 3, three types of cathode material were used in these studies: gold, silver, and copper. The gold (Gold Target, 99.99% Pure, Kurt J. Lesker, Clairton, PA) and silver (Silver Target, 99.99% Pure, Kurt J. Lesker, Clairton, PA) are high purity blocks of metal. The copper cathode is a certified standard reference material, NIST 1113. NIST 1113 is 95.03% Cu and 4.80% Zinc.

The same procedure was employed for sputter rate determination as described for the nitrogen studies in Chapter 3. Samples for obtaining sputter rates were high purity elemental foils (gold, silver, copper) approximately 1 mm thick (Puratronic, 99.9%, Alfa Aesar, Ward Hill, MA). The foils were cut into small discs 15 mm in diameter and weighed with an analytical microbalance (Model: M2P, Sartorius, Corp., Edgewood, NY). To calculate the weight difference, the foils were weighed prior to and after sputter analysis. Each element was sputtered three times for 30 minutes, using a new sample for each analysis.

## **Results and Discussion**

### **Direct Current Glow Discharge: Comparison of Ar and 5%CH<sub>4</sub>**

Low pressure glow discharge studies introducing methane into the plasma gas have been studied to determine the contribution of Penning ionization in the discharge. Methane has been reported to quench the argon signals and consequently, the analyte ion populations also decrease. Despite these reports, a methane-argon discharge was studied in this present research to investigate the possibility of methane as a chemical ionization gas in glow discharge. Initial investigations utilized the direct current glow discharge to

establish the effect of methane content on the steady state ion population. The type and intensity of gas ions were monitored as a function of methane gas content.

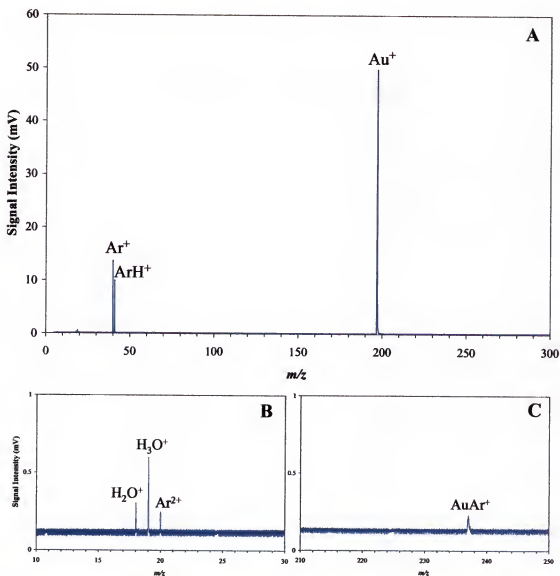


Figure 5-1 Mass spectra of an argon direct current glow discharge with time-of-flight mass spectrometry detection. A) Full mass spectrum B) 60x magnified view of  $m/z$  10-30 and C) 60x magnified view of  $m/z$  210-250. Sample material: high purity gold.

**Pure Argon.** For the present investigation, a direct current argon discharge was analyzed initially. As in the nitrogen and oxygen gas studies, gold was initially employed as the target material to eliminate any surface interactions that might occur with more

reactive targets. A constant voltage (1 kV) and current (8 mA) were maintained for the dcGD methane-argon mixed gas experiment. Figure 5-1 shows the resulting spectra of an argon dcGD using a gold target. This mass spectrum serves as a reference for the pulsed glow discharge experiments that follow. Part A is the full mass spectrum and parts B and C are 60x magnified views of the  $m/z$  regions 10-30 and 210-250 respectively. As reported previously, the main ions in the discharge are  $\text{Ar}^+$ ,  $\text{ArH}^+$ , and  $^{197}\text{Au}^+$ . The minor ions detected in this discharge are  $\text{H}_2\text{O}^+$ ,  $\text{H}_3\text{O}^+$ ,  $\text{Ar}^{2+}$ , and  $\text{AuAr}^+$ . The ions detected in the pure argon discharge are the same as those for a pure argon discharge found in Chapter 3 and 4; however, the ratios of the signals changed. This is due to slightly different discharge conditions.

Argon provides an inert stable environment for a glow discharge. What happens if 5% methane is added to the argon matrix?

**5% Methane in Argon.** Lower concentrations of methane are added to argon for effective reagent ion formation in chemical ionization. The major ions generated by a modified electron ionization source (ion gun)<sup>123</sup> at 1 Torr total pressure are  $\text{CH}_5^+$ ,  $\text{C}_2\text{H}_5^+$ , and  $\text{C}_3\text{H}_5^+$  when the most widely used reagent gas is used (i.e., methane). Reagent ions produced at lower yields are  $\text{C}_2\text{H}_4^+$  and  $\text{C}_3\text{H}_7^+$ .<sup>104,105,118,124</sup> The source pressure and other instrument variables determine the reagent ion yields. In the following experiments, a percentage of argon was replaced with methane.

The effect of a 5%  $\text{CH}_4$  plasma gas on a dcGD (gold target) is illustrated in Figure 5-2. Note that the y-axis scale is magnified 40 times compared to Figure 5-1. With 5% methane added to argon, the gold ion signal decreases by a factor of 50 compared to a pure argon plasma; therefore, the dominant ion in the 5% methane discharge is  $\text{C}_2\text{H}_5^+$  at

$m/z$  29 as shown in Figure 5-2A. Of the gas ions detected,  $\text{Ar}^+$  has the second most intense peak. This is to be expected since 95% of the gas mixture is argon. Other methane derivatives present in the discharge are  $\text{C}_2\text{H}_4^+$ ,  $\text{C}_3\text{H}_3^+$ , and  $\text{C}_3\text{H}_5^+$  as illustrated in Figure 5-2B. Table 5-1 compares the ions formed under convention CI conditions<sup>118</sup> and 5%  $\text{CH}_4$  glow discharge conditions. The most significant difference is that  $\text{CH}_5^+$  is not detected in a dcGD.

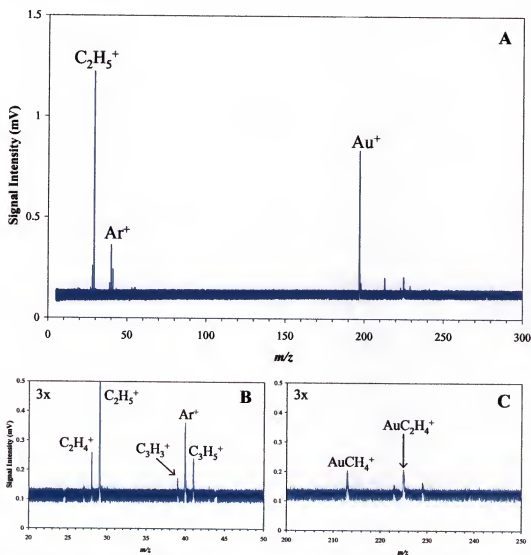


Figure 5-2 Mass spectra of a 5% methane in argon direct current glow discharge with time-of-flight mass spectrometry detection. A) Full mass spectrum B) 3x magnified view of  $m/z$  20-50 and C) 60x magnified view of  $m/z$  210-250. Sample material: high purity gold.

Table 5-1 Comparison of methane ions in a conventional CI mass spectrum and a 5% CH<sub>4</sub> in argon direct current glow discharge mass spectrum.

Conventional CI	5% CH <sub>4</sub> GD
CH <sub>5</sub> <sup>+</sup> (48%)	C <sub>2</sub> H <sub>5</sub> <sup>+</sup>
C <sub>2</sub> H <sub>5</sub> <sup>+</sup> (41%)	C <sub>2</sub> H <sub>4</sub> <sup>+</sup>
C <sub>3</sub> H <sub>5</sub> <sup>+</sup> (6%)	C <sub>3</sub> H <sub>5</sub> <sup>+</sup>
C <sub>2</sub> H <sub>4</sub> <sup>+</sup>	C <sub>3</sub> H <sub>3</sub> <sup>+</sup>
C <sub>3</sub> H <sub>7</sub> <sup>+</sup>	

Similar to the argon discharge, the gas species form adducts with the sputtered atom. Even though the plasma gas is 95% argon, the major adduct ion is AuCH<sub>4</sub><sup>+</sup>. Also present in the mass spectrum at  $m/z$  225 is the gold adduct AuC<sub>2</sub>H<sub>4</sub><sup>+</sup>. The C<sub>2</sub>H<sub>4</sub><sup>+</sup> methane molecule is also found in the lower molecular weight region. The relative signal intensities of the gold-methane adducts are similar in intensity to AuAr<sup>+</sup> in a pure argon GD. In a methane-argon dc glow discharge, the mass spectra remain fairly simplistic compared to the pure argon data; however, the signal intensities of all ions decrease by a factor of 25 or more. The following section presents the effect of methane concentration on ion signals in a dcGD.

**Effect of Gas Concentration on Ionization.** The previous sections reported the common ions formed in a dc glow discharge with the discharge gases argon and 5% CH<sub>4</sub> (in argon). Obvious changes occur in the discharge when 5% CH<sub>4</sub> is added to the argon plasma gas. Between 0-5% methane, what methane content has the greatest effect on the ion signals? In these experiments, the discharge conditions are the same as those stated in the pure argon segment: constant voltage and current and a 0.2 Torr pressure variation. Total gas flow rate was maintained at 150 mL·min<sup>-1</sup>. Figure 5-3 illustrates the change in

ion signals versus methane content in a dc glow discharge. Argon was systematically replaced with methane until a five-percent methane discharge was established.

As shown in Figure 5-3A, the gold ion signal is drastically reduced within the first 3% methane addition at which point the ion signal is at the level of impurities. Contributions from  $C_2H_3^+$ ,  $C_2H_4^+$ ,  $C_2H_5^+$ , and  $C_3H_3^+$  begin to emerge and dominate as gas ions with less than one-percent methane addition. The other ions monitored as a function of methane content are  $Ar^+$ ,  $ArH^+$ , and  $Au^+$ . As methane fragmentation products begin to emerge in the mass spectrum, the argon gas ions disappear. Figure 5-4 displays ions in the lower molecular weight region ( $m/z$  10-60) for 0.5, 1, 2, and 3%  $CH_4$ . The strong signal at  $m/z$  32 ( $O_2^+$ ) in Figure 5-4B is likely due to a poor seal between the sample and cathode plate. From 0.5% to 2%  $CH_4$ , the argon signal gradually decreases, but appears to reach a steady state level by 3%  $CH_4$ . The same methane gas ions appear at all four concentrations and at relatively the same levels. In the literature, a report<sup>107</sup> lists methane-related peaks detected in an rf methane discharge. The few methane derivatives detected (Figure 5-4) in this research are part of the ion list in the report by Evans.

An increase in methane concentration parallels a decrease in the gold ion population, yet gold adducts with methane become more prevalent as illustrated in Figure 5-5. The methane-gold adducts are slightly larger in intensity relative to  $AuAr^+$  in a pure argon discharge. As stated previously, methane acts as a quenching agent to argon. The results in the dc glow discharge section act as reference spectra for the microsecond pulsed glow discharge data. The final section introduces what happens in a pulsed discharge with methane addition.

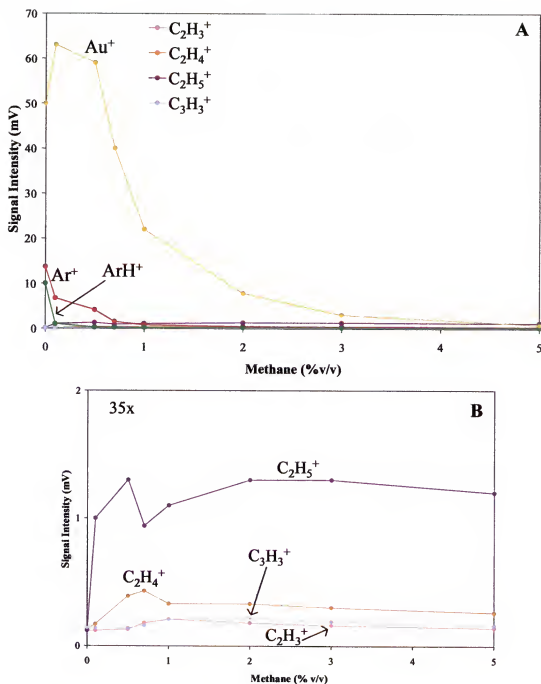


Figure 5-3 The effect of methane addition to an argon dc glow discharge. Methane concentration ranges from 0-5%  $\text{CH}_4$ . A) The primary ions are indicated. B) 35x zoomed in view of plot A.

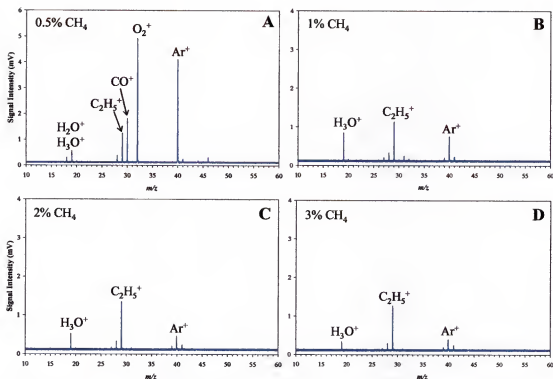


Figure 5-4 Direct current glow discharge mass spectra of A) 0.5% methane, B) 1% methane, C) 2% methane, and D) 3% methane.  $m/z$  region 10-60.

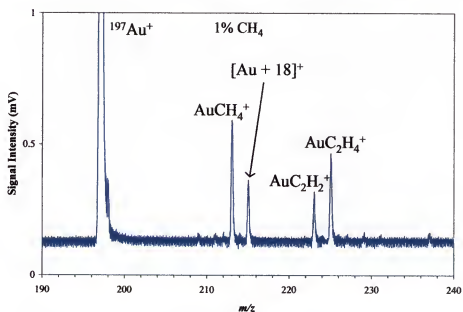


Figure 5-5 Direct current glow discharge mass spectrum of 1%  $\text{CH}_4$  in an argon matrix depicting the  $m/z$  region 190-240 magnified 60x. This figure correlates to Figure 5-3. Sample material: high purity gold.

### Microsecond Pulsed Glow Discharge: Comparison of Ar and 5% CH<sub>4</sub>

A direct current glow discharge provides information on the steady-state level of reagent ions; however, the pulsed glow discharge offers increased sputtered atom density and therefore increased ion (or emission) intensity.<sup>46,125</sup> By pulsing the discharge, discrimination of gas ions and sputtered species is possible. Ions are detected at specific times during the pulse cycle. In the  $\mu$ sPGD-TOFMS used in this research, data is collected between a 10-300  $\mu$ s time period. Gas species are found at earlier delay times while sputtered species are located at higher delay times. A “dc like” spectrum is found at delay times between the two species. Since the pulsed discharge is known to increase ion intensities (compared to dc), methane addition to a pulsed discharge was investigated.

**Pure Argon.** Before making definitive conclusions about the results from the dc glow discharge, it is beneficial to observe the effect of a pulsed glow discharge. For the pulsed glow discharge experiments in the remainder of the document, a 600 Hz frequency and 20  $\mu$ s pulse width are used to maintain the same duty cycle. Pulsed voltage is -1750 V and a constant pressure is maintained.

Experimental data for a pure argon  $\mu$ sPGD was reported in the previous chapters. Refer to Figures 3-7 and 4-5 for a delay time plot and waterfall plot of an argon discharge. Each corresponding section described the argon plasma, so it is not necessary to restate the entire sections. As a review, Ar<sup>+</sup>, ArH<sup>+</sup>, and Au<sup>+</sup> are the dominant peaks in an argon glow discharge and the plasma was stable. Signal intensities of these species vary with respect to delay time.

**5% Methane.** Methane is a common CI reagent gas for conventional chemical ionization experiments. A previous study<sup>109</sup> compares a 3% CH<sub>4</sub> (in argon) direct current glow discharge to a conventional chemical ionization mass spectrum, also 3% CH<sub>4</sub>. A

direct insertion probe (pin-type cathode) was employed in these studies using 1.6 Torr and the low voltage of 500 V. A pin-type cathode differs from a Grimm-type GD by the anode-cathode distance, plasma volume, and orientation of sample. The dcGD mass spectrum displays hydrocarbon peaks up to very high mass of relatively high intensity (Figure 5-6). Little was mentioned about the sputtered atoms. As shown in the previous section, very few peaks associated with methane are displayed in the mass spectra (Figure 5-4); hence, the array of hydrocarbon peaks does not form (Figure 5-6). Does changing the voltage parameter affect the hydrocarbon series associated with methane?

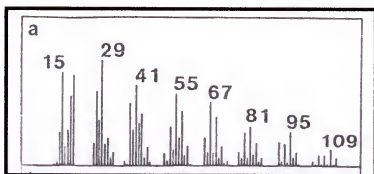


Figure 5-6 Direct current glow discharge mass spectrum of 3% CH<sub>4</sub> in argon (1.6 Torr, V = 500 V). (Ref. 109)

In this section a 5% CH<sub>4</sub> plasma gas is interrogated with a high voltage pulse of -1750 V at a duty cycle of ~1%. Figure 5-7 is a delay time plot of a 5% CH<sub>4</sub> in argon microsecond pulsed glow discharge. Discharge ions are monitored as a function of time. The major species are C<sub>2</sub>H<sub>5</sub><sup>+</sup> and C<sub>3</sub>H<sub>3</sub><sup>+</sup>. At early delay times the C<sub>2</sub>-based molecule dominates; however, the C<sub>3</sub>-based molecule is the predominant ion at the higher delay times. A possible explanation for the C<sub>2</sub>-based and C<sub>3</sub>-based molecule trend is that C<sub>2</sub>H<sub>5</sub><sup>+</sup> reacts with CH<sub>4</sub> to form a C<sub>3</sub>-based molecule. The proposed reaction is expressed as



The increase in hydrogen as a by-product could account for the significant decrease in sputtered analyte ion signal ( $\text{Au}^+$ ), but this will be described later in the document. The sputtered analyte is usually prevalent at these higher delay times, yet the  $\text{Au}^+$  signal is close to background level. Typical  $m/z$  40 and 41 peaks correspond to  $\text{Ar}^+$  and  $\text{ArH}^+$ , but methane is known to quench these species so most likely the masses are associated with methane ( $\text{C}_3\text{H}_4^+$  and  $\text{C}_3\text{H}_5^+$ ).

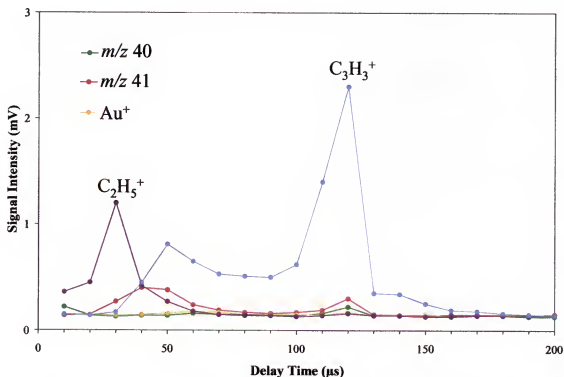


Figure 5-7 Microsecond pulsed glow discharge delay time plot of 5%  $\text{CH}_4$  in argon. Sample material: high purity gold.

Figures 5-8 and 5-9 are mass spectra of a 5%  $\text{CH}_4$  glow discharge at the delay times of 30  $\mu\text{s}$  and 120  $\mu\text{s}$  respectively. Gas ions are prevalent at the earlier delay times (e.g., 30  $\mu\text{s}$ ) as shown in Figure 5-8. The labeled peaks are proposed molecules. Similar to Figure 5-4 (dcGD), the dominant ion is  $\text{C}_2\text{H}_5^+$ . According to Field and Munson,<sup>124</sup>  $\text{C}_2\text{H}_5^+$  is the second most abundant ion in a chemical ionization source at 2 Torr. Other

methane fragmentation peaks are not dominant because  $\text{C}_2\text{H}_5^+$  does not react appreciably with methane.

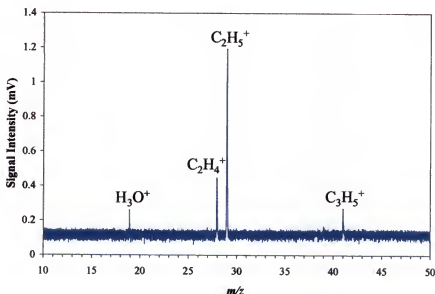


Figure 5-8 Microsecond pulsed glow discharge mass spectrum of 5%  $\text{CH}_4$  in argon at a  $30\ \mu\text{s}$  delay time.  $m/z$  region 10-50. Sample material: high purity gold.

As illustrated in Figure 5-7, gas ions associated with methane are detected at earlier delay times. After the discharge pulse is terminated, there is the possibility of additional reactions (Figure 5-9). Figure 5-9 includes a series of mass spectra for 5%  $\text{CH}_4$  in argon collected at a  $120\ \mu\text{s}$  delay time. At longer delay times, analyte ions are commonly prevalent. Plot B and C are magnified views of plot A. At the  $120\ \mu\text{s}$  delay time  $^{197}\text{Au}^+$  is not present, and  $\text{C}_3\text{H}_3^+$  predominates over all other ions. With respect to Figure 5-9B and C, it is evident that reactions continue after pulse termination. This is evident since gas ions are detected at longer delay times. Additionally, gold adduct peaks are also prevalent at 5%  $\text{CH}_4$  (Figure 5-9C) even though  $\text{Au}^+$  is not detected. After pulse termination, an influx of  $\text{CH}_4$  molecules is available (continuous gas flow) to further react with methane associated ions. This could contribute to an increase in the  $\text{C}_3$ -based and  $\text{C}_4$ -based ions, which form adducts with gold.

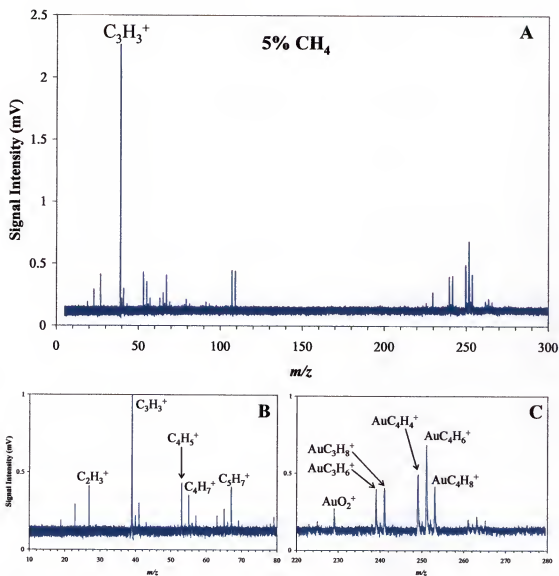


Figure 5-9 Microsecond pulsed glow discharge mass spectra in 5%  $CH_4$  at a 120  $\mu s$  delay time. A) Full mass spectrum, B)  $m/z$  10-80 magnified 3x, and C)  $m/z$  230-280 magnified 3x. Sample material: high purity gold.

**Effect of Gas Concentration on Ionization.** Described in the previous two sections are a pure argon and a 5%  $CH_4$  microsecond pulsed glow discharge with time-of-flight mass spectrometry detection. By pulsing the applied voltage, temporal discrimination of ions is possible and as described above, affects the ionization schemes. The greatest difference between the argon and 5%  $CH_4$  discharge is the loss of the gold ion. In this section, the effect of methane concentration on the gold ion signal and

methane related species will be analyzed. Additionally, the target material was also investigated in response to a methane discharge.

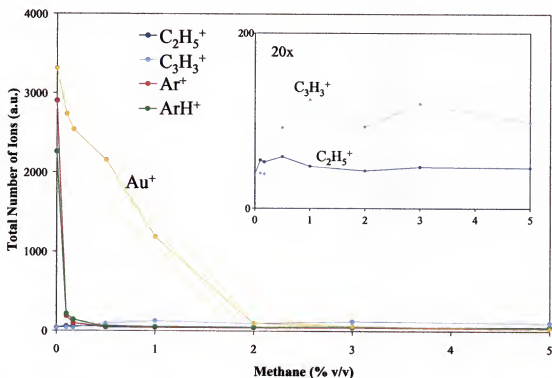


Figure 5-10 Microsecond pulsed glow discharge plot of ion population versus methane content in argon. Methane concentration ranges from 0-5%. Sample material: high purity gold.

To continue from the previous two sections, gold is used as the target material. The methane content in the discharge ranged from 0-5% and the total flow rate was maintained at  $150 \text{ mL} \cdot \text{min}^{-1}$ . Figure 5-10 illustrates ion signal intensity with respect to methane content in argon. Between 0-2%  $\text{CH}_4$  addition, the population of gold ions drastically decreases until the gold ion signal is at the level of the background (2%  $\text{CH}_4$ ). The gold ion population remains at this level. As the argon and argon-hydride ions drastically decrease (<0.5%  $\text{CH}_4$ ), the methane related ions begin to evolve. The inset in Figure 5-9 is a 20x magnified view illustrating the  $\text{C}_2\text{H}_5^+$  and  $\text{C}_3\text{H}_3^+$  ions with respect to methane content; however, only a small increase in  $\text{C}_2\text{H}_5^+$  is evident. A delay time plot

only presents part of the story for a methane discharge. Additional phenomena are occurring in the pulsed discharge as methane is introduced, which can only be seen when viewing a mass spectrum.

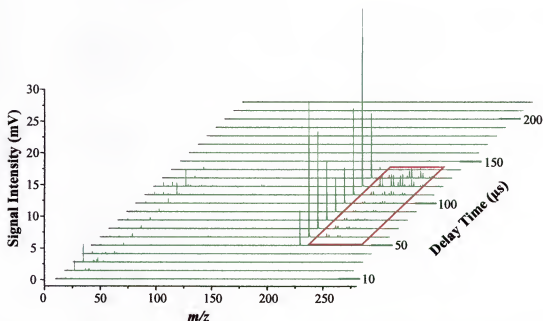


Figure 5-11 A 1%  $\text{CH}_4$   $\mu\text{SPGD}$ . A series of mass spectra collected at delay times between 10–220  $\mu\text{s}$  compiled to generate a waterfall plot. The red box indicates the delay times, which gold-methane adducts are detected. Cathode material: high purity gold.

Figure 5-11 illustrates the change in ions at different delay times with a waterfall plot for 1%  $\text{CH}_4$ . Ions associated with the discharge gas typically are only detected at earlier times; however, methane related ions are also apparent at longer delay times ( $\text{C}_3\text{H}_3^+$ ). Also noteworthy is the group of ions between  $m/z$  200 and 250, which are enclosed by a red box. The presence of lower molecular weight ions (due to the discharge gas) may be related to the increase in ion peaks  $>m/z$  200. In the dcGD mass spectrum of 5%  $\text{CH}_4$  (Figure 5-5) a few peaks are present at  $>m/z$  200; however, Figure 5-12 illustrates the increased number of peaks in a mass spectrum at 1%  $\text{CH}_4$  for a

$\mu$ sPGD. At  $m/z$  197, the gold ion peak dominates at the 120  $\mu$ s delay time as expected compared to Figure 5-9.

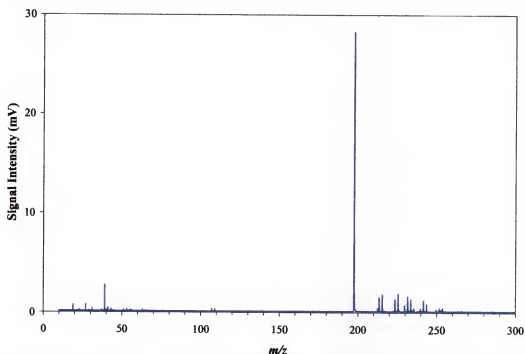
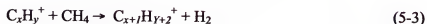


Figure 5-12 Microsecond pulsed glow discharge mass spectrum of 1%  $\text{CH}_4$  in argon collected at a 120  $\mu$ s delay time. Sample material: high purity gold.

Figure 5-13 consists of two mass spectra depicting magnified views of the mass regions 10-70 (A) and 200-270 (B), which correlate to Figure 5-12. In plot A, a series of methane related peaks are identified. A report by Mason and Milton<sup>109</sup> describes a series of hydrocarbon peaks from  $m/z$  13-123 that appear in a 3%  $\text{CH}_4$  in argon dcGD (refer to Figure 5-6). A periodicity in the hydrocarbon distribution of 12 or 14 mass units was evident. The pattern and extensive hydrocarbon peaks were not evident in the data presented in Figures 5-12 and 5-13. Higher mass ions associated with methane grow by the reaction sequence expressed by<sup>105</sup>



The hydrocarbon ions can also be expressed in sequences: (a)  $m/z = 13 \rightarrow 27 \rightarrow 41 \rightarrow 55 \rightarrow 69 \rightarrow 83 \rightarrow 97 \rightarrow 111$ , (b)  $m/z = 15 \rightarrow 29 \rightarrow 42 \rightarrow 57 \rightarrow 71 \rightarrow 85$ , and (c)  $m/z = 39 \rightarrow 53 \rightarrow 67 \rightarrow 81 \rightarrow 95 \rightarrow 109 \rightarrow 123$ .

Figure 5-13A displays the mass range 10-70 depicting some of the hydrocarbon peaks just mentioned. A few ion signals in plot A correspond to those noted in the series (a), (b), and (c). The sequences should stop as the process becomes endothermic; however, larger hydrocarbons form because these ions are probably highly energetic. Table 5-2 lists the methane related ions detected in dc and microsecond pulsed discharges. Never reported before for the pulsed glow discharge are the series of ions illustrated in Figure 5-13B in the  $m/z$  range 200-270. As depicted in Figures 5-11 and 5-12, a strong ion signal for gold is present at the 120  $\mu\text{s}$  delay time. In the mass range greater than 197 are a series of ion signals related to gold, otherwise considered gold adducts. The signal intensities of the gold adduct peaks are greater than the hydrocarbon ion signals.

Table 5-2 Comparison of the methane derived ions in a dc glow discharge compared to a microsecond pulsed glow discharge.

dcGD	$\mu\text{sPGD}$
$\text{C}_2\text{H}_5^+$	$\text{C}_3\text{H}_3^+$
$\text{C}_2\text{H}_4^+$	$\text{C}_2\text{H}_3^+$
$\text{C}_3\text{H}_5^+$	$\text{C}_3\text{H}_5^+$
$\text{C}_3\text{H}_3^+$	$\text{C}_3\text{H}_7^+$
	$\text{C}_4\text{H}_5^+$
	$\text{C}_5\text{H}_3^+$
	$\text{C}_4\text{H}_7^+$
	$\text{C}_5\text{H}_7^+$

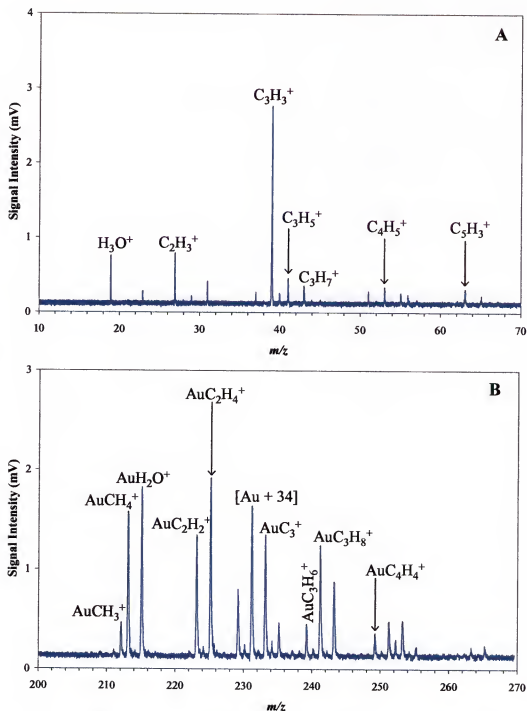


Figure 5-13 Microsecond pulsed glow discharge mass spectrum of 1%  $\text{CH}_4$  in argon collected at a 120  $\mu\text{s}$  delay time. A) Magnified 7.5x illustrating  $m/z$  10-70 and B) Magnified 10x illustrating  $m/z$  200-270. Sample material: high purity gold.

The extensive gold adduct formation is not as prevalent in the dcGD as shown in Figure 5-9C. Signal intensities in the dcGD are one-third less than the  $\mu\text{sPGD}$ . An

interesting phenomenon is occurring after pulse termination in the pulsed glow discharge. As the discharge pulse is terminated, the potential field is gone, and ions continue to react. A continuous flow of methane through the GD source produces a constant supply of methane molecules to react with gold. What happens if other target materials are subjected to a methane discharge? Analyzing copper and silver might provide insight into the gold adduct formation.

**Mixed-Gas Plasma – Alternative Elements.** To better understand the phenomena of adduct formation occurring in the pulsed discharge, both copper (NIST 1113) and silver were used as target materials in place of gold. The effect of methane will be monitored to see if a similar phenomenon occurs with other target materials. Figure 5-14 consists of two plots depicting a copper (A) and silver (B) target when subjected to various concentrations of methane (0-5%) in a microsecond pulsed glow discharge. The two plots are not drastically different. The silver ion signals gradually decrease with up to 3% methane addition and then reach a steady-state up to 5% CH<sub>4</sub>. The greatest drop in copper ion signals occurs within the first percent of methane addition and at 5% CH<sub>4</sub> the ion signals are around background level. Between copper and silver targets, the copper ion population trend more closely resembles the gold ion trend as illustrated in Figure 5-10. If the copper ion population trend is similar to gold, then does adduct formation occur?

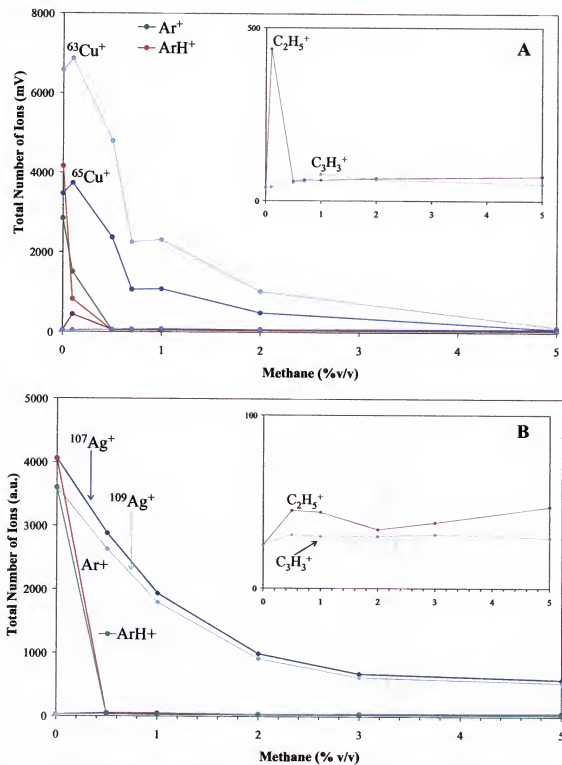


Figure 5-14 Microsecond pulsed glow discharge of ion population with respect to methane concentration (0-5%). A) NIST 1113 and B) High purity silver.

At 1% CH<sub>4</sub> in argon for a  $\mu$ sPGD, a series of peaks greater than  $m/z$  65 are prevalent at longer delay times. Since copper has two strong isotope signals, the copper-hydrocarbon adducts become more complex. Figure 5-15 illustrates the ions detected at an early delay time of 50  $\mu$ s, and Figure 5-16 shows the extensive adducts at a later delay time of 120  $\mu$ s. Figure 5-15 is more representative of a dcGD mass spectrum because it was collected at a middle delay time. Labeled in the inset are hydrocarbon species associated with methane, which are also detected with a gold target.

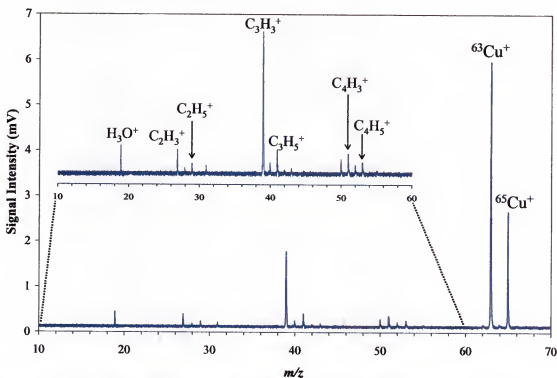


Figure 5-15 1% CH<sub>4</sub> in argon  $\mu$ s pulsed glow discharge mass spectrum at a 50  $\mu$ s delay time. Inset is magnified 3.5x. Sample material: NIST 1113.

Figure 5-16 illustrates the effect that 1% CH<sub>4</sub> in argon has on the ionization mechanisms in a pulsed glow discharge at a 120  $\mu$ s delay time. Plot A is dominated by the two copper isotope ions, but with a 25x magnification a series of peaks are present between  $m/z$  75-215 as shown in plot B. In plot B, the first two cluster sets have ion distributions that are similar to the  $^{63}\text{Cu}^+$  and  $^{65}\text{Cu}^+$  ratio. Ion peaks at  $m/z$  81 and 83

indicate a +18 ( $\text{H}_2\text{O}$ ) to  $^{63}\text{Cu}$  and  $^{65}\text{Cu}$ . A methane adduct with copper is likely at  $m/z$  91 and 93, a difference of 28 ( $\text{C}_2\text{H}_4^+$ ). Other identifiable peaks are illustrated in the inset.

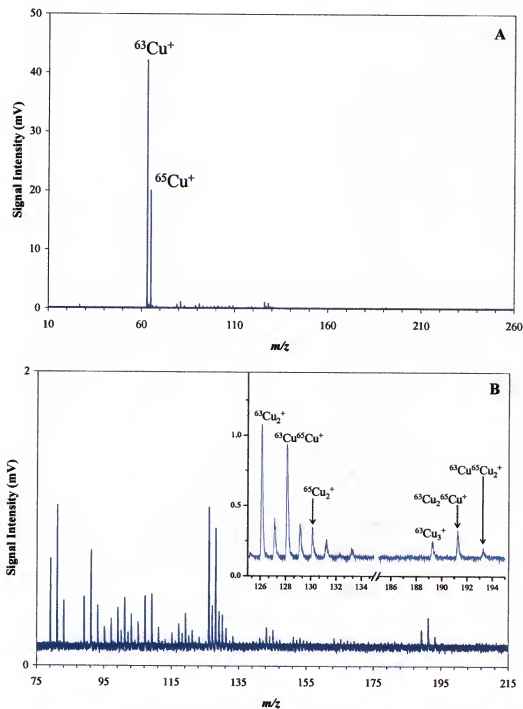


Figure 5-16 Mass spectra of 1%  $\text{CH}_4$  in argon for a  $\mu\text{SPGD}$  collected at a 120  $\mu\text{s}$  delay time. A)  $m/z$  region 10-260 and B)  $m/z$  region 75-215. Sample material: NIST 1113.

The inset in plot B is a mass spectrum of  $m/z$  122-134 and  $m/z$  184-194. In these mass regions are peaks corresponding to the copper dimers and trimers, which are not detected in an argon plasma for the source and conditions employed. Formation of dimers and trimers in a glow discharge has been observed previously<sup>71,126-128</sup> and dimers have also been used as a way of quantification in a dcGD.<sup>127</sup> During the sputtering event, either bound metal atoms are ejected or single atoms, which recombine after ejection; therefore, it is possible to detect polyatomic species under suitable conditions. In the current experiments, the dimers and trimers of copper are prevalent only when methane is added to an argon plasma; however, Mohill<sup>71</sup> reported detecting copper dimers and trimers in an argon  $\mu$ SPGD using a different glow discharge source, mass spectrometer, and conditions. Variations between results exist because a different set of conditions and source were implemented for experimentation. The ratios of the polyatomic ions for copper match the calculated distribution as shown in Figure 5-17. Isopro calculates the distribution based on a binomial expansion relative to the natural isotope abundance and the number of atoms in the cluster.

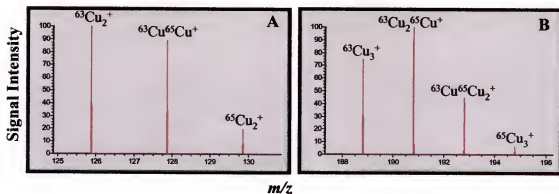


Figure 5-17 Mass spectra generated from Isopro indicating the isotope distribution of copper dimers (A) and trimers (B).

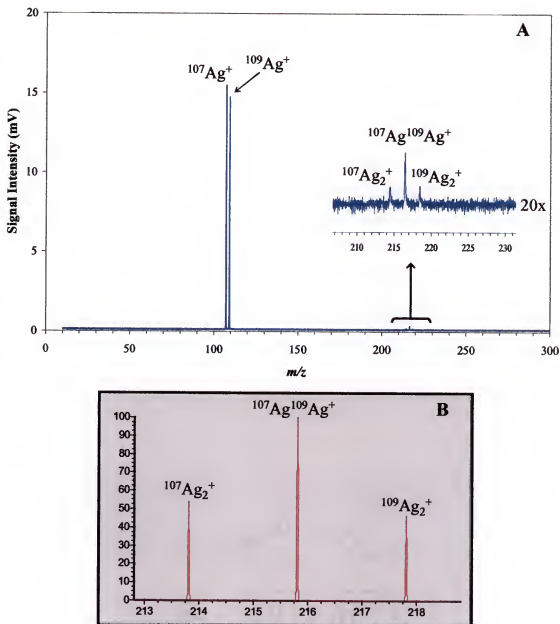


Figure 5-18 A) Microsecond pulsed glow discharge mass spectrum of 1% CH<sub>4</sub> in argon, experimental data. B) Distribution of silver dimers using Isopro calculation.

Does the polyatomic ion formation only occur with the copper atoms? Due to instrumental constraints, the gold polyatomic ions could not be analyzed. Detecting silver diatomic species is within the instrument constraints. Figure 5-18 is a mass spectrum of (A) experimental data for 1% CH<sub>4</sub> at 110  $\mu\text{s}$  delay time and (B) theoretical

data based on Isopro calculations. The experimental data of copper and silver matches the distribution calculations of Isopro.

According to Mohill,<sup>71</sup> the copper dimer population is greatest at smaller cathode-to-sampling orifice distances. As the distance between the cathode and sampling orifice is increased, the copper dimer must travel a longer distance through the energetic plasma. Higher probabilities of collisions exist at greater plasma volumes. Adding methane to an argon plasma reduces the sputter rate (described in following section), quenches the argon metastable population, and reduces the net analyte ion population. Because of these conditions, the plasma volume most likely changes. Sputter rate results may provide further insight into the polyatomic ion formation.

**Sputter Rate.** As illustrated in the previous sections, the addition of up to five percent methane causes significant changes in the sputtered analyte ion populations. The sputter rate is one indication of why the ion population is decreasing. Figure 5-19 illustrates the effect of 0-5% CH<sub>4</sub> in argon on the net sputter rate of gold, copper, and silver. The sputter rate for each target decreases gradually with increasing concentration of methane. Of the three metals, the silver sputter rate most closely matches the ion population trend. Sputter rate decreases because the major byproduct of methane reactions is hydrogen. Due to the weight and size of hydrogen, its ability to transfer enough energy to the target surface for atom liberation is limited. With at least 95% of the plasma gas being argon, then argon must still be contributing significantly to sputtering. Since the sputter rate does not directly correspond to the ion population trend of copper and gold, then other considerations must be taken into account.

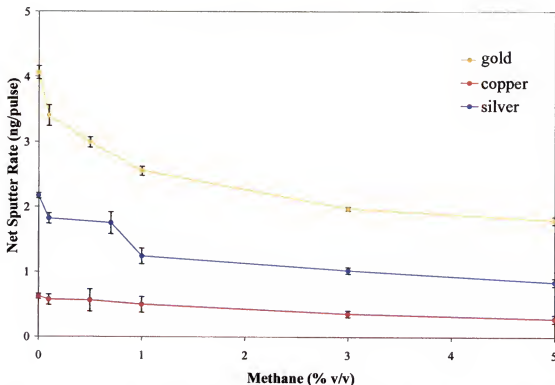


Figure 5-19 Net pulsed sputter rate of gold, copper, and silver as a function of methane concentration.

**Penning Ionization.** Since the dominant reason for a decrease in analyte ion population with increasing methane concentration is not sputter rate (fewer atoms liberated), then ionization mechanisms are considered. As mentioned previously, methane plays a role in the reduction of argon metastables. According to Velazco et al.,<sup>129</sup> the quenching rate constant ( $k_Q$ ) is  $33 \cdot 10^{-11} \text{ cm}^3 \text{ s}^{-1}$  for the Ar ( $^3\text{P}_2$ ) metastable and  $55 \cdot 10^{-11}$  for the Ar ( $^3\text{P}_0$ ) metastable. These quenching constants are almost two times that of oxygen. A loss of argon metastables in negative glow results in a significant reduction in ionization of sputtered atoms; hence, a decrease in the sputtered analyte ion populations.

**Chemical Ionization.** Studies indicate the possibility of utilizing methane as a CI reagent gas in a microsecond pulsed glow discharge. Other glow discharge studies have

introduced organic vapors into the argon plasma to study the structural, molecular, and elemental information. In these studies, toluene vapor ( $\text{C}_6\text{H}_5\text{CH}_3$ ) was introduced into the pulsed glow discharge *via* a separate gas line. To promote chemical ionization, a mixture of 1% methane in argon was employed as the plasma gas. Gold was used as the target material.

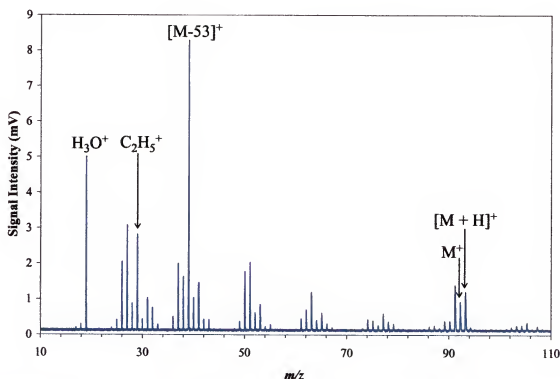


Figure 5-20 Mass spectrum of a microsecond pulsed glow discharge with a 1% methane in argon plasma gas. Toluene vapor was added to the plasma. Sample material: high purity gold.

Figure 5-20 illustrates the effect of toluene vapor on a methane glow discharge. With 1%  $\text{CH}_4$  and toluene added to the plasma gas, the sputtered analyte signal (gold) is around background level. In addition, the gold-methane adducts are also removed. The series of ion peaks in the mass spectrum are indicative of the toluene molecular ion ( $m/z$  92), protonated species ( $m/z$  93), and extensive fragmentation peaks. Amidst the

fragmentation is a prevalent methane reagent ion ( $\text{C}_2\text{H}_5^+$ ) at  $m/z$  29. A pulsed glow discharge offers the advantage of producing both electron impact and chemical ionization-like spectra. In an electron impact mass spectrum, the molecular ion peak would be much higher in signal than the protonated species; however, as shown in Figure 5-20, the protonated toluene peak is slightly more intense than the molecular ion. A previous study reports that only the molecular ion peak for toluene was detected in a pure argon plasma verifying that chemical ionization is occurring to a small extent in a methane discharge. The microsecond pulsed glow discharge has the capability of promoting chemical ionization with a methane-argon plasma.

### Conclusions

Chemical ionization involves the ion/molecule reaction of the reagent gas ions and molecule of interest. Multiple papers and books have been written on chemical ionization describing the many gases used to promote CI reactions; however, methane is the most commonly used and studied reaction gas.

In these studies, methane was introduced into an argon microsecond pulsed glow discharge until a 5% methane discharge was established. With increasing additions of methane, both the sputtered analyte ion signals and net sputter rate decreased. The decrease in sputter rate results from lower molecular weight species impinging upon the target, which includes methane and hydrogen molecules (the byproduct of methane reactions). A decrease in the sputter rate correlates with the loss of analyte signal; however, other factors contribute to a decrease in this signal. Methane is known to quench the argon signal (as shown in Figures 5-10 and 5-13). A decrease in the argon metastable population affects the significant contribution of Penning ionization.

Adding methane to a pulsed discharge also contributes to adduct and cluster formation. Extensive adduct formation is found for both gold and copper. Adduct formation occurs at longer delay times, after pulse termination, signifying possible recombination occurring in the afterpeak region of the discharge. A continuous gas flow of methane offers a steady supply of methane molecules in the discharge region. Conditions within the discharge are also favorable for cluster formation as shown for both copper and silver. With the addition of methane, the plasma volume is possibly smaller, and therefore a shorter distance exists for metal clusters to travel from the target (or negative glow) to the orifice. A shorter travel distance means a lower probability of collision to break the cluster. The greatest amount of clustering and adduct formation occurs in a 1% methane discharge.

The effect of methane on the plasma and discharge ions was investigated. Because of the results, a 1% CH<sub>4</sub> in argon plasma gas was used to study the chemical ionization in a microsecond pulsed glow discharge. Addition of toluene vapor to the plasma gas illustrates the capability of utilizing a glow discharge for CI. In these studies, it was found that the protonated toluene peak was greater in signal intensity than the molecular ion, which is more typical of CI-like spectra. A microsecond pulsed glow discharge has the capability of promoting both electron ionization and chemical ionization under suitable conditions.

## CHAPTER 6

### CONCLUDING REMARKS

This dissertation has focused on the glow discharge source encompassing both sputtering and ionization studies in reactive gas environments. Electrical breakdown of a gas between two electrodes causes current to flow, thus creating a glow discharge (GD). Due to the nature of the glow discharge, atomization and ionization is a two-step process. The sample is atomized during the sputtering event followed by ionization through collisions with the gas species. While glow discharge sources are commonly operated in constant voltage mode, applying a transient pulse alters the reaction environment. For example, after pulse termination, reactions between sputtered analytes and gas species continue. The projects presented in this dissertation involve interfering with the stable discharge environment by replacing inert argon gas with reactive gases. Because the mechanism of ionization in the discharge is important, time-of-flight mass spectrometry was used to monitor changes in ion signals.

Two of the projects were based on impurities often present in the plasma environment. These impurities are nitrogen and oxygen, which are typically associated with vacuum leaks or a poor seal between the sample and source. Based on direct current glow discharge studies with optical emission spectrometry, nitrogen and oxygen addition are considered to quench signals formed in the discharge. Argon metastables, which cannot be monitored with mass spectrometry, show the most significant drop in signal with nitrogen or oxygen addition. A loss in the argon metastable signal parallels a

reduction in signal of sputtered analyte species. Despite these reports, nitrogen and oxygen provide opportunities for improving the analytical utility of the GD source.

Nitrogen, the primary constituent in air, has been considered a primary reagent ion, besides water, in atmospheric pressure ionization. In this project, the participation of nitrogen in the ionization events was studied. For the studies, nitrogen was systematically added to a stable argon plasma until a pure nitrogen discharge was established. By introducing nitrogen in increments, ionization in the discharge could be monitored as a function of gas concentration. The direct current (dc) GD provided conditions suitable for steady-state ion analysis. Data collected in dc mode presented a reference point when analyzing ion trends generated in the microsecond pulsed discharge mode. As expected, pulsing the discharge offers a unique ionization environment with a nitrogen-argon plasma gas. Not only does, the analyte ion population decrease with increasing nitrogen concentration, but the nitrogen ion populations do not dominate. Since the difference in ionization energies between nitrogen and argon is only 0.2 eV, ionization competition prevents either ion from dominating. Even though nitrogen may be an integral component in atmospheric pressure ionization, efficient ionization at low pressures may be hindered. In addition to competitive ionization, the secondary electron emission in a nitrogen discharge is almost two times lower than for argon. Fewer electrons means a lower probability of electron impact ionization of gas species; fewer gas ions results in a lower sputter yield, and therefore a loss in analyte ion signal.

Nitrogen's involvement in the ionization process of a glow discharge may be minimal, but analytical utility of a nitrogen discharge exists. With increasing nitrogen content, the net pulsed sputter rate decreases. In an argon microsecond pulsed glow

discharge, depth profiling of thin films is limited to ~25 nm, yet thin layer analysis can be improved by adding nitrogen to the plasma. In essence, a decrease in sputter rate lends to <25 nm layers being removed. Additionally, a pure nitrogen discharge reduces the number of interferences. After evaluating the capabilities of nitrogen, a more reactive gas was introduced into the glow discharge.

Oxygen, the second most prevalent gas in the atmosphere, is a detrimental impurity because of oxide layers that can form, which hinder efficient sputtering. Instead of oxygen acting as an impurity, these studies monitored oxygen's involvement in glow discharge ionization. For ionization sources with mass spectrometry detection, oxygen is often used as a means for generating negative ions; however, this project entailed utilizing oxygen for positive ionization.

Compared to nitrogen, a pure oxygen discharge generated an  $O_2^+$  ion population almost equal in population to the  $Ar^+$  population in a pure argon discharge. Despite the surplus of gas ions available for ionization, the sputtered analyte ion population decreased with increasing amounts of oxygen content. This trend corresponds to the lower net sputter rates at higher oxygen concentrations. In the microsecond pulsed discharge, the voltage-on time is 20  $\mu s$  with a short duty cycle indicating long off-times. Long off times allows plasma equilibration and the sample surface can become coated with surface layers of absorbed gases such as oxygen. Further investigation is required to determine the possible utility of  $O_2^+$  ions in the plasma. In an effort to study of the effect of a range of reactive gases on the plasma, methane was incorporated into discharge gas.

The final phase of research focused on 0-5% methane addition to an argon plasma. Methane is the most common gas used in chemical ionization (CI) due the extensive

reagent ions generated. Ionization in the glow discharge plasma is dominated by electron impact and Penning ionization, so the possibility of chemical ionization in the low pressure discharge was considered. Adding methane to argon quickly quenched the sputtered analyte ion signal. A primary by-product of methane reagent ion formation is hydrogen, which is a poor sputtering agent. In addition, an unusual phenomenon of methane adduct formation with metal species occurred at longer delay times, which indicates reactions taking place after pulse termination. To test methane's ability in chemical ionization, toluene vapor was introduced into the plasma gas. Compared to an electron impact mass spectrum, the molecular toluene ion was lower in signal than the protonated toluene molecule indicating that CI was predominating.

In this dissertation, ionization studies on reactive discharge environments in a glow discharge were investigated. Studies reveal chemical sputtering is occurring and ionization patterns are changing. Many future studies will provide additional insight into the effect of alternative gases on a microsecond pulsed glow discharge.

## CHAPTER 7

### FUTURE CONSIDERATIONS

The studies in this dissertation leave many unanswered questions about the fundamental processes occurring in the pulsed discharge with reactive gas additions. Experiments to be considered in the future include not only mass spectrometry detection, but also emission measurements.

With the addition of nitrogen, oxygen, or methane, obvious changes in the argon ion signals occur. As ion species associated with nitrogen, oxygen, or methane become prevalent due to greater amounts of these gases in the plasma, the  $\text{Ar}^+$  signal decreases or reaches a level equivalent to background. Previous optical emission studies report a decrease in the emission lines associated with Ar I, Ar II, and argon metastables with increasing concentrations of alternative gases. However, these reports are based on direct current glow discharges with varying source conditions. In addition, the monoatomic ion of nitrogen is non-existent and  $^{16}\text{O}^+$  from oxygen is close to background level. Emission studies report larger populations of the monoatomic species as atomic lines. No ion lines were monitored. Future gas studies would include complementary emission data to observe the trends for both atomic and ionic populations. This would include monitoring metastable states of argon and nitrogen to determine their contribution in the ionization of sputtered analyte atoms. For example, in the dc glow discharge, as nitrogen content increases (Figure 3-4) the gold signal intensity remains relatively constant from 0-100%  $\text{N}_2$ . Is a large population of argon metastables present? Is there a large population of nitrogen metastables available? Optical emission spectrometry could provide

complementary information to mass spectrometry for a better understanding of the fundamental processes in the plasma.

With respect to the emission studies, two setups are possible: 1) a glow discharge source with scanning monochromator or 2) modify the existing source to include either a window to collect the emission or introduce a fiber optic element to collect the emission. Due to the constraints of the glow discharge source associated with the time-of-flight mass spectrometer, a separate glow discharge optical emission spectrometer set up would be needed.

A second parameter of the discharge to investigate is the plasma's axial profile. Even though the atomic ions of oxygen and nitrogen are not detected, they could be prevalent closer to the cathode. By developing an axial profile of each mixed gas plasma, one can determine ion distributions at known distances from the cathode, if plasma size changes based on gas composition, and speculate possible ionization mechanisms. To accomplish axial profiling an imaging system is required.

In addition to profiling the plasma, profiling the ion signals as a function of the pulse profile would provide further insight into mixed-gas plasmas. An advantage of a microsecond pulsed glow discharge is the ability to temporally discriminate between gas and analyte species. For example, in a microsecond pulsed glow discharge, argon no longer interferes with calcium at  $m/z$  40. Signals are enhanced by the higher instantaneous energies generated per pulse and create intense ion signals. By using both emission spectrometry and mass spectrometry for pulse profiling, additional insight on atom and ion interaction can be generated. This would provide information on why sputter rate is decreasing, gas ions are decreasing, or gas ions are not increasing. For

example, with increasing additions of nitrogen gas the gas ions associated with nitrogen do not increase as significantly as the molecular oxygen ion (in the oxygen discharge). Analyzing the population of ions during the pre-peak, plateau, and after-peak could indicate how nitrogen ions are contributing to ionization in the plasma.

Plasma and pulse profiling of a methane plasma would be advantageous for understanding the appearances of certain species, yet additional studies could provide information on the structures' energies. Methane generated interesting results, for example the adduct formation of the metal (gold or copper) with methane derivatives. The exact formation or structure of the metal adducts is not known; however, using a computer modeling program for molecular structures would be beneficial. Methane is also a known chemical ionization (CI) gas, and preliminary studies report that CI is possible in a glow discharge. This was shown with the addition of toluene. Additional experiments based on methane concentration and analyte molecule are required to further determine the utility of chemical ionization in a microsecond pulsed glow discharge.

Even though insight into the mixed-gas plasmas of nitrogen, oxygen, and methane has been introduced, many holes exist in the research to make strong conclusions. The proposed experiments will provide the additional information needed to better understand the sputtering and ionization processes in mixed-gas plasmas.

## LIST OF REFERENCES

1. Llewellyn-Jones, F. *The Glow Discharge and An Introduction to Plasma Physics*, John Wiley & Sons Inc.: New York, 1966.
2. *Measuring Mass from Positive Rays to Proteins*, Chemical Heritage Press: Philadelphia, 2002.
3. *Nobel Lectures: Physics 1901-1921*, Elsevier Publishing Company: Amsterdam, 1967.
4. Aston, F. W. *Mass Spectra and Isotopes*, 2 ed.; Longmans: New York, 1942.
5. Aston, F. W. *Proc. Roy. Soc. A* **1937**, *163*, 391.
6. Bainbridge, K. T.; Jordan, E. B. *Phys. Rev.* **1936**, *50*.
7. Coburn, J. W. *Rev. Sci. Instrum.* **1970**, *41*, 1219.
8. Coburn, J. W.; Kay, E. *Appl. Phys. Lett.* **1971**, *18*, 435-438.
9. Coburn, J. W.; Kay, E. *J. Appl. Phys.* **1972**, *43*, 4965-4971.
10. Grimm, W. *Spectrochim. Acta, Part B* **1968**, *23*, 443.
11. Daughtrey Jr., E. H.; Harrison, W. W. *Anal. Chem.* **1975**, *47*, 1024-1028.
12. Donohue, D. L.; Harrison, W. W. *Anal. Chem.* **1975**, *47*, 1528-1531.
13. Harrison, W. W.; Magee, C. W. *Anal. Chem.* **1974**, *46*, 461-464.
14. Mattson, W. A.; Bentz, B. L.; Harrison, W. W. *Anal. Chem.* **1976**, *48*, 489-491.
15. Harrison, W. W.; Prakash, N. J. *Anal. Chim. Acta* **1970**, *49*, 151-159.
16. Broekaert, J. A. C. *Spectrochim. Acta, Part B* **1980**, *35*, 225-232.
17. Brackett, J. M.; Vickers, T. J. *Spectrochim. Acta, Part B* **1982**, *37*, 841-847.
18. Jakubowski, N.; Stuewer, D.; Toelg, G. *Spectrochim. Acta, Part B* **1991**, *46*, 155-163.

19. Bogaerts, A.; Wilken, L.; Hoffmann, V.; Gijbels, R.; Wetzig, K. *Spectrochim. Acta, Part B* **2002**, *57*, 109-119.
20. Anfone, A. B.; Marcus, R. K. *J. Anal. At. Spectrom.* **2004**, *19*, 333-344.
21. Pisonero, J.; Pérez, C.; Pereiro, R.; Bordel, N.; Sanz-Medel, A. *J. Anal. At. Spectrom.* **2001**, *16*, 370-375.
22. Michler, J.; Aeberhard, M.; Velten, D.; Winter, S.; Payling, R.; Breme, J. *Thin Solid Films* **2004**, *447*, 278-283.
23. Bengtson, A. *J. Anal. At. Spectrom.* **2003**, *18*, 1066-1068.
24. Palaez, M. V.; Costa-Fernández, J. M.; Pereiro, R.; Bordel, N.; Sanz-Medel, A. *J. Anal. At. Spectrom.* **2003**, *18*, 864-871.
25. Yang, C. L.; Ingeneri, K.; Mohill, M.; Harrison, W. W. *J. Anal. At. Spectrom.* **1999**, *15*, 73-78.
26. Shimizu, K.; Habazaki, H.; Skeldon, P.; Thompson, G. E.; Wood, G. C. *Surf. Interf. Anal.* **2000**, *29*, 155-159.
27. Oxley, E.; Yang, C. L.; Harrison, W. W. *J. Anal. At. Spectrom.* **2000**, *15*, 1241-1245.
28. Li, L.; Barshick, C. M.; Millay, J. T.; Welty, A. V.; King, F. L. *Anal. Chem.* **2003**, *75*, 3953-3961.
29. Davis, W. C.; Venzie, J. L.; Willis, B.; Coffee Jr., R. L.; Arya, D. P.; Marcus, R. K. *Rapid* **2003**, *17*, 1749-1758.
30. Bogaerts, A.; Gijbels, R. *J. Anal. At. Spectrom.* **2001**, *16*, 239-249.
31. Bogaerts, A.; Gijbels, R.; Jackson, G. P. *J. Anal. At. Spectrom.* **2003**, *18*, 533-548.
32. Bogaerts, A.; Chen, Z. Y.; Gijbels, R. *Surf. Interf. Anal.* **2003**, *35*, 593-603.
33. Beyer, C.; Feldmann, I.; Gilmour, D.; Hoffmann, V.; Jakubowski, N. *Spectrochim. Acta, Part B* **2002**, *57*, 1521-1533.
34. Oxley, E.; Yang, C.; Liu, J.; Harrison, W. W. *Anal. Chem.* **2003**, *75*, 6478-6484.
35. Yang, C.; Mohill, M.; Harrison, W. W. *J. Anal. At. Spectrom.* **2000**, *15*, 1255-1260.
36. Lewis, C. L.; Moser, M. A.; Dale Jr., D. E.; Hang, W.; Hassell, C.; King, F. L.; Majidi, V. *Anal. Chem.* **2003**, *75*, 1983-1996.

37. Li, L.; Millay, J. T.; Turner, J. P.; King, F. L. *J. Am. Soc. Mass. Spectrom.* **2004**, *15*, 87-102.
38. Majidi, Vahid; Moser, Matt; Lewis, Cris; Hang, Wei; King, F. L. *J. Anal. At. Spectrom.* **2000**, *15*, 19-25.
39. Chapman, B. *Glow Discharge Processes: Sputtering and Plasma Etching*, John Wiley & Sons: New York, 1980.
40. Fang, D.; Marcus, R. K. *Glow Discharge Spectroscopies*, Marcus, R. K., Ed.; Plenum Press: New York, 1993; Chapter 2.
41. Howatson, A. M. *An Introduction to Gas Discharges*, 2 ed.; Pergamon Press: Oxford, 1976.
42. Llewellyn-Jones, F. *The Glow Discharge and an Introduction to Plasma Physics*, John Wiley & Sons Inc.: New York, 1966.
43. Howatson, A. M. *An Introduction to Gas Discharges*, 2 ed.; Pergamon Press: Oxford, 1965; Chapter 4.
44. Barshick, C. M. *Inorganic Mass Spectrometry: Fundamentals and Mass Spectrometry*, Barshick, C. M.; Duckworth, D. C. Smith, D. H., Eds.; Marcel Dekker, Inc.: New York, 2000; Chapter 2.
45. von Engel, A. *Ionized Gases*, 2 ed.; Oxford University Press: Oxford, 1965; Chapter 8.
46. Harrison, W. W.; Yang, C.; Oxley, E. *Anal. Chem.* **2001**, *73*, 480A-487A.
47. Bruhn, C. G.; Harrison, W. W. *Anal. Chem.* **1977**, *50*, 16-21.
48. Chapman, B. *Glow Discharge Processes*, John Wiley & Sons: New York, 1980; Chapter 6.
49. Wehner, G. K. *Physical Rev.* **1955**, *102*, 690-704.
50. Boumans, P. W. *Anal. Chem.* **1972**, *44*, 1219-1228.
51. Sigmund, P. *Phys. Rev.* **1969**, *184*, 383-416.
52. Rosenberg, D.; Wehner, G. K. *J. Appl. Phys.* **1962**, *33*, 1842.
53. Carter, G.; Colligon, J. S. *Ion Bombardment of Solids*, Heinemann Educational Books Ltd: London, 1968; Chapter 7.
54. Laegreid, N.; Wehner, G. K. *J. Appl. Phys.* **1961**, *32*, 365-369.

55. Harrison , W. W. *Inorganic Mass Spectrometry*, Adams, F.; Gijbels, R. van Grieken, R., Eds.; John Wiley & Sons: New York, 1988; Chapter 3.
56. McDaniel, E. W. *Collision Phenomena in Ionized Gases*, John Wiley & Sons: New York, 1964.
57. Harrison , W. W.; Yang, C.; Oxley, E. *Glow Discharge Plasmas in Analytical Spectroscopy*, Marcus, R. K.; Broekaert, J. A. C., Eds.; John Wiley & Sons: West Sussex, 2003; Chapter 3.
58. Chapman, B. *Glow Discharge Processes: Sputtering and Plasma Etching*, John Wiley & Sons: New York, 1980; Chapter 4.
59. Levy, M. K.; Serxner, D.; Angstadt, A. D.; Smith, R. L.; Hess, K. R. *Spectrochim. Acta, Part B* **1991**, *46*, 253-267.
60. Jackson, G. P.; King, F. L. *Spectrochim. Acta, Part B* **2003**, *58*, 185-209.
61. Chapman, B. *Glow Discharge Processes: Sputtering and Plasma Etching*, John Wiley & Sons: New York, 1980; Chapter 2.
62. Hang, W.; Baker, C.; Smith, B. W.; Winefordner, J. D.; Harri *J. Anal. At. Spectrom.* **1997**, *12*, 143-149.
63. Oxley, E. University of Florida, Ph.D. Dissertation 2002.
64. Broekaert, J. A. C. *Glow Discharge Spectroscopies*, Marcus, R. K., Ed.; Plenum Press: New York, 1993; Chapter 4.
65. Cotter, R. J. *Time-of-Flight Mass Spectrometry*, American Chemical Society: Washington DC, 1994.
66. Cotter, R. J. *Anal. Chem.* **1992**, *64*, 1027A-1039A.
67. Mamyrin, B. A.; Shmikk, D. V. *Zh. Eksp. Teor. Fiz.* **1979**, *76*, 1500-1505.
68. Lewis, C. L.; Oxley, O.; Pan, C. K.; Steiner, R. E; King, F. L. *Anal. Chem.* **1999**, *71*, 230-234.
69. Harrison , W. W.; Hang, W. *J. Anal. At. Spectrom.* **1996**, *11*, 835-840.
70. Barshick, C. M. University of Florida, Ph.D. Dissertation 1991.
71. Mohill, M. University of Florida, Ph.D. Dissertation 2001.
72. Hess, K. R.; Harrison, W. W. *Anal. Chem.* **1988**, *60*, 691-696.
73. Carroll, D. I.; Dzidic, I.; Horning, E. C.; Stillwell, R. N. *Appl. Spectrosc. Rev.* **1995**, *49*, 338-406.

74. Bruins, A. P. *Trends Anal. Chem.* **1994**, *13*, 37-43.
75. Turney, K.; Harrison, W. W. *Rapid Commun. Mass. Spectrom.* **2004**, *18*, 629-635.
76. Fernández, B.; Bordel, N.; Pérez, C.; Pereiro, R.; Sanz-Medel, A. *J. Anal. At. Spectrom.* **2002**, *17*, 1549-1555.
77. Šmid, P.; Steers, E. B.; Weiss, Z.; Vlcek, J. *J. Anal. At. Spectrom.* **2003**, *18*, 549-556.
78. Wagatsuma, K.; Hirokawa, K. *Anal. Chem.* **1989**, *61*, 326-329.
79. Knewstubb, P. F.; Dawson, P. H.; Tickner, A. W. *J. Chem. Phys.* **1963**, 1031-1032.
80. Wagatsuma, K. *Spectrochim. Acta, Part B* **2001**, *56*, 465-486.
81. Fischer, W.; Naoumidis, A.; Nickel, H. *Fresenius' J. Anal. Chem.* **1993**, *349*, 210-213.
82. Fischer, W.; Naoumidis, A.; Nickel, H. *J. Anal. At. Spectrom.* **1994**, *9*, 375-380.
83. Wagatsuma, K.; Hirokawa, K. *Anal. Chim. Acta* **1995**, *306*, 193-200.
84. Giglio, J. J.; Caruso, J. A. *Appl. Spectrosc.* **1995**, *49*, 900-906.
85. Matsuda, S.; Shimosato, H.; Yumoto, M.; Sakai, T. *Electrical Engineering in Japan* **2004**, *147*, 17-24.
86. Wright, A. N.; Winkler, C. A. *Active Nitrogen*, Academic Press: New York, 1968.
87. Wagatsuma, K. *Z. Phys. D* **1996**, *37*, 231-239.
88. Fernández, B.; Bordel, N.; Pereiro, R.; Sanz-Medel, A. *J. Anal. At. Spectrom.* **2003**, *18*, 151-156.
89. Junk, G.; Svec, H. J. *J. Am. Chem. Soc.* **1958**, *80*, 2908-2909.
90. Knewstubb, P. F.; Tickner, A. W. *J. Chem. Phys.* **1962**, *37*, 2941-2949.
91. Keller, G. E.; Martin, D. W.; McDaniel, E. W. *Phys. Rev.* **1965**, *140*, 1535A-1546A.
92. Hwang, H. H.; Olthoff, J. K.; Van Brunt, R. J.; Radovanov, S. B.; Kushner, M. J. *J. Appl. Phys.* **1996**, *79*, 93-98.
93. Stephan, K.; Märk, T. D.; Futrell, J. H.; Helm, H. *J. Chem. Phys.* **1984**, *80*, 3185-3188.

94. Saporoschenko, M. *Phys. Rev.* **1965**, *139*, 352A-356A.
95. Bentz, B. L.; Harrison, W. W. *Int. J. Mass Spectrom. Ion Phys.* **1981**, *37*, 167-176.
96. Fernández, B.; Bordel, N.; Pereiro, R.; Sanz-Medel, A. *Anal. Chem.* **2004**, *76*, 1039-1044.
97. Hecq, M.; Hecq, A. *Thin Solid Films* **1981**, *76*, 35-43.
98. Heller, J. *Thin Solid Films* **1973**, *17*, 163-176.
99. Knewstubb, P. F.; Dawson, P. H.; Tickner, A. W. *J. Chem. Phys.* **1963**, *38*, 1031-1032.
100. Lounsbury, J. B. *J. Vac. Sci. Tech.* **1968**, *6*, 838-842.
101. Purdes, A. J.; Bolker, B. F. T.; Bucci, J. D.; Tisone, T. C. *J. Vac. Sci. Technol.* **1977**, *14*, 98-101.
102. Adams, N. G.; Dean, A. G.; Smith, D. *Int. J. Mass Spectrom. Ion Phys.* **1972**, *10*, 63-76.
103. Hunt, D. F.; McEwen, C. N.; Harvey, T. M. *Anal. Chem.* **1975**, *47*, 1730-1734.
104. Munson, B. *Int. J. Mass Spectrom.* **2000**, *200*, 243-251.
105. Munson, M. S. B.; Field, F. H. *J. Am. Chem. Soc.* **1966**, *88*, 2621-2630.
106. Harrison, A. G. *Chemical Ionization Mass Spectrometry*, 2nd ed.; CRC Press: New York, 1992.
107. Evans, H. E.; Jennings, P. P. *J. Phys. Chem.* **1966**, *70*, 1265-1267.
108. Smith, R. L.; Serxner, D.; Hess, K. R. *Anal. Chem.* **1989**, *61*, 1103-1108.
109. Mason, R.; Milton, D. *Int. J. Mass Spectrom. Ion Processes* **1989**, *91*, 209-225.
110. Boumans, P. W.; Broekaert, J. A. C., and Marcus, R. K. *Spectrochim. Acta, Part B* **1991**, *46*, 457-545.
111. MKS Type 247D: Four Channel Readout. 1998. Andover, MKS Instruments, Inc.
112. Hess, K. R. University of Virginia, Ph.D. Dissertation 1986.
113. Raizer, Y. P. *Gas Discharge Physics*, 2nd ed.; Springer: New York, 1997.
114. Hagstrum, H. D. *Phys. Rev.* **1956**, *104*, 672-683.

115. Cobine, J. D. *Gaseous Conductors: Theory and Engineering Applications*, Dover Publications: New York, 1958.
116. von Engel, A. *Ionized Gases*, 2 ed.; Oxford University Press: London, 1965.
117. Keefe, R. B. University of Virginia, Ph.D. Dissertation 1983.
118. Harrison, A. G. *Chemical Ionization Mass Spectrometry*, 2nd ed.; CRC Press: New York, 1992.
119. Roth, J. *Sputtering by Particle Bombardment II: Sputtering of Alloys and Compounds, Electron and Neutron Sputtering, Surface Topography*, Behrisch, R., Ed.; Springer-Verlag: Berlin, 1983; Chapter 3.
120. Hecq, A.; Vandy, M.; Hecq, M. *J. Chem. Phys.* **1980**, *72*, 2876-2878.
121. Long, G. L.; Bolton, J. S. *Spectrochim. Acta, Part B* **1987**, *42*, 581-589.
122. Adler, J. F.; Mermet, J. M. *Spectrochim. Acta, Part B* **1973**, *23*, 421.
123. Field, F. H. *J. Am. Chem. Soc.* **1961**, *83*, 1523-1534.
124. Field, F. H.; Munson, M. S. B. *J. Am. Chem. Soc.* **1965**, *87*, 3289-3294.
125. Savickas, P. J. University of Virginia, Ph.D. Dissertation 1984.
126. Gerhard, W.; Oechsner, H. *Z. Physik B* **1975**, *22*, 41-48.
127. Goodner, K. L.; Eyler, J. R.; Barshick, C. M.; Smith, D. H. *Int. J. Mass Spectrom. Ion Processes* **1995**, *146/147*, 65-73.
128. Oechsner, H.; Gerhard, W. *Surface Science* **1974**, *44*, 480-488.
129. Velazco, J. E.; Kolts, J. H.; Setser, D. W. *J. Chem. Phys.* **1978**, *69*, 4357-4373.

### BIOGRAPHICAL SKETCH


Elizabeth Pierz Hastings was born in Oneida, NY on November 17, 1977. She attended Mount Holyoke College, an all women liberal arts school, in South Hadley, MA. After graduating with her Bachelors of Arts degree in May 1999, Beth spent the summer hiking The Long Trail, which traverses 270+ miles through the Green Mountains in Vermont. In the fall of 1999, she continued her education at the University of Florida in the analytical chemistry division. Under the direction of Dr. W. W. Harrison, she completed her graduate studies with a Doctor of Philosophy in August 2004. Beth has accepted a post-doctoral position with Dr. George Havrilla at Los Alamos National Lab in New Mexico.

I certify that I have read this study and that in my opinion it conforms to acceptable standards of scholarly presentation and is fully adequate, in scope and quality, as a dissertation for the degree of Doctor of Philosophy.

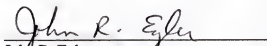


Willard, W. Harrison, Chair  
Professor of Chemistry


I certify that I have read this study and that in my opinion it conforms to acceptable standards of scholarly presentation and is fully adequate, in scope and quality, as a dissertation for the degree of Doctor of Philosophy.

  
James D. Winefordner  
Graduate Research Professor of Chemistry


I certify that I have read this study and that in my opinion it conforms to acceptable standards of scholarly presentation and is fully adequate, in scope and quality, as a dissertation for the degree of Doctor of Philosophy.

  
John R. Eyler  
Professor of Chemistry

I certify that I have read this study and that in my opinion it conforms to acceptable standards of scholarly presentation and is fully adequate, in scope and quality, as a dissertation for the degree of Doctor of Philosophy.

  
David H. Powell  
Scientist of Chemistry

I certify that I have read this study and that in my opinion it conforms to acceptable standards of scholarly presentation and is fully adequate, in scope and quality, as a dissertation for the degree of Doctor of Philosophy.

  
Nancy D. Denslow  
Scientist of Biochemistry and Molecular  
Biology

This dissertation was submitted to the Graduate Faculty of the Department of Chemistry in the College of Liberal Arts and Sciences and to the Graduate School and was accepted as partial fulfillment of the requirements for the degree of Doctor of Philosophy.

August 2004

---

Dean, Graduate School